Surface Evolution during Gallium Arsenide Homoepitaxy with Molecular Beam Epitaxy

by

Michael Brian Whitwick

B.Sc. University of Northern British Columbia, 2000
M.Sc. University of British Columbia, 2003

A THESIS SUBMITTED IN PARTIAL FULFILMENT OF
THE REQUIREMENTS FOR THE DEGREE OF

Doctor of Philosophy

in

The Faculty of Graduate Studies

(Physics)

The University of British Columbia

(Vancouver)

December 2009

Abstract

GaAs grown with MBE is the basis for many useful optoelectric devices. Measurements are presented of the smoothing of patterned and randomly roughened GaAs surfaces during homoepitaxy over a large range of Ga flux, substrate temperatures, As_2 fluxes, and Bi surfactant. The bulk of these measurements were taken by in-situ elastic light scattering or ex-situ AFM. These measurements provide experimental support for a non-linear continuum growth model [1] that has been derived analytically from basic atomic level phenomena that occur in epitaxial film growth.

During epitaxial growth the smoothing is observed to change in nature as the surface amplitude decreases. One of the regimes of smoothing is associated with the linear smoothing coefficients from the physically based non-linear continuum growth equation. The temperature and growth rate dependence of the smoothing coefficients are presented and found to be in good agreement with predictions from the continuum growth model. A key parameter in the continuum growth equation, the density of atomic steps, is measured independently using AFM. The step density, which agrees with theoretical predictions, is used to compute smoothing coefficients and is shown to be in agreement with the light scattering measurements.

Complex shapes are observed for epitaxial growth on patterned GaAs substrates. Two characteristic surface morphologies were observed. The first

is characterized by downward V-shaped cusps and rounded mounds caused by non-linear smoothing. The second morphology is similar, however the symmetry of the surface structure was inverted. This surface morphology has not been previously observed in GaAs. Step edge attachment was found to be the driving mechanism that produced both of these morphologies.

Bismuth is observed to act as a surfactant in GaAs homoepitaxy. While Bi assisted growth is found to decrease the overall surface roughness, it is also found to alter the characteristics of the surface morphology. Notably, roughness at low spatial frequency was increased with the addition of Bi, while at high spatial frequency roughness was decreased. Significant changes to the shape evolution of patterned substrate are also observed when Bi is added to GaAs epitaxial growth.

Table of Contents

Appendices

List of Tables

List of Figures

List of Notations

AFM	Atomic Force Microscope
BCF	Burton Cabrera Frank
BEP	Beam Equivalent Pressure
ES	Ehrlich Schwoebel
kMC	kinetic Monte Carlo
KPZ	Kardar Parisi Zhang
MBE	Molecular Beam Epitaxy
ML	Monolayer
PSD	Power Spectral Density
RHEED	Reflection High Energy Electron Diffraction
RMS	Root Mean Square
SIMS	Secondary Ion Mass Spectrometry
STM	Scanning Tunnelling Microscope
UHV	Ultra High Vacuum
XRD	X-ray Diffraction
A,L^2	Surface area (μm^2)
$\bar{A}$	Average surface amplitude (nm)
$\dot{A}$	Step capture efficiency anisotropy
a	Lattice parameter (nm)
β	Dimensionless structure constant
D	Adatom diffusion constant (nm^2/s)

E_{ES}	ES potential barrier (eV)
E_{inc}	Adatom incorporation barrier (eV)
E_{lat}	Lateral binding energy (eV)
E_{sub}	Diffusion activation energy (eV)
η_i	Ion gauge sensitivity coefficient
F, F_{As}, F_{Bi}	Ga, As_2, or Bi flux (ML/s)
$h(\vec{x})$	Local surface height (nm)
I	Optical intensity (W/m^2)
κ	2nd order linear smoothing coefficient (nm^4/s)
λ	Optical wavelength (nm)
λ_2	Non-linear smoothing coefficient (nm^3/s)
ISR	Initial smoothing rate (1/s)
$\hat{m}$	Average number of lateral bonds
N	Number of data points
n	Average adatom density ($1/nm^2$)
ν	Linear smoothing coefficient (nm^2/s)
P	Pressure (Pa)
ϕ_s	Out-of-plane angle of scattered beam
$\vec{q}$	Spatial frequency (μm^{-1})
σ	RMS roughness
S, S_o	Step density (nm/nm^2)
T	Substrate temperature (^{o}C)
θ_i	Angle of incident beam
θ_s	Angle of scattered beam
x	Stable island critical size
$\vec{x}$	Local position (μm)
ζ	ES step edge barrier coefficient

Acknowledgements

I would like to thank my supervisor, Dr. Thomas Tiedje for the opportunity to work in his lab and for his guidance, insight, and advice on research matters. I particularly enjoyed the countless discussions and stories on topics that ranged from science to outdoorsmanship, to history, to travel.

Also, I would like to acknowledge the time and effort spent by the other members of my supervisory committee, Dr. Joerg Rottler, Dr. Lukas Chrostowski, and Dr. Andrea Damascelli.

I wish to thank my colleagues and friends that have helped so much over the years, the people in the MBE lab and AMPEL have made my time at UBC fun and enlightening. First I will acknowledge Dr. Martin Adamcyk, Dr. Sebastien Tixier, and Dr. Jens Schmit, who taught me how to operate, maintain, and get useful results from the lab's group III/V MBE. I thank my fellow MBE growers, Dr. Erin Young, Dr. Nikolaj Zangenberg, Dan Beaton, and Ryan Lewis for helping me grow films and for their perseverance through the long downtimes. I wish to thank Jim MacKenzie for his diligent efforts in maintaining and repairing vital equipment and Dr. Mario Beaudoin for bringing professionalism to the AMPEL cleanroom. I would like to thank Dr. Anders Ballestand for engaging me in numerous discussions on surface physics. Finally I thank my friends and colleagues for their help and support: Miryam Elouneg, Dr. Walter Hardy, Johanna Hansen, Aleksy Jones, Raveen

Kumaran, Dr. Xianfeng Lu, Dr. Wei Li, Kevin Mitchell, Eric Nodwell, Shawn Penson, Mostafa Shirazi, Scott Webster, and Arvin Yazdi.

Especially, I would like to thank my beautiful wife Xin Whitwick and my parents, Daphne and Donald Whitwick for their love and support.

Chapter 1

Introduction

Over the past 30 years advances in compound semiconductors have significantly improved the quality of the civilization that we live in. The development of new semiconducting materials has paved the way for many wondrous devices and technologies. Cellular phones, solid-state lasers, long distance fibre optic communications, precision optical sensors and numerous other applications have changed the very basis of society. Research in this diverse field continues to produce new and novel materials which are incorporated into increasingly smaller devices. A large amount of resources have been applied to the development of optical-electronic devices and materials that are based on group III-V elements [7–9]. In the field of nanoscale compound semiconductor devices there is a need to understand and control the surface and interface structure in a more quantitative way. The complexities involved in the growth of compound semiconductors makes the development of physical based theoretical models difficult.

Additionally, epitaxial crystal growth is an interesting case of atomic self assembly. By definition epitaxy means that atoms deposited from the vapour (or liquid) on the surface of a seed crystal will form a crystalline structure with the same lattice as the original substrate. Studying materials grown epitaxially can yield insights into the numerous and complex atomic scale dynamics that occur on the surface in this unusual physical state. Even for

a narrower field such as the epitaxial growth of group III-V semiconductors there are many interesting phenomenon that are not understood.

This thesis investigates the evolution of the (001) GaAs surface morphology during homoepitaxial growth with molecular beam epitaxy (MBE), and probes the atomic scale mechanisms of this material system. Emphasis is placed on providing the research community with a substantial set of experiments which can be used to compare and test theoretical models of epitaxial growth. Since GaAs substrates are the foundation of many devices there is great interest in predicting the surface morphology over a large range of differing growth conditions. This work seeks to develop a more quantitative description of the surface morphology evolution in semiconductors to learn how to make better devices. To do so, a physically based growth model that accurately predicts the surface morphology over a large set of experimental conditions needs to be developed and tested. For GaAs, numerous models have been developed to describe the observed evolution of the surface shape during growth [1, 3, 10–13]. A general description of GaAs homoepitaxy has been developed but needs better experimental confirmation. Additionally, studying GaAs serves as a basis for the more general problem of group III-V heteroepitaxy. Models are needed for the growth of new alloys that consist primarily of Ga and As atoms such as dilute bismides or nitrides ($GaAs_{1-x}Bi_x$, $GaAs_{1-x}N_x$) [14–16]. A solid well tested model for GaAs homoepitaxy will help this progress.

The growth techniques used to fabricate compound semiconductors such as molecular beam epitaxy or metal-organic chemical vapour deposition are not particularly conducive to in-situ measurements on the surface. The substrate is inaccessible as it is located in a ultra high vacuum (UHV) chamber, typically at high temperatures. Ex-situ measurements are not

surprisingly, more common then in-situ measurements. For example, the surface morphology is typically measured directly with an atomic force microscope (AFM), a scanning tunnelling microscope (STM) or an electron beam imaging technique. However, the dynamics that occur during growth are of particular interest, for which in-situ measurement methods are needed. For MBE, reflection high energy electron diffraction (RHEED) is the most common in-situ observational tool. RHEED can measure the surface reconstruction and even in some cases the density of atomic steps. Reviews of STM and RHEED studies on GaAs can be found in [2, 17]. An in-situ measurement technique which this work focuses on is diffuse light scattering [18]. In this method the surface morphology can be measured from light scattered off the surface roughness in non-specular directions. This allows the surface shape evolution to be monitored throughout the growth.

The (001) GaAs surface morphology has been the subject of many studies. A review of GaAs growth with MBE can be found in [3]. In the case of the (001) GaAs surface grown under typical MBE conditions, the roughness produced by the oxide thermal evaporation is reduced to an atomically flat surface with the deposition of a few hundred nanometers of material [19]. Consistently, in many independent experiments an initially rough or patterned substrate was observed to smooth during GaAs homoepitaxy. Atomically smooth interfaces are normally preferred for electronic and optical devices. Even with these previous studies on GaAs there is not a complete understanding of how the surface evolves during epitaxy.

There is a history of theoretical models for the shape evolution of the (001) GaAs surface during homoepitaxial growth. Unfortunately, early work on the GaAs surface morphology identified the growth as being unstable [20, 21]. Unstable growth implies that atoms diffusing on the surface migrate

uphill in the presence of local surface topography. In this situation mounds would form, leading to the creation of significant roughness on the surface, even if the growth started with an atomically flat surface. Unstable growth is often seen in epitaxy on metals, examples of this can be seen in [22, 23]. However for GaAs, experiments have found that homoepitaxial growth is stable [24–28]. Rough surfaces will smooth to an atomically flat morphology. It is clear that the net atom diffusion is downhill, as valleys and pits fill in during growth. Originally researchers missed the roughening process that occurs when the native GaAs oxide is thermally desorbed from the surface at the start of the growth [29]. It is common practice to remove the native oxide this way in GaAs growth. Without knowing that the GaAs surface had previously roughened, the initially flat surface was observed to form mounds during epitaxial growth. This initial confusion led to a heated debate about the stability of GaAs growth [3].

Models that make predictions on the epitaxial growth of GaAs are typically based on the Burton-Cabrera-Frank (BCF) picture of crystal growth [30]. This solid-on-solid description of the surface is reviewed in Section 2.2. There are two major classes of models that are used for GaAs, atomistic kinetic Monte Carlo (kMC) simulations, and continuum growth equation models. A good review of the various models applied to GaAs can be found in [4]. KMC simulations involve modeling the motion of individual atoms on the surface, using relative binding energies to determine the probability of individual atomic transition events. These models reproduce the experimentally observed phenomenon very well and are an excellent tool for probing atomic scale mechanisms. However, kMC simulations are limited by computational power and cannot reproduce the large scale features and timescales seen in actual MBE growth. On the other hand, the continuum growth

equation approach provides a simple way to describe the time evolution of the surface morphology [31–33]. Although continuum models do not provide atomic scale information as do kMC simulations, continuum growth equations require less computational resources and can mimic typical MBE growth. For GaAs this approach is found experimentally to give a good description of the surface morphology on mesoscopic length scales greater than ∼30 nm, and for small-angle surface topography on the order of a few degrees or less [27, 28]. This work tests a continuum growth equation that has been derived analytically from basic atomic-level phenomena seen in growth of epitaxial films [1].

Surfactants are useful in the growth of compound semiconductor devices and have been found to improve the opto-electrical properties of materials [5, 34, 35] or reduce the inherent surface roughness at the interface [36, 37]. Atoms that wet the surface and do not incorporate into the bulk material during growth are defined as surfactants. The nature of a surfactant depends on the chemistry of the growth system. For group III-V materials bismuth is considered to be an ideal surfactant [38–40]. This is due to the large atomic radii of Bi which prevents it from incorporating into the bulk while binding to the surface. Although these atoms do not incorporate they do have a significant effect on the surface chemistry. This thesis includes a study of the effect of a Bi surfactant on the homoepitaxial growth of GaAs.

This thesis is ordered in the following way: Chapter 2 reviews the physical nature of the (001) GaAs surface and the atomic dynamics on the surface during growth. This chapter also describes the theoretical model of GaAs growth that is used in this work. Additionally, the mathematics that are used to statistically characterize the surface are provided. In Chapter 3 the experimental methods used to obtain the results presented in Chapters 4,

5, and 6 are reviewed. Chapter 4 presents an experimental study of the surface shape evolution for smoothing on randomly rough GaAs substrates and a comparison of these results to a physically based continuum equation model. The chapter focuses on smoothing observed with an in-situ light scattering apparatus. Chapter 5 presents the shape evolution of patterned GaAs substrates during epitaxy. Finally, in-situ and ex-situ observations of GaAs grown with the assistance of the surfactant bismuth are presented in Chapter 6. Smoothing on both patterned and randomly rough surfaces are examined in this chapter. A discussion of the results of Chapters 4, 5, and 6 and the final conclusions are summarized in Chapter 7.

Chapter 2

Theoretical Framework of Nanoscale Surfaces

Quantitative characterization of a surface is a necessity in the complex field of surface physics. Important quantities such as surface shape can be measured directly but statistical characterization is needed to observe finer details. Additionally, physically based models that predict the time evolution of the surface shape are desired. This chapter reviews the current state of knowledge in surface physics with regard to the (001) GaAs surface. The chapter starts by reviewing the crystalline structure of GaAs and the (001) GaAs surface. Then in Section 2.2, a theoretical picture of the atomic scale mechanisms involved in epitaxial growth is presented. This section introduces the continuum growth equation that is used in this thesis. Finally, the mathematics used to statistically characterize the surface in experimental measurements are reviewed.

2.1 Structural Framework of (001) GaAs

Both gallium and arsenic atoms have highly directional covalent bonds. Combined together in a GaAs crystal they form a diamond-like zinc-blend crystal structure as displayed in the upper portion of Figure 2.1. The struc-

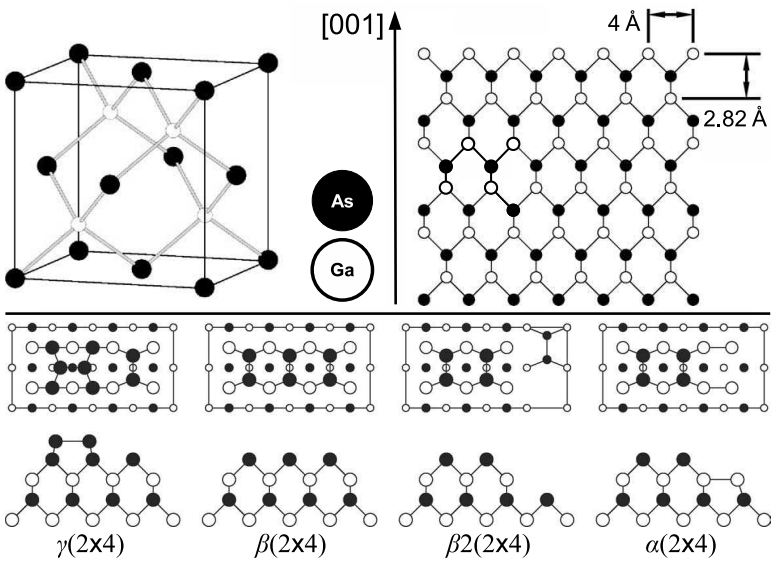

Figure 2.1: Top: a representation of the zinc-blend crystal structure found in bulk GaAs. A there dimensional view is shown on the left and a side view is shown on the right. Bottom: aerial and side views of four of the predicted configurations of the arsenic rich (2×4) surface reconstruction. This figure is reproduced from [2].

ture at the surface interface is more complicated then the bulk lattice. On the surface incorporated atoms will rearrange themselves to an energetically favourable configuration, this rearrangement of atoms is called a surface reconstruction. Predicted configurations of the common As-rich (2×4) reconstruction are illustrated in the bottom half of Figure 2.1. Models and explanations as to how the surface reconstructs vary, but essentially the atoms near the surface shift to minimize the surface free energy caused by the excess of free dangling bonds at the termination of the crystal lattice.

The configuration of a surface reconstruction is dependent on the atomic

bonds of the base element(s) and the temperature of the surface. Surface reconstructions have been measured experimentally with RHEED and STM. It should be noted that experimental techniques do not directly reveal the atomic structure at the surface. Models and simulations (compared to STM or RHEED measurements) are needed to provide fine details of the surface reconstruction. For (001) GaAs surface at MBE growth conditions several maps of the surface reconstruction phase have been produced. Typically the reconstruction phase diagram is plotted as a function of temperature and As_4/Ga flux ratio [41–46]. In these works there are minor inconsistencies between the boundaries of the phases presented in the phase maps. Variations in the techniques used to measure flux and substrate temperature are often the cause of these inconsistencies. Thus these maps are best used as a general guide and not exact measurements.

Despite the complicated nature of the surface, the problem of diffusion on the surface can be simplified. Consider only the effective potential barriers seen by a single Ga atom (or Ga-As molecule) at each atomic site. The Ga atom will see a potential barrier when it diffuses to a new atomic site on a terrace and may see potential barriers when it approaches a step edge from the upper or lower terraces, as exemplified in Figure 2.2. The potentials seen by an Ga adatom can be estimated from STM measurements of the GaAs surface, in conjunction density functional theory calculations of the surface reconstruction [47] and tested with kMC simulations of the GaAs surface evolution.

Surfactants have been observed to alter the (001) GaAs surface reconstruction during MBE growth. For low substrate temperatures (400^oC-500^oC) the arsenic rich (2×4) GaAs surface reconstruction was observed to change to a (3×1) configuration [48] or a (2×1) configuration [49, 50]

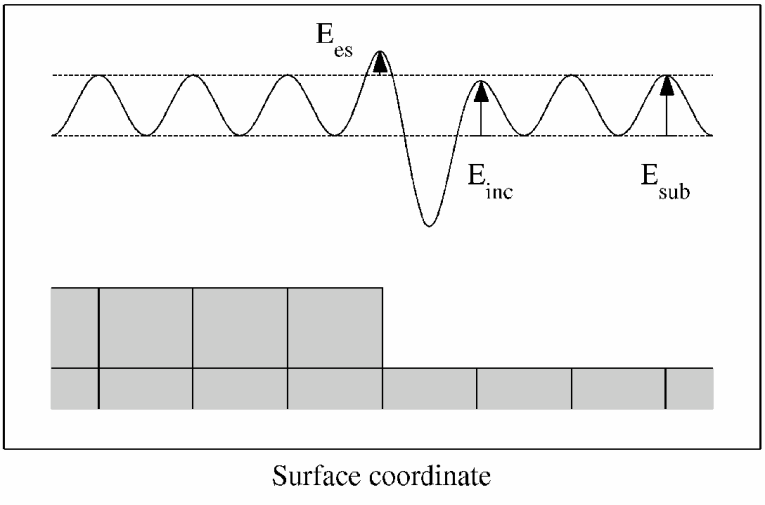

Figure 2.2: The local one-dimensional potential seen by an unincorporated Ga atom on the surface due to the lattice and a step edge. This figure is from [3].

with the addition of bismuth. A surfactant, which sits on top of the surface, is likely to change the effective free energy of the surface. This would lead to a change in the surface reconstruction and a change in the local potential seen by unincorporated atoms on the surface due to the lattice and step edges.

2.2 Continuum Growth Equation Approximation

On an atomic scale, the evolution of the surface morphology that occurs during epitaxial growth can be thought of in terms of the movements on individual atoms. A representation of the atomic dynamics that occur on the surface during epitaxial growth is shown in Figure 2.3. In the Burton-

Cabrera-Frank (BCF) picture of crystal growth adatoms land on an crystalline surface from the vapour and various surface mechanics occur before the adatom is incorporated into the bulk material. After the adatom has dissipated its initial kinetic energy into the lattice it will diffuse on the surface. Diffusing adatoms will eventually encounter a step edge or additional adatom. When two or more adatoms encounter each other on a flat terrace they can nucleate a new island. In typical GaAs epitaxial growth it is more probable that an adatom will encounter an existing step edge. Growth in which all the adatoms attach to the existing step edges with little to no nucleation is called step-flow growth. Typically, step-flow growth is observed on vicinal surfaces. At a step edge an adatom can incorporate into the step edge, hop up or down to another atomic terrace (interlayer transport), or be reflected away from the step edge. The rate at which these events occur will depend on the potential barriers at the step edge which are exemplified in Figure 2.2. For (001) GaAs, the Ehrlich-Schwoebel (ES) step edge barrier seen by an adatom encountering a step edge from an upper terrace is expected to be small and negative [3]. In this case adatoms are more likely to hop down to the lower terrace and the net flux of adatoms is downhill. Note that a large incorporation barrier seen by an adatom encountering a step edge from the lower terrace would have the same effect as a negative ES barrier [51]. Reverse processes are also thermodynamically possible and adatoms may be released from the terraces or desorbed into the vapour.

The epitaxial growth of GaAs is complicated by the two components (Ga and As) involved in the surface chemistry. Examples of two component models for GaAs have been suggested in [10, 52]. However, the atomic dynamics of arsenic are often ignored. Under normal MBE conditions the growth of GaAs is limited by the gallium flux. Arsenic is supplied to the

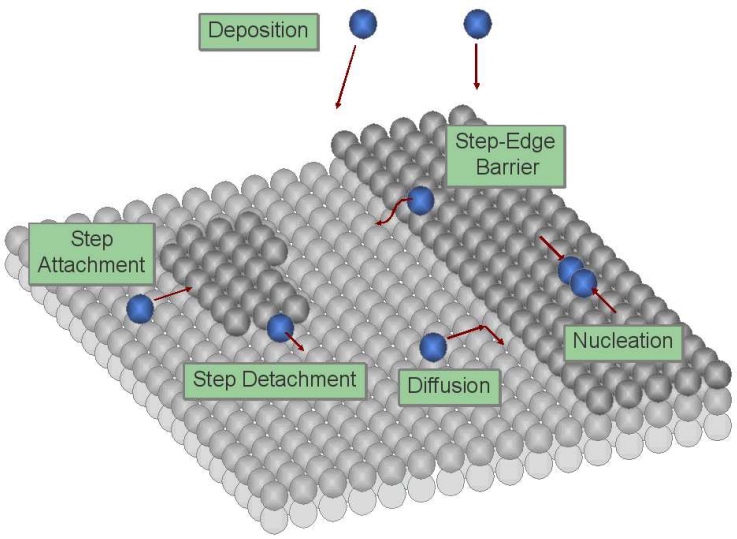

Figure 2.3: A schematic of the atomic dynamics that occur on the surface during epitaxial growth. This figure was taken from by A. Ballestad [4].

surface well in excess of the gallium, typically the As_2/Ga ratio is between 6 and 20. Also, gallium evaporation events are improbable, unlike excess arsenic which is volatile by comparison. Thus, it is reasonable to treat the two component GaAs system as a one component system dominated by a gallium single 'adatom'. The binding energies of this Ga 'adatom' are scaled to account for the arsenic dynamics.

The study of complex systems such as group III/V semiconductors presents a difficult challenge. An atomic scale picture is difficult to compare to macroscale experimentally measured physical quantities. Atomistic models such as kMC simulations require extensive computational resources and cannot effectively reproduce macroscale features. An alternative to direct atomistic models is the continuum growth equation approach, which de-

scribes the surface with continuous ordinary differential equations [4, 31–33]. This approximation assumes that the surface is a continuous function with no discrete steps or spacings. A general continuum equation describing the time evolution of the surface height, $h(\vec{x}, t)$ is [53]:

$$\partial_t h \propto \nabla^2 h + \nabla^4 h + (\nabla h)^2 + \nabla^2(\nabla h)^2 + \nabla(\nabla h)^3 + \ldots + F \tag{2.1}$$

where F is the flux of adatoms from the vapour. In this thesis F has units of monolayers per second (ML/s). Terms that are proportional to h, such as $\nabla^2 h$ or $\nabla^4 h$, are call linear terms, while terms that are proportional to h^2 (eg $(\nabla h)^2$ or $\nabla^2(\nabla h)^2$) are call non-linear terms. Two common continuum equations used to describe GaAs homoepitaxy are the Kardar-Parisi-Zhang (KPZ) equation [54, 55]:

$$\partial_t h = aF + \nu\nabla^2 h + \frac{\lambda_1}{2}(\nabla h)^2 \tag{2.2}$$

and the MBE equation [56]:

$$\partial_t h = aF - \kappa\nabla^4 h - \lambda_2\nabla^2(\nabla h)^2 \tag{2.3}$$

where ν, κ, λ_1 and λ_2 are growth parameters of Equations 2.2 and 2.3, and a is the lattice parameter. Both the KPZ and MBE equations have been used to model the GaAs surface during epitaxial growth and are found to agree with AFM measurements of the surface morphology [26, 27]. In these works, continuum growth equations were numerically solved to simulate the surface morphology of GaAs from the same starting surface that is seen at the start of epitaxial growth (measured with AFM). Features in the surface morphology generated by these simulations were compared to features observed on GaAs samples grown with MBE under equivalent conditions. Though, numerical solutions to both Equations 2.2 and 2.3 reproduce experimentally observed features of the GaAs surface, neither of these equations

have a solid basis in the fundamental physics of the GaAs surface. They are commonly used empirical fits to experimental observations, since the physical significance of the growth parameters are not obvious in these equation. Additionally, the KPZ equation does not conserve the mass of incoming molecules, i.e. the growth rate of the KPZ equation depends on the surface shape and not the flux of incoming atoms as is the case in GaAs growth.

A physically based non-linear continuum equation has been developed [1] which is derived from the adatom transport equation in a BCF crystal growth picture. This equation is:

$$\partial_t h = aF + \nu\nabla^2 h - \lambda_2\nabla^2(\nabla h)^2 \tag{2.4}$$

where the growth coefficients, ν and λ_2 are derived from first principles and can be expressed in terms of physical quantities:

$$\nu = \frac{\zeta a F}{S_o} \tag{2.5}$$

$$\lambda_2 = \frac{F}{\beta a S_o^4} \tag{2.6}$$

where ζ is the ES step edge coefficient that is based on the interaction of an adatom with a step edge, β is a dimensionless structure constant, and S_o is the average atomic step density. In this model the step density of sloped surfaces is assumed to depend on surface slope as follows:

$$S = \sqrt{S_o^2 + (\nabla h/a)^2} \tag{2.7}$$

Equation 2.4 has the form of a conservative KPZ equation [54], which has been used to simulate GaAs growth which agree qualitatively with AFM measurements of experimentally grown films [27, 57]. However, Equation 2.4 differs from the conservative KPZ equation as the smoothing coefficients, ν

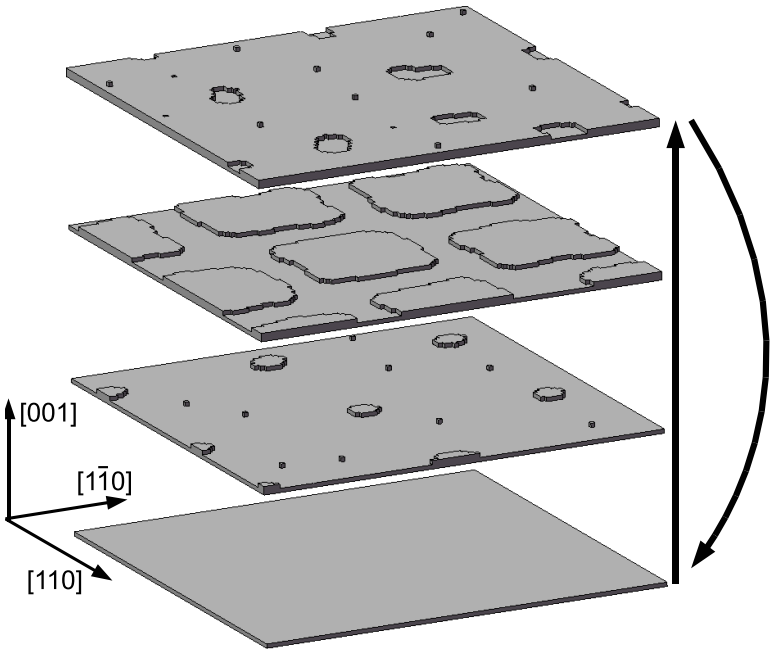

Figure 2.4: A representation of layer filling for a single monolayer during growth nucleation dominated growth.

and λ_2, depend on physical parameters such as the growth rate or step density.

During epitaxial growth the atomic step density can be determined by considering an equilibrium between two competing rates: the rate of filling of the terraces and the nucleation rate of new islands [32]. For growth on a atomically flat surface, new islands must be nucleated on the surface every monolayer of growth or else the growth is unstable. These new islands will serve as adatom sinks and the new monolayer will fill until the surface is flat again, in which more new islands will need to be nucleated. Figure 2.4 shows a pictorial description of this process. The rate of adatom nucleation

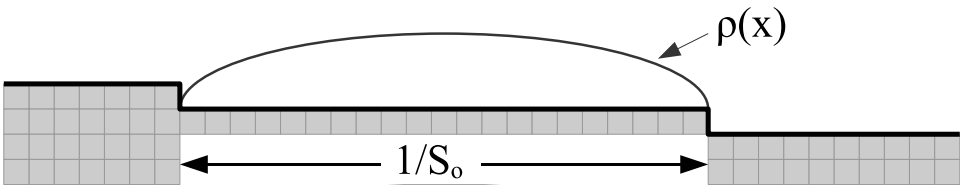

Figure 2.5: The adatom density on a one-dimensional terrace of length $1/S_o$. In this picture adatoms that encounter a step edge are incorporation into the bulk material.

is balanced by the rate of monolayer filling [32]:

$$n^{x+1}a^{2x-2}D = FS_o^2 \tag{2.8}$$

where n is the average adatom density, D is the adatom diffusion constant, and x is the number of adatoms needed to form a stable island on the surface called the critical island size. For example a stable island of 4 atoms would have a critical island size of 3.

Now consider the adatom density on a single one dimensional terrace of length S_o^{-1} as shown in Figure 2.5. In this picture, assume that the uphill and downhill steps act as adatom sinks and the flux of incoming atoms act as an uniform source. The local adatom density will be zero at the steps. The local adatom density can be determined by solving the steady-state adatom diffusion equation ($\partial_t n = 0 = D\nabla^2 n + F/a^2$) with the boundary conditions of $n = 0$ at the position of 0 and S_o^{-1}. Thus the average adatom density can be determined:

$$n = \frac{F}{a^2 \beta D S_o^2} \tag{2.9}$$

where β is a dimensionless structure constant, for straight parallel step $\beta = 12$. By combining Equations 2.8 and 2.9 an atomic mechanism depen-

dent form of the atomic step density can be written as:

$$S_o = \left[\frac{1}{\beta^{x+1}a^4}\left[\frac{F}{D}\right]^x\right]^{\frac{1}{2x+4}} \tag{2.10}$$

Using Equation 2.10 with Equations 2.5 and 2.6 yields growth equation coefficients that are dependent on physical quantities such as the Ga flux and the substrate temperature (through D and ζ) and atomic scale parameters such as the critical island size:

$$\nu = a^{\frac{x+4}{x+2}}\beta^{\frac{x+1}{2x+4}}\zeta F^{\frac{x+4}{2x+4}}D^{\frac{x}{2x+4}} \tag{2.11}$$

$$\lambda_2 = a^{\frac{6-x}{x+2}}\beta^{\frac{x}{x+2}}F^{\frac{2-x}{x+2}}D^{\frac{2x}{x+2}} \tag{2.12}$$

Both the diffusion constant, D and the ES step edge coefficient, ζ, are dependent on substrate temperature. The temperature dependent form of the ES step edge coefficient is [3]:

$$\zeta = \frac{1}{2}\left[\frac{1}{e^{-(E_{inc}-E_{sub})/k_BT}} - \frac{1}{e^{-E_{ES}/k_BT}}\right] \tag{2.13}$$

where E_{ES} is the Ehrlich-Schwoebel step edge barrier and E_{inc} is the adatom incorporation barrier at a step edge, as shown in Figure 2.2. The diffusion constant has the form:

$$D = a^2 w_o e^{-\frac{E_{sub}}{k_BT}} \tag{2.14}$$

where w_o is the attempt frequency and E_{sub} is the energy needed to overcome in order to move to a nearby lattice site, as shown in Figure 2.2. This activation energy has been measured by RHEED to be between 1.5 eV and 2.0 eV [58–60]. The attempt frequency, $w_o = \frac{2k_BT}{h}$ is dependent on temperature as determined from the theory of chemical reactions [61].

Now consider a surfactant atom such as Bi on the surface. The surfactant atom has a large atomic radius which prevents incorporation. As with any

atom on the surface the most favourable location for the surfactant to sit is on the lower terrace of an atomic step edge. This will have a profound effect on the step edge barriers shown in Figure 2.2 and the ES step edge coefficient in Equation 2.13. Gallium adatoms approaching this step edge from the lower terrace will likely see a large repulsive incorporation barrier, since a large bismuth atom sits in the way. Adatoms approaching the step edge from the upper terrace may see a different ES step edge barrier when a Bi atom is located on the lower terrace of the step edge, however the change in the incorporation barrier is expected to be more significant. The addition of a large repulsive incorporation barrier would reflect Ga adatoms away from the upper step edge increasing downhill flow. This would change the boundary conditions used to determine Equation 2.9 since the upper step edge no longer acts as a perfect sink. Surfactant atoms also could change Ga adatom diffusion in the atomic terraces (Equation 2.14), since nearby Bi atoms could assist Ga atoms when they move to new atomic sites. The atomic step density in Equation 2.10 would be changed by Bi surfactant since it depends on the diffusion constant and is derived from Equation 2.9.

2.3 Surface Statistical Characterization

2.3.1 Power Spectral Density and RMS-roughness

The following section presents details of the mathematics and statistics used in this work for the characterization and analysis of the physical surface morphology. There are several experimental methods capable of a direct and accurate measurement of surfaces to nanometer precision, such as the atomic force microscope and diffuse light scattering as used in this work. A human's image recognition, although quite adept, is limited in quantitative

analytical ability. Thus some sort of statistical approach is required.

The Power Spectral Density (PSD) is an useful method to characterize a surface in a statistical way. Consider a surface image of area A, and a local height, $h(\vec{x})$. Then the two-dimensional PSD is defined as [62]:

$$PSD_{2d}(\vec{q}) = \frac{1}{(2\pi)^2 A}\left|\int_A h(\vec{x})e^{-i\vec{q}\cdot\vec{x}}d^2\vec{x}\right|^2 \tag{2.15}$$

where $\vec{q}$ is the spatial frequency. The discrete nature of digital images will lead to the discretization of $\vec{q}$. Consider an image of area, $A = L \times L$ measured over an $N \times N$ grid. This results in an upper and lower limit on the spatial frequency; $|\vec{q}|_{min} = 2\pi/\mathrm{L}$ and $|\vec{q}|_{max} = 2\pi\mathrm{N/L}$. The spatial frequency will range between $|\vec{q}|_{min}$ and $|\vec{q}|_{max}$ in integer multiples of $|\vec{q}|_{min}$. The PSD and $\vec{q}$ are real quantities since they are derived from the real quantities of A, N, and $h(\vec{x})$ having units of nm^4 and $\mu\mathrm{m}^{-1}$ respectively. Additionally since $h(\vec{x})$ is real, the PSD will be symmetric: PSD($\vec{q}$) = PSD(-$\vec{q}$).

The Root Mean Square (RMS) roughness, σ, is another useful quantity used in this work, defined by:

$$\sigma^2 = \frac{1}{A}\int_A h(\vec{x})^2 d^2\vec{x} = \int_{q_x}\int_{q_y} PSD(\vec{q})d^2\vec{q} \tag{2.16}$$

The RMS roughness is perhaps the most used and important surface quantity in terms of the growth of material or structures.

2.3.2 Diffuse Optical Scattering

For a MBE system, physical contact with a growing film is limited. A UHV system is needed to protect the sample from contamination and the sample needs to be free to move and rotate within this vacuum chamber. Optical observation of the surface is an excellent non-invasive way to see the substrate in-situ. For this work, diffuse light scattered from the surface

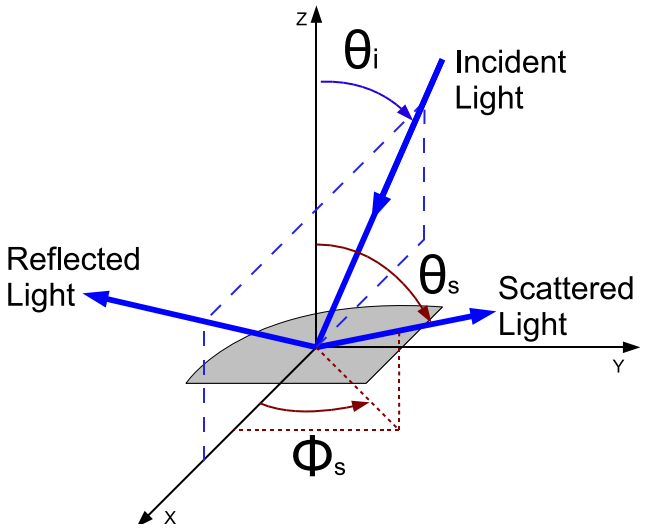

Figure 2.6: Configuration of the incident, reflected and scattered beams with respect to the surface normal of the substrate in the light scattering setup.

roughness of a GaAs substrate is used to monitor the process of epitaxial growth. This section describes the mathematical relationship between the surface roughness and the diffusely scattered light intensity.

Light scattered at non-specular angles from a rough surface will depend on the surface morphology of that surface [18]. Consider the geometric arrangement of the incident optical beam, the reflected optical beam, a beam of scattered non-specular light and the substrate as presented in Figure 2.6. The angular distribution of the scattered light intensity is given by:

$$\frac{dP}{P_o d\Omega} = \frac{16\pi^2}{\lambda^4} \cos\theta_i \cos^2\theta_s Q(\theta_i, \theta_s, \phi_s) PSD_{2D}(\vec{q}) \tag{2.17}$$

where dP is the fractional power measured in solid angle $d\Omega$, and P_o is the initial power of the light incident on the surface. λ is the optical wavelength

and θ_i, θ_s and ϕ_s are the angles of the incident beam and detected scattered light as shown in Figure 2.6. $PSD_{2D}(\vec{q})$ is the power spectral density as defined by Equation 2.15 at the spatial frequency $\vec{q}$. For light scattered off a rough surface the spatial frequency represents the momentum transfer that must occur on the surface. Thus $\vec{q}$ is determined by the angles and wavelength:

$$\vec{q} = \frac{2\pi}{\lambda}(\sin\theta_i - \sin\theta_s\cos\phi_s)\hat{x} + \frac{2\pi}{\lambda}(\sin\theta_s\sin\phi_s)\hat{y} \tag{2.18}$$

The polarization factor, $Q(\theta_i, \theta_s, \phi_s)$ accounts for polarization dependent reflections from the surface [63]. For unpolarized light scattered off a surface with a complex dielectric constant, ϵ, the polarization factor is:

$$Q = \frac{1}{2}(Q_{ss} + Q_{pp} + Q_{sp} + Q_{ps}) \tag{2.19}$$

where Q_{yz} are directional components of the polarization factor with y and z denoting s or p. Notation in the y position denotes the polarization of the optical source and the z position denotes the polarization sensitivity of detector measuring the reflected light. The notation of s indicates that the electric field vector of the electromagnetic wave of the incident laser beam is parallel to the surface and p indicates that the electric field vector is parallel to the plane of incidence. The directional components can be found in [63]:

$$Q_{ss} = \frac{(\epsilon-1)\cos(\phi_s)}{(\cos(\theta_i) + \sqrt{\epsilon - \sin^2\theta_i})(\cos\theta_s + \sqrt{\epsilon - \sin^2\theta_s})} \tag{2.20}$$

$$Q_{sp} = \frac{(\epsilon-1)\sqrt{\epsilon - \sin^2\theta_s}\sin\phi_s}{(\cos(\theta_i) + \sqrt{\epsilon - \sin^2\theta_i})(\epsilon\cos\theta_s + \sqrt{\epsilon - \sin^2\theta_s})}$$

$$Q_{ps} = \frac{(\epsilon-1)\sqrt{\epsilon - \sin^2\theta_s}\sin\phi_s}{(\epsilon\cos(\theta_i) + \sqrt{\epsilon - \sin^2\theta_i})(\cos\theta_s + \sqrt{\epsilon - \sin^2\theta_s})}$$

$$Q_{pp} = \frac{(\epsilon-1)(\sqrt{\epsilon - \sin^2\theta_s}\sqrt{\epsilon - \sin^2\theta_i}\cos\phi_s - \epsilon\sin\theta_i\sin\theta_s)}{(\epsilon\cos(\theta_i) + \sqrt{\epsilon - \sin^2\theta_i})(\epsilon\cos\theta_s + \sqrt{\epsilon - \sin^2\theta_s})}$$

The dielectric constant, ϵ for (001) GaAs at the wavelengths used in this thesis can be found in [64].

Optical light scattering has been used on the (001) GaAs system before. Earlier work by Lavoie [65] attempted to measure the shape evolution during growth, but the smoothing and roughening observed was not completely understood. For GaAs growth by MBE it has been established that the observed light scattering signal is due to the surface roughness and not particles on the surface as demonstrated by Pinnington's work on the InGaAs/GaAs system [66, 67].

Chapter 3

Experimental Methods

This chapter describes the experimental methods, sample characterization and computational techniques used to obtain the results presented in the following chapters of this work. To start, the molecular beam epitaxy technique of growing crystalline structures and related equipment will be discussed. Then the in-situ light scattering apparatus constructed on the MBE will be presented and the interpretation of the resulting light scattering data will be discussed. Then the lithographic processes used to manufacture periodic structures in GaAs and the surface preparation of samples will be presented. Details of the atomic force microscope (AFM) measurements of GaAs and the practical calculation of PSD and step densities from these images are then discussed.

3.1 Molecular Beam Epitaxy

The homoepitaxial growth of GaAs was done in a VG V80H MBE reactor equipped with gallium and bismuth Knudsen effusion cells, and an As_2 dual zone gas cracker source. The system is equipped with a RHEED gun and screen and a residual gas analyzer. The MBE growth chamber is attached to a UHV sample preparation chamber which is attached to a HV load lock. The growth chamber is pumped with ion, titanium sublimation and cryo

pumps and contains a liquid nitrogen cooled (77 K) shroud. The chamber pressure is measured with an ion gauge, and the base pressure of the growth chamber is measured to be 1-3$\times 10^{-8}$ Pa after baking the MBE at 180^{o}C for 2-3 days.

Fluxes from the molecular sources are measured with an ion gauge moved into the beam path. These flux measurements are calibrated by measuring layer thicknesses of multilayered films with high resolution X-ray diffraction. The thickness is determined by fitting to the Pendellosung interference fringes that are seen in X-ray diffraction from thin films [68]. For calibration samples a simple structure is grown with the material of interest capping a contrasting material. The growth rate of GaAs is determined by the Ga flux. Relative fluxes of different materials can be compared by [69]:

$$\frac{F_i}{F_j} = \frac{P_i \eta_j}{P_j \eta_i} \left[\frac{T_i m_j}{T_j m_i}\right]^{\frac{1}{2}} \tag{3.1}$$

where i and j denote different materials, F_i is the flux, P_i represents the beam pressure measured with an ion gauge, T_i is the absolute temperature of the molecular source, m_i is the molecular mass of the material, and η_i is the ion gauge sensitivity coefficient. For simple molecules, η_i can be approximated as [70]:

$$\eta_i = \frac{0.6 Z_i}{14} + 0.4 \tag{3.2}$$

where Z_i is the number of electrons in a molecule from source i. From Equation 3.2, η_{Ga} is 1.74 and η_{Bi} is 3.96. From measurements on a quartz crystal monitor by [69], η_{As_2} is 4.0 and for comparison η_{As_4} is 6.8. In this thesis, fluxes are given in units of monolayers per second (ML/s). For As_2 and Bi fluxes these units refer to the amount of incoming material (per second) in relation to the Ga Flux.

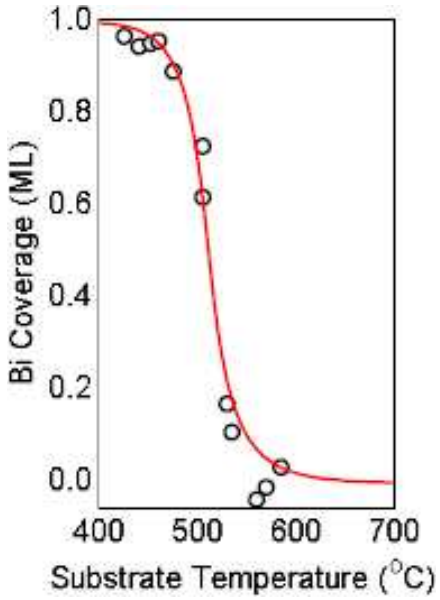

Figure 3.1: The surface coverage of Bi on a (001) GaAs surface at various temperatures. The data points were measured by examining the surface reconstruction change from (2x4) to (1x2) with RHEED. This figure is reproduced from Young at al. [5].

For this work, the Ga flux ranged between 0.01-6 ML/s, with an As_2 overpressure from 8-16 ML/s and the Bi flux ranged from 0.01-4 ML/s if applied. The amount of As_2 and Bi on the surface depends on the substrate temperature since surface desorption is probable for these atoms on GaAs at the temperature used. The Bi coverage on GaAs is shown in Figure 3.1 as a function of temperature for a Bi flux of 1.9×10^{-3}Pa. Unless otherwise stated, GaAs samples used in this work were grown with the following conditions: a substrate temperature of 590^oC, a Ga flux of 1 ML/s, and an As_2 flux of 8 ML/s.

The GaAs wafers used were either mechanical or epi-grade and had a polished (001) surface oriented on-axis ($\pm 0.5^o$) with a light (rough surface) textured back surface. Before growth, GaAs substrates were outgassed at $\sim 200^o$C for over one hour in a isolated preparation chamber to remove H_2O attached to the substrate. The substrate temperature was measured with optical bandgap thermometry [71, 72]. For GaAs growths the substrate temperature ranged from 400 to 610^oC.

The native oxide on GaAs can be removed in a number of ways: by an atomic hydrogen etch [73, 74], with successive gallium monolayer depositions and thermal cycles [75, 76], or by thermally desorbing the oxide [77]. The thermal desorption method was used to create the starting surface for the in-situ smoothing measurements, and the hydrogen etched surface was used for step density measurements and the grating regrowth experiments.

For the thermal oxide desorption the substrate was rapidly brought to $\sim 610^o$C and held at this temperature for over ten minutes. The oxide desorbs in two steps, the first occurs around 400^oC when the arsenic oxide evaporates in a layer-by-layer fashion. An As_2 overpressure is maintained during the time that GaAs substrates are at a temperature higher than 300^oC to prevent loss of bulk As. When the substrate is heated to 600^oC the native gallium oxide evaporates explosively from the surface. This results in a significant roughening of the surface (RMS roughness $\sim$5 nm). Random pits are created on the surface when the oxide is removed this method, typically the pits are about 400 nm in diameter, 30 nm deep and 1 μm apart [29]. The explosive surface reaction could be caused by volatile Ga_2O breaking through a capping layer of stable Ga_2O_3 [3]. An example GaAs surface with the native oxide thermally desorbed is shown in Figure 3.2. The thermally desorbed surface is used as a starting surface to observe smoothing

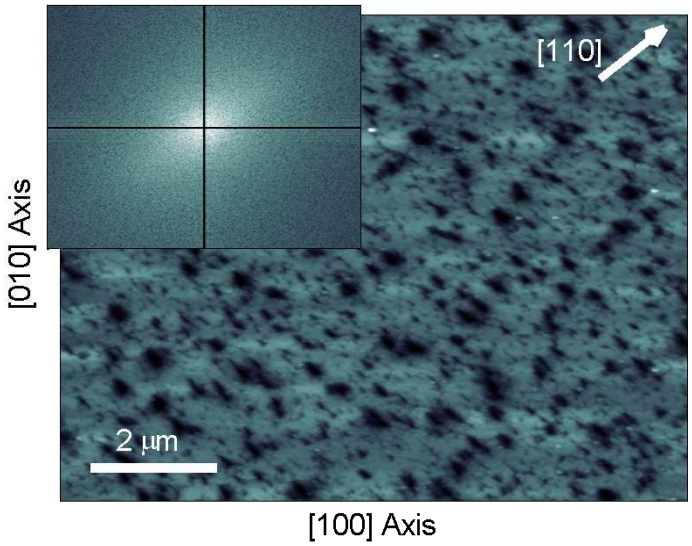

Figure 3.2: A 10 μm^2 AFM image of a (001) GaAs surface after the native oxide is thermally desorbed. The insert is the two-dimensional PSD calculated from this surface on a log scale. This image has a vertical scale of 22.1 nm and a RMS roughness of 4.9 nm.

(or roughening) with the light scattering apparatus.

Etching with atomic hydrogen was used to remove the oxide on samples that are used for the step density or grating regrowth experiments. Atomic hydrogen is supplied to the growth chamber through a cracker source (at a filament temperature of 1650^{o}C) directed at the substrate. H_2 gas is supplied to the cracker through an independent gas line UHV system. The H_2 pressure is controlled by a precision leak valve and monitored with the growth chamber ion gauge. The typical H_2 background pressure in the chamber was 4×10^{-4} Pa. During the hydrogen etch an As_2 overpressure of 5.3-9.3$\times10^{-5}$ Pa was applied and the substrate was held at 350^{o}C. The

hydrogen etch lasted 20 minutes to ensure that the oxide was completely removed. The atomic hydrogen etch method of removing the oxide yields a mirror-like surface with RMS roughness of ∼0.3 nm [19].

Before growth all substrates are baked at 200^{o}C in a preparation chamber to remove absorbed water that results from exposure to air. Unless stated, no additional cleaning procedure was used beyond that of the initial manufacturer's process (AXT or Wafer Technology wafers). The light scattering apparatus is highly sensitive to the impurities on the surface and will roughen to visible levels if the sample is unclean and thus provides an excellent gauge of the cleanliness of a surface.

Samples were often rapidly quenched at the end of the growth in order to freeze the surface. The initial rate of cooling is ∼50^{o}C/min as measured with optical bandgap thermometry. For this work, samples that were quenched first had the Ga flux shuttered, then the substrate heater power was shut off, and then the As_2 flux was valved off as fast the equipment allowed (∼1 min). Note that excess arsenic remains in the chamber at sufficient levels to ensure that the sample does not lose arsenic while it remains briefly above 400^{o}C. Samples prepared for AFM imaging were quenched at the end of growth.

3.2 Lithography and Sample Preparation

For this work, 3 μm line gratings were fabricated for the purpose of exploring the shape evolution of GaAs during growth using lithographic techniques adapted from [11, 78, 79]. The fabrication of gratings consisted of the creation of a photoresist mask and the etching of a pattern into GaAs which are outlined in Tables 3.1 and 3.2 respectively. Both the etching and photolithography were done in a class 1000 cleanroom and epi-ready chemicals

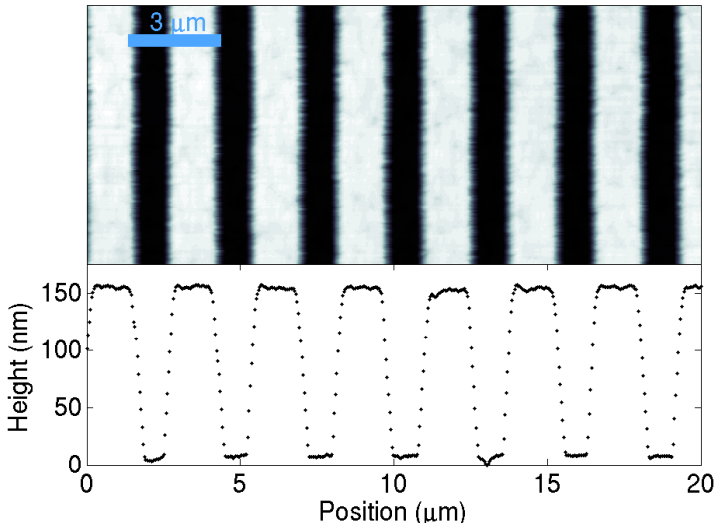

Figure 3.3: An AFM image of a line grating in GaAs used as a starting surface for regrowth experiments.

were used to ensure the quality of the sample. The photoresist layer is typically 1 μm thick and a Karl Suss MJ-3 aligner was used for the exposure. Ultrasonically agitated acetone was found to completely remove the photoresist. Figure 3.3 shows an example of a line grating in GaAs fabricated for this work.

The etching processes detailed in Table 3.2 were also used to clean GaAs wafers. Typically the line gratings were etched 150 nm deep. The initial part of GaAs growth is highly sensitive to surface impurities and contact even with epi-ready liquids had a noticeable effect. It was found that samples cleaned with the procedure in Table 3.2 showed little to no signs of surface impurities.

1	Spin on AZ4110 photoresist at 8300 rpm for 60 sec
2	Bake at 100^oC for 10 minutes
3	Align contact mask to sample
4	Expose to 254 nm light at 100 W/cm^2 for 30 sec
5	Develop photoresist with $3H_2O$:AZ400K ($\sim$2 min)
6	Rinse with DI H_2O, dry with N_2

Table 3.1: Recipe for patterning photoresist on GaAs.

1	Etch in $2H_2SO_4$:$2H_2O_2$:$75H_2O$ for $\sim$1 min per 200 nm
2	Remove photoresist in ultrasonically agitated acetone
3	Clean with acetone, methanol, then isopropanol. Dry with N_2
4	Etch in $2H_2SO_4$:$2H_2O_2$:$75H_2O$ for 1 sec.
5	Expose to UV generated ozone for 10 min
6	Dip in conc. H_2SO_4 for 30 sec.

Table 3.2: Recipe for etching and cleaning GaAs.

3.3 In-Situ Light Scattering

As discussed in Section 2.3.2 the surface structure can be observed from light scattered in non-specular directions. For this thesis a light scattering apparatus was designed and constructed on the growth chamber of the MBE, in order to examine the surface structure during epitaxial growth. The configuration of this apparatus is shown in Figures 3.4 and 3.7.

The light scattering apparatus is limited by the positions of the available optical ports. In terms of the sample's PSD (as exemplified in the insert of Figure 3.2) the light scattering apparatus is sensitive to the PSD at a

λ (nm)	θ_i (deg)	θ_s (deg)	ϕ_s (deg)	$\lvert\vec{q}\rvert$ (μm^{-1})
632.8	55	-25	0	12.3
514.5	55	-25	0	15.2
457.9	55	-25	0	17.0
244.0	55	-25	0	32.0
244.0	55	-65	22.5	43.5

Table 3.3: List of the viewport configurations available and the resulting spatial frequencies. $|\vec{q}|$ is calculated from Equation 2.18.

specific spatial frequency. The angles of optical ports and the wavelength used determine this spatial frequency, which can be calculated from Equation 2.18. Figure 3.6 shows how the PSD, as measured by ex-situ AFM of GaAs surface evolves over time during a typical growth. During the growth GaAs, the surface is subject to random non-conservative noise cause by the random deposition of atoms from the molecular sources. This random non-conservative noise will cause some inherent roughness on the surface, in the PSD this roughness will be of the form $PSD = F/\nu q^2$ [27, 32]. A rough surface, such as one produced by thermally desorbing the native GaAs oxide shown in Figure 3.2, will smooth over time until the PSD saturates to the roughness caused by the random deposition of atoms. The in-situ light scattering apparatus observes the PSD at a single spatial frequency as indicated by the vertical dashed line. A summary of the MBE growth chamber ports and the resulting spatial frequencies is given in Table 3.3.

Three separate light sources were used in this work. The most frequently used light source was a beam of coherent UV light of wavelength 244.0 nm. The UV light was generated by frequency doubling 488.0 nm light from a 2 W

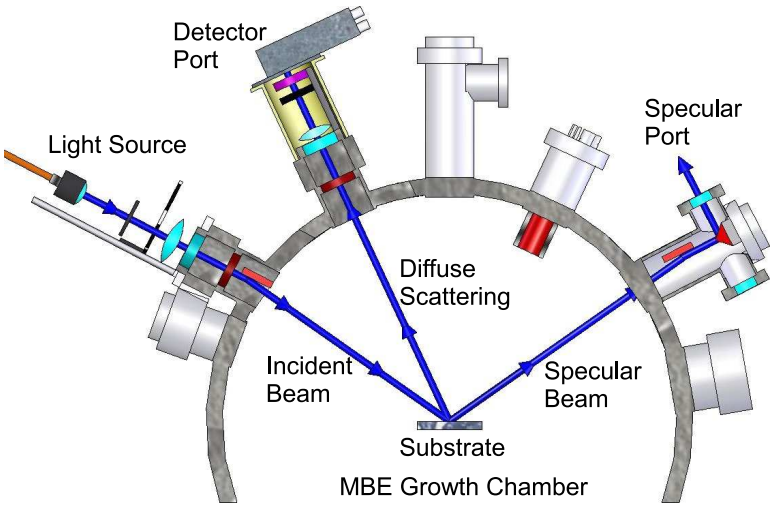

Figure 3.4: Schematic of the in-situ light scattering apparatus on the MBE growth chamber. The laser sources are isolated from the MBE system and connected through a 16 m fibre optic cable.

Spectra Physics Argon Ion laser which contained a Beamlok Etalon for increased stability. The frequency doubler was a Spectra Wavetrain equipped with a LBO non-linear optical crystal. This setup, shown in Figure 3.5 was capable of generating 15-100 mW of UV light. Typically 40 mW was used. The optical beam was coupled to a 10 m UV transmitting fibre optic cable that was attached to an optical port on the MBE growth chamber, as shown in Figure 3.4. Losses for UV light transmitted through the optical fibre are large (0.35 dB/m), and this light source had 2 mW incident on the GaAs sample. Optical power is not an issue with the light scattering apparatus. The main experimental limitation in the light scattering experiment is the ratio of the signal to the background due to scattering inside the chamber.

The second light source used was a tunable Ar ion laser with optics

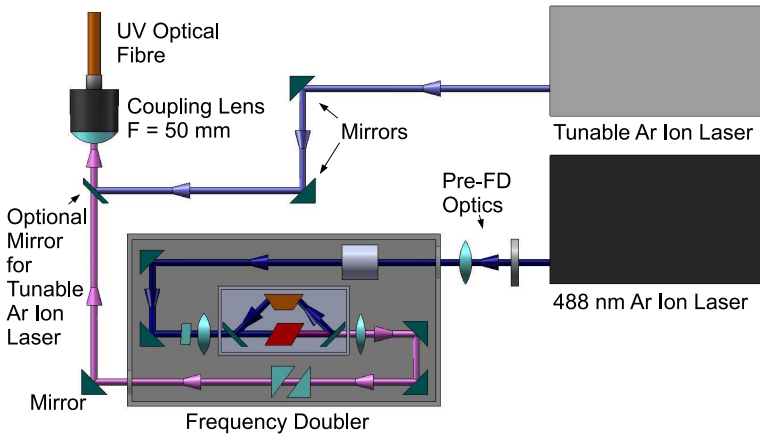

Figure 3.5: Optical light sources used in the light scattering apparatus.

for the laser lines of 457.9 nm, 465.8 nm, 476.5 nm, 488.0 nm, 496.5 nm, 501.7 nm, and 514.5 nm. The 457.9 nm laser line was typically used. The laser beam was coupled to the optical fibre used for the UV source, as shown in Figure 3.5. For visible light the absorption in the fibre cable is less and the power incident to the sample is greater, typically ∼30 mW. The third light source used was a He-Ne laser (632.8 nm) that was mounted directly on a MBE optical viewport.

Figure 3.7 shows the optical assembly that prepared light from the optical fibre cable. For the UV light a collimating lens (focal length 10 mm) was mounted on the optical fibre cable, which focuses the beam to a circular spot (radius ∼2 mm) on the sample. For visible light from the tunable Ar source an additional lens (f=451 mm) was placed near the optical viewport to compensate for the fact that the UV optical fibre and related optics are designed for UV light. The spot size on the sample was larger (radius ∼2.3 mm) for

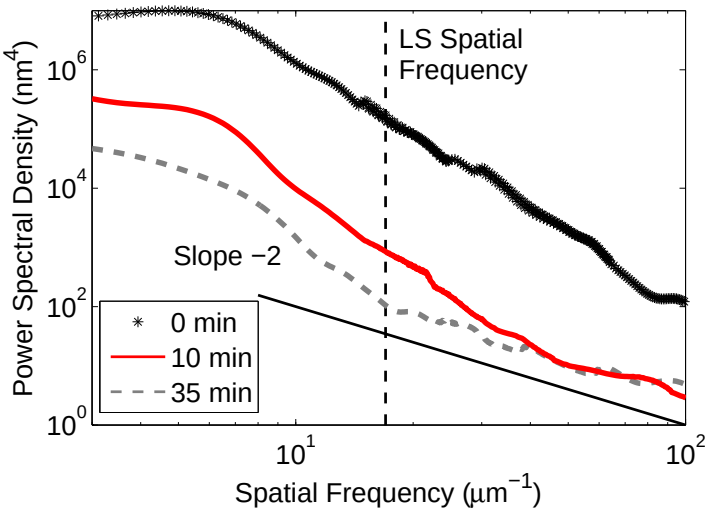

Figure 3.6: 1D PSD along the $[1\bar{1}0]$ crystalline axis of the GaAs surfaces at various times during growth, determined from AFM images with the method discussed in Sectionsec:AFMExp. This GaAs sample was grown at 1.1 ML/s and a temperature of 590^{o}C.

the visible light. An iris aperture was placed around the optical beam to reduce stray light scattered from the cladding layer in the optical fibre. An optical chopper was placed in the beam path so that detected scattered light can be distinguished from background sources. The optical chopper was connected to a SR810 or SR510 lock-in amplifier. The optical viewport had UV enhanced quartz windows and were heated to ∼300^{o}C in order to prevent arsenic from accumulating during growth. The UV light was found to increase the deposition of arsenic on the windows.

The detector assembly that measures light scattered from the sample is shown in Figure 3.7. A collecting lens (f=50 mm) is placed near the optical

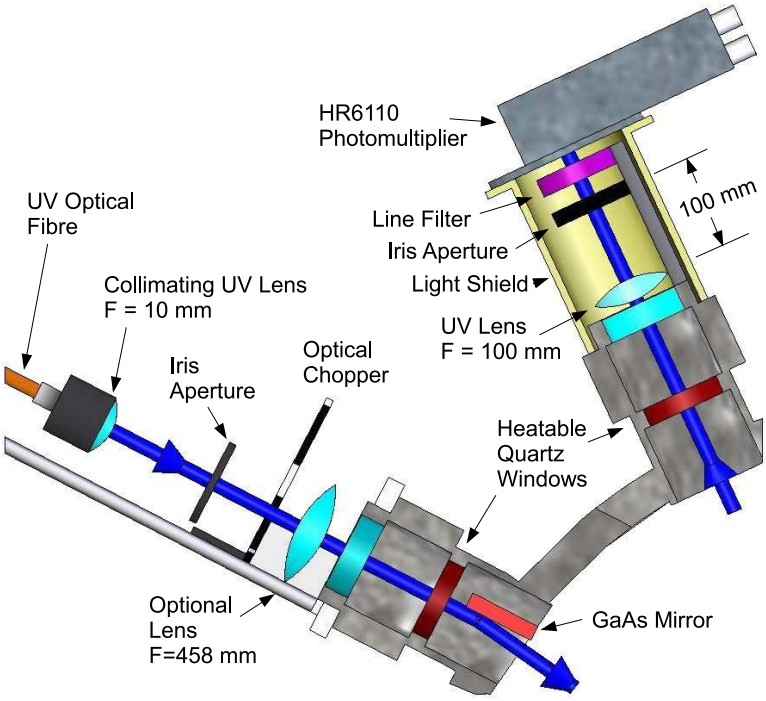

Figure 3.7: The optical assemblies used in the in-situ light scattering apparatus. The photomultiplier is powered with a 1.1 kV high voltage source, and output the measured intensity which is read with an SR810 lock-in amplifier. The optical beam is chopped at a frequency between 150-230 Hz.

window to increase the light on the detector. An iris aperture is placed at the focal plane of this lens and positioned such that it blocks scattered light from the substrate holder. The majority of background light is scattered off the substrate holder whereas the sample is the smoothest object in the chamber and scatters a relatively low amount of light. A Hamamatsu R6353 Si UV diode and photomultiplier are placed close to the iris aperture. A line filter of the correct wavelength was placed in front of the detector to block light from the effusion cells and prevent the detector from overloading.

The incident beam enters the growth chamber through a converted shutter port. A mirror was mounted within the shutter port to direct the port's line of sight to the substrate. Either a GaAs or Si wafer was used as the mirror. The detector assembly was mounted on a source port. The specular beam was directed out of the growth chamber through another converted shutter port and blocked with black paper to reduce the overall background intensity.

Differential heating induced by optical absorption from the incident laser beam used by the light scattering apparatus will occur [80]. The light-induced surface temperature rise can be calculated by solving the heat flux equation for a GaAs substrate in contact with a thermal reservoir (the substrate holder) with a Gaussian heat source (the laser spot) [81]. The surface temperature has been calculated for $\lambda = 488\ nm, 40\ mW$ of input power. The calculated difference in temperature is less than 2^oC between the illuminated spot and the edge of the substrate. This temperature rise is negligible.

GaAs substrates were often reused for light scattering experiments. For all samples that would be reused, the GaAs growth ended as follows: the substrate temperature was ramped to 570-590^{o}C, the Ga flux was changed to $\sim$1 ML/s, the As_2 flux was changed to 8 ML/s, and the sample was rotated to ensure uniformity. The substrate was then removed from the growth chamber and re-oxidized by exposure to ozone for 10 minutes. The ozone was produced by exposing air to UV light generated by a mercury arc lamp. Although an ozoned surface produces a significantly rougher starting surface after the oxide is desorbed, the surface quickly anneals to a surface whose roughness is similar to that produced from the desorption of a native oxide.

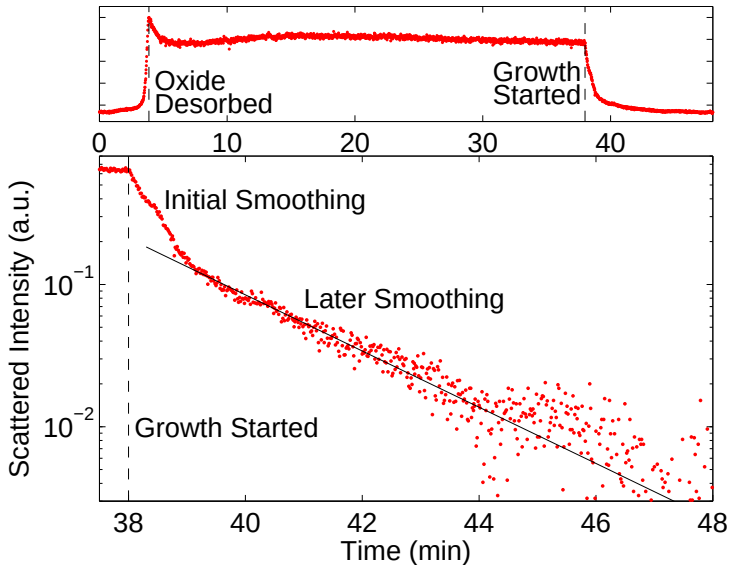

Figure 3.8: An example of the diffuse light scattering signal from a thermally cleaned GaAs surface followed by the growth of GaAs. The bottom part of this figure is a semilog plot of the GaAs growth with the background scattered light intensity subtracted. The solid line is a fit to an exponential decay with time. This sample was grown at 1 ML/s, 550^{o}C and measured along the [1$\bar{1}$0] direction.

An example of the observed light scattering signal during growth of GaAs is shown Figure 3.8. In the top part of Figure 3.8 the light scattering signal increases dramatically when the oxide is thermally desorbed, then decreases rapidly when the GaAs growth starts. Before the oxide is desorbed the sample is atomically flat and scatters a nominal amount of light. At this point, the observed intensity is from light scattered off other objects in the growth chamber. When the native oxide is desorbed the light scattering signal increases by 1-2 orders of magnitude, allowing the light scattering

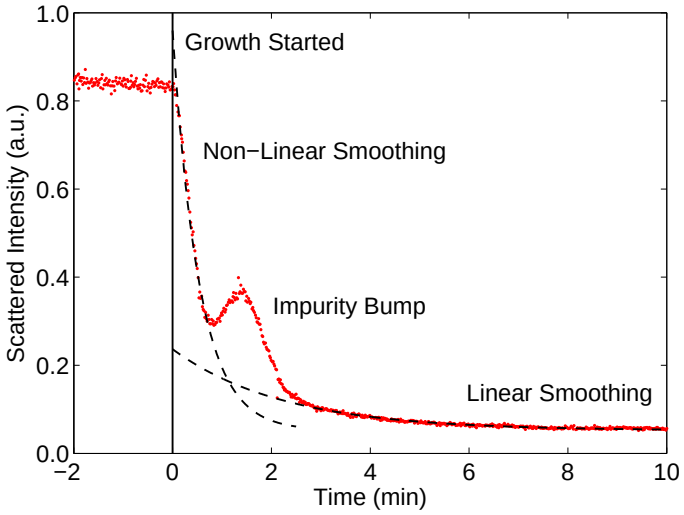

Figure 3.9: Diffuse light scattering signal displaying the commonly seen impurity bump that is sometimes seen near the start of growth. The sample was grown at a Ga flux of 0.1 ML/s and a substrate temperature of 590^{o}C. The dashed lines are fits to exponential decays with time.

apparatus to observe the GaAs sample. Although the surface does anneal and smooth before the growth, the surface is observed to relax to a stable surface morphology after a period of time as measured by light scattering, as long as the substrate temperature is less than 610^{o}C. Introducing a Ga flux starts the GaAs growth and causes rapid smoothing of the surface as shown in the lower panel of Figure 3.8. The smoothing is characterized by two regimes: an initial rapid smoothing followed by a slower exponential decay of the light scattering signal. This behaviour is always seen for smoothing of the oxide-desorbed surface.

On occasion, a period of roughening was observed with the light scat-

tering near the start of the GaAs growth. An example of this roughening is shown in Figure 3.9. It is believed that this bump is caused by carbon or SiO_2 contamination on the surface [82]. The deposited GaAs does not wet the contaminated areas which results in a rougher surface. This bump becomes more pronounced for smaller growth rates or unclean substrates. The second indication is that carbon and oxygen impurities are always seen at layer or substrate interfaces with Secondary Ion Mass Spectrometry (SIMS). In SIMS the sample is sputtered away with a focused ion beam and the sputtered material is measured with mass spectrometry. Figure 3.10 shows a SIMS measurement of a GaAs sample in which ∼600 nm of material was grown on the substrate. The growth was then interrupted, allowing more impurities to land on the sample, after that ∼250 nm of material was deposited. The SIMS measurement in Figure 3.10 measured impurities on the surface, the growth interrupt interface and the substrate-sample interface. This impurity bump has little effect on the measurements of the smoothing coefficients. Smoothing coefficient measurements of samples in which large impurity bumps were observed are in agreement with growths under similar conditions in which no bump was seen.

The fact that the light scattering apparatus is able to observe changes on the substrate accurately is a challenging technical feat. The substrate is nearly atomically flat, and even after the oxide is removed only scatters a marginal amount of light in non-specular directions. Other fixtures in the MBE such as the nearby substrate holder or the in-chamber optics are rough and scatter light strongly. The scattered light from the inside of the growth chamber has orders of magnitude more intensity then light scattered from the substrate. Only careful alignment of optical beam paths to reduce these effects allows the light scattering apparatus to work.

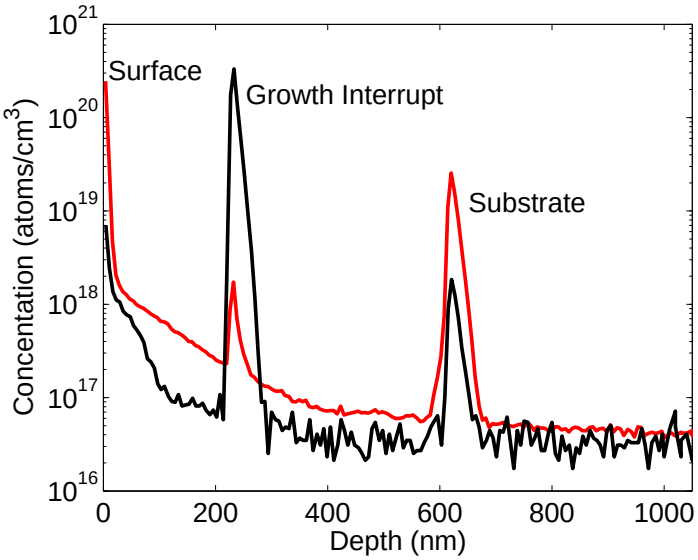

Figure 3.10: SIMS measurements of the carbon and oxygen concentration (C: – O: –) in a grown film as a function of depth. Two GaAs film growths were carried out on this sample with a growth interrupt in between. In the interrupt, the substrate was removed from the MBE and re-oxidized by exposure to ozone for 10 minutes. Interfaces can be seen at 225 nm and 620 nm depth.

3.4 Atomic Force Microscopy

An atomic force microscope (AFM) (Digital Instruments MMAFM-2) was used to measure ex-situ surfaces of homoepitaxially grown GaAs samples. The AFM was used to collect images for the calculation of PSD for surfaces, the measurement of step densities, and the shape of GaAs structures. The AFM imaged surfaces in air and was equipped with either a 10 nm radius silicon tip or a 1 nm radius tungsten tip on a silicon cantilever (Mikromasch

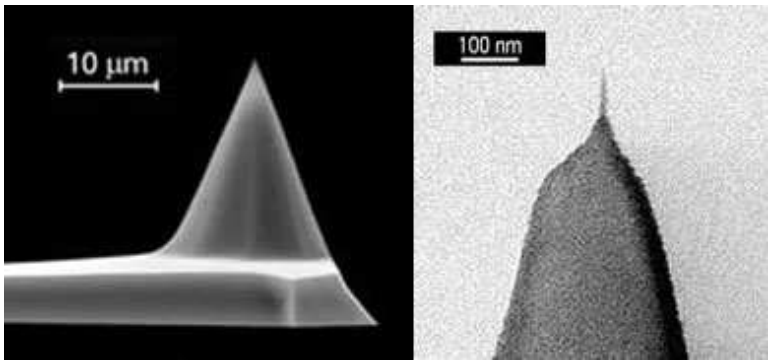

Figure 3.11: SEM images of a 10 nm radius silicon tip (left) and a high resolution 1 nm radius tungsten tip (right) used for AFM measurements. These images were provided by the tip manufacturer, Mikromasch.

NSC15 or NSC15-HiRes) with a resonant frequency in the 300-400 Hz range. Figure 3.11 shows a detailed picture of the AFM tips used in this work. The lateral resolution of the AFM is either the scan size divided by 512 (a limitation of the controlling software) or the radius of the tip, whichever is larger. The vertical resolution of the AFM is 0.1 nm. The high resolution tips significantly improved the lateral resolution and were used for step density measurements.

The power spectral densities shown in this work were determined from a series of images taken at increasing scan sizes in order to achieve a wide spatial frequency range. In the PSDs of individual images the PSD at low and high spatial frequencies is inaccurate. The features that correspond to the PSD at low q have lengthscales similar to the image size. These features are lost when the AFM image is flattened resulting in an artificial levelling off of the PSD. At high spatial frequencies the PSD is sensitive to noise in the AFM image. For the these reasons the PSD at high and low spatial

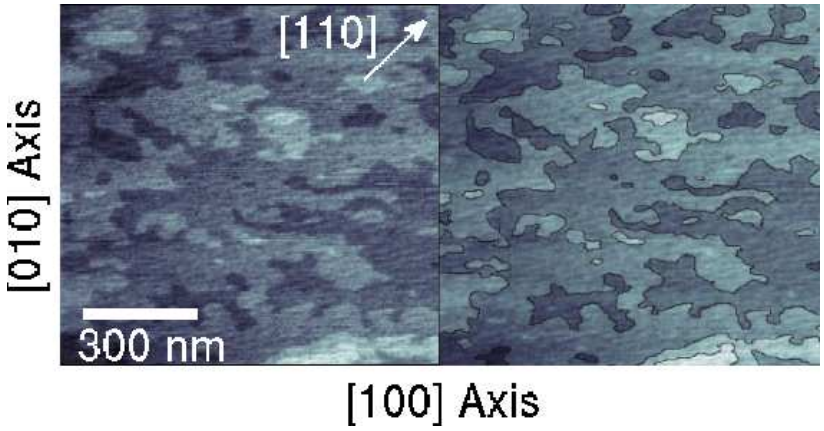

Figure 3.12: An AFM image used to determine the step density. In the right hand image the step edges are highlighted with a Canny edge-finding routine; the $\vec{z}$ scale is 2.08 nm and the average step density is 0.079 nm^{-1}. For this sample 500 nm of GaAs was grown at a substrate temperature of 590^{o}C and a Ga flux of 0.27 ML/s.

frequencies are not included in the final merged PSD. Figure 3.6 and the upper left insert in Figure 3.2 show examples of PSDs calculated according to this method. Physical and electronic noise in the AFM will introduce a noise floor in the PSD. By measuring the PSD for flat GaAs surface with little variation in surface height the noise floor was determined to be on the order of 10^{-3} nm^4 at high spatial frequencies, which is significantly lower than the power spectral densities shown in this thesis.

The step density, S_o was measured from AFM images with clear and visible step edges. An edge finding routine based on the Canny algorithm, which is part of the Matlab software package was used to locate the step edges. The edge finding routine determined for number of pixels containing a step. The step density was determined by multiplying by the size of a

pixel (the lateral resolution of the AFM) and dividing by the image size. An example of the edge finding method is shown in Figure 3.12, which gives the original image and the steps determined by the edge finding routine. The results of the step density measurements will be discussed in Section 4.3.

3.5 Numerical Simulations

In Section 5.4, dynamic numerical methods have been used to simulate the surface the shape evolution that occurs during GaAs growth. The purpose of these simulations was to compare theoretical predictions to experimentally measured quantities. These simulations consist of solving continuum model equations with numerical methods for simple one dimensional lines using the Isoda ordinary differential equation package in Matlab. This package is dynamic and chooses the appropriate numerical method and time step based on the current conditions of the simulation. The simulations were limited to one-dimensional line scans to keep computational times reasonable. Line scans from AFM images of patterned GaAs surfaces were used as initial starting surfaces for the simulations.

Since this thesis focuses on testing the non-linear continuum model described by Equation 2.4 it would have been ideal to simulate this equation directly. However, Equation 2.4 does not converge to a stable solution when it is numerically solved. It was found that the addition of the second order linear term, $\kappa\nabla^4 h$ to Equation 2.4 relieves this problem. Thus, the following equation was used for numerical simulations presented in this thesis:

$$\partial_t h = aF + \nu\nabla^2 h - \lambda_2\nabla^2(\nabla h)^2 - \kappa\nabla^4 h \tag{3.3}$$

Equation 3.3 with the additional second order term is not expected to signif-

icantly differ from Equation 2.4 for small κ since the first order linear term and second non-linear term dominate. In the simulations the value of κ was chosen to be as small as possible, such that if κ was lowered the numerical simulation would not converge to a stable solution. To test if the second order linear had an effect on the simulation, κ was increased to in order observed when the second order linear term had an effect of the numerical solutions of the surface morphology. Typically, no observable change in the simulated surface morphology was observed until κ was increased by 2 orders of magnitude.

3.6 Error Analysis

For the measurements presented in this thesis the primary source of uncertainty is due to systematic variations in the parameters of the GaAs growth. For this thesis all samples were grown with a MBE reactor, which can unfortunately introduce uncertainties that are difficult to control or determine. In a MBE system the growth parameters and sample quality will change over time. This is particularly true for a MBE that is being used in a wide variety of research projects, as was the case for the MBE reactor used to grow the samples used in this work.

As mentioned previously in Section 3.1, the fluxes of the molecular sources were calibrated with an in-beam ion gauge and x-ray diffraction. Unfortunately, during use the molecular flux of the sources will change over time. As the source uses material (which is deposited on the substrate) the output flux will be slowly reduced. Also, material in a source can melt and undergo a change in shape over time, which could potentially change the outgoing flux. Note that regular flux calibrations were conducted to track

and account for this unavoidable drift in the molecular fluxes.

During the growth of GaAs, the substrate temperature may vary or drift in an undesired manner. In the growth, GaAs substrates are radiatively heated by the substrate heater and radiatively cooled by the surrounding MBE growth chamber. The MBE growth chamber primarily consist of a cyro-shroud that is held at -196^{o}C (liquid N_2). However, there are other elements in the growth chamber such as the molecular sources (typically 600-1000^{o}C), which are often blocked with a shutter. Opening or closing a shutter will rapidly change the radiative cooling of the substrate and it will take time for the substrate heater to adjust to this change. This often results in a short period of time (less than 2 mins) in which the substrate is not held at the desired temperature. Fortunately, the substrate temperature is accurately measured with bandgap thermometer. From these measurements the error in the substrate temperature is estimated to be approximately $\pm 5^o$C.

Elements in the growth chamber in a MBE reactor, such as the chamber walls or the sample holder, will be coated with material from the molecular sources over time. This is particularly true when a arsenic source is used, as is the case in GaAs growth. Layers of arsenic or arsenic related compounds will coat any surfaces in the MBE growth chamber that are not regularly heated above 200^{o}C. This can potentially introduce systematic errors. One known effect is that a clean molybdenum sample holder (shiny grey in color) will quickly be coated with arsenic (black in color). In this case, the emissivity of the sample holder changes rapidly, making it difficult to control the substrate temperature. Fortunately, after about a month the sample holder is sufficiently coated with arsenic such that the emissivity does not change during growth. Another known effect of the chamber being coated

with arsenic is that when a new area in the growth chamber is heated (eg, a new molecular source added to the chamber) the based chamber pressure will be increased until all the arsenic is thermally evaporated from the newly heated area, potentially introducing impurities.

This thesis primarily used two techniques to measure and characterize the (100) GaAs surface; atomic force microscopy and elastic light scattering. These techniques measure the surface morphology fairly accurately, however there are some uncertainties involved with these measurements. In the AFM measurements on smooth surfaces errors are introduced when GaAs samples reoxide over time after being removed from vacuum, since this will alter the surface morphology slightly. Measurements of the step density are particularly sensitive to these changes, while measurements of patterned surfaces are insensitive to the reoxidation of the GaAs surface. For measurements of patterned surface the main source of error arises from unavoidable variations in the grating fabrication. Fortunately, it takes time for GaAs surface reoxidize, no noticeable change in the surface shape is seen until approximately 2 hrs after the sample is removed from vacuum. Most AFM measurements were conducted immediately after that samples were exposed to air inorder to reduce this effect.

In the light scattering apparatus the main source of error is due the difficulties in aligning the light beam with GaAs substrate. There is some mechanical play in the device in the MBE growth that holds the sample holder (the sample manipulator) and it is difficult to consistently place the substrate at the exact same angle relative to the incident light beam for each run. To account for this uncertainty the position of the sample manipulator was adjusted until position of the reflected beam on a screen outside the growth chamber was approximately the same as it was in previous experi-

ments. The error in the in-plane angles of the incident and scattered beams (θ_i and θ_s) is approximately ± 3 degrees given the observed variations in the position of the reflected beam. Additional uncertainty is added the light scattering measurement since the incident light beam is aligned to a crystalline axis of the GaAs substrate by matching by eye the crystalline flat to the flat of a known element in the MBE growth chamber.

Overall, the main sources of error that exist in the data presented in the following chapters is do to the reproducibility of the GaAs growth, the fabrication of the patterned surfaces and the alignment of the light scattering apparatus. Whenever possible measurements were conducted as a set to minimize run-to-run variations. However, this were not always possible and some of the experiments presented in this thesis were conducted over long periods of time.

Chapter 4

GaAs Homoepitaxy on Roughened Substrates

An understanding of the GaAs surface during epitaxial growth is needed for the development of compound semiconductor devices. In this chapter the results of the in-situ light scattering and AFM step density experiments on GaAs are presented and compared to the predictions of the non-linear continuum model described in Section 2.2. The chapter starts by presenting the smoothing coefficients and smoothing rates for GaAs homoepitaxy over a range of spatial frequencies (lengthscales), Ga flux, As_2 flux, substrate temperature and crystalline orientation. The continuum equation derived by [1] which predicts the effect of Ga flux and temperature is compared to these results. The effect of the arsenic flux and crystal orientation are discussed with respect to the surface reconstruction and surface diffusion. The chapter will then present independent ex-situ measurements of step densities from AFM.

4.1 In-situ Light Scattering Measurements

4.1.1 Linear Smoothing

The smoothing of (001) GaAs observed at long times in the growth shown in Figure 3.8 is represented well by the linear smoothing coefficient in Equation 2.4 [28]. For the first test of this, the smoothing rate constants were measured by fitting the long time light scattering data to an exponential decay with time and presented in Figure 4.1 at multiple spatial frequencies. The variation in spatial frequency was obtained by using multiple light sources and incident angles in the light scattering apparatus. In order to determine the expected spatial frequency dependence of the rate constants consider the limit of a weak surface topography ($h < \nu/\lambda_2$) for Equation 2.4 which is the case for long time smoothing of GaAs. In this case the surface smoothing is dominated by the linear term, $\nu\nabla^2 h(\vec{x})$ and the non-linear term, $\lambda_2\nabla^2(\nabla h(\vec{x}))^2$ can be neglected. The noise term, η can also be neglected since it only contributes to the steady state roughness at very long times. The reduced form of Equation 2.4 in this limit can be analytically solved by considering a Fourier series expansion of $h(\vec{x})$:

$$h(\vec{x},t) = \left[\frac{A_o}{2} + \sum_n A_n cos(\vec{q_n}\cdot\vec{x}) + \sum_n B_n sin(\vec{q_n}\cdot\vec{x})\right] h(t) \tag{4.1}$$

Equation 4.1 can be applied to the low amplitude limit form of Equation 2.4 and using Equations 2.15 and 2.17 the scattered light intensity has the time dependence:

$$I(q,t) = I_o(q)e^{-2\nu q^2 t} + I_{bg} \tag{4.2}$$

where $I_o(q)$ is the initial intensity due the inherent roughness that is present at the start of the smoothing regime, and I_{bg} is the background intensity due to scattering off the surrounding chamber.

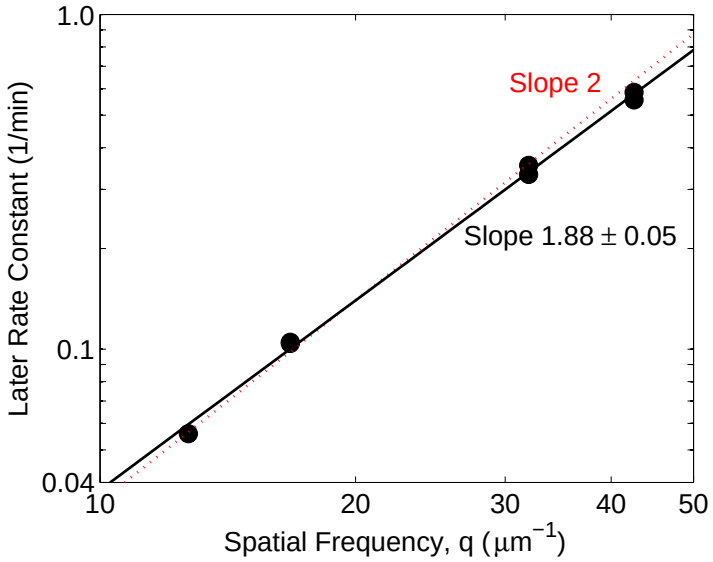

Figure 4.1: Rate constant versus spatial frequency as measured along the [110] direction with the light scattering apparatus at later times in the growth. The GaAs was grown at a substrate temperature of 590^{o}C and a Ga flux of 1 ML/s.

The spatial frequency dependence of the smoothing rate constants in Figure 4.1 is very close to the expected $\vec{q}$ dependence of the linear term, ν. A fit to a power law in spatial frequency of these rate constants yields an exponent of 1.88±0.05. As shown by the dotted red line in Figure 4.1, this exponent is close to an exponent of 2 which is predicted by Equation 4.2. This agreement between the measured and predicted exponents validates the statement that the linear term, $\nu\nabla^2 h(\vec{x})$ dominates Equation 2.4 at low amplitudes (which occur at longer growth times). The linear smoothing coefficients presented in the rest of this section are obtained by fitting the

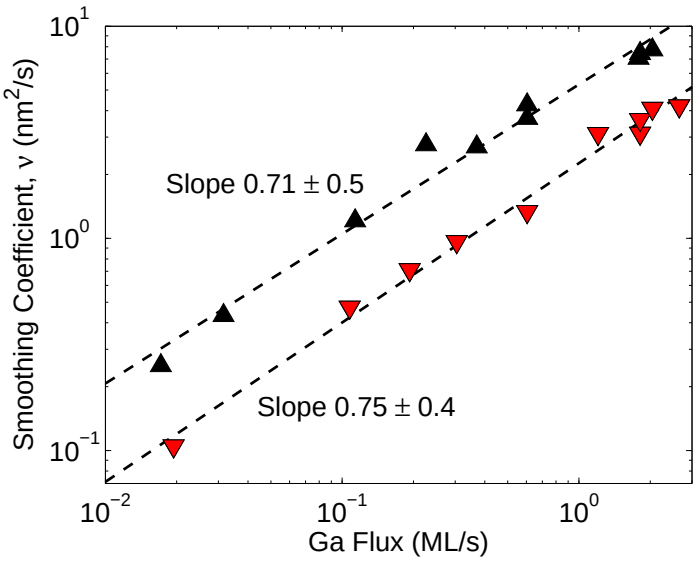

Figure 4.2: Linear smoothing coefficient inferred from light scattering data as a function of Ga flux at a substrate temperature of 590^{o}C and a fixed As_2 overpressure. Measurements in the $[1\bar{1}0]$ direction are indicated by ▲, and in the [110] direction by ▼. The dashed lines are least-square fits to $\nu \propto F^y$.

data to Equation 4.2.

The linear smoothing coefficient has been measured over a large range of Ga flux at three substrate temperatures. These results are presented in Figures 4.2 and 4.3. The gallium flux is important to study as it controls the growth rate under typical MBE growth conditions. For this smoothing measured at a later growth time, two functional dependencies on Ga flux are observed. At lower Ga fluxes, ν increases with increasing Ga flux, while at higher fluxes the smoothing decreases with increasing flux. The transition between the two flux dependencies of ν is at ∼1.5 ML/s. This flux is where the linear smoothing coefficient has its maximum value. The linear smooth-

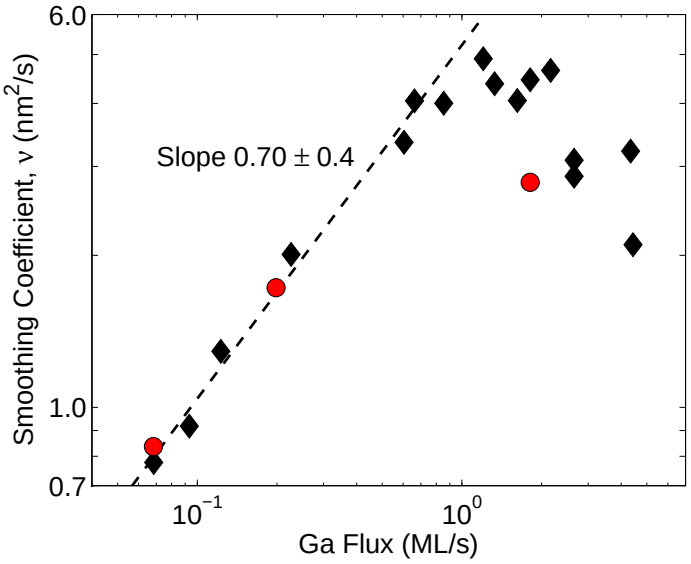

Figure 4.3: Linear smoothing coefficient as a function of Ga flux measured with the light scattering apparatus along the $[1\bar{1}0]$ direction. The substrate temperatures were 550^oC (♦) and 500^oC (●). The dashed line is a least-square fit to a power law in flux for the 550^oC data set.

ing coefficient has a power law dependence on Ga flux with an exponent that is less than 1 for Ga fluxes less than 1.5 ML/s. This indicates that, for the same amount of material deposited a sample grown at a low Ga flux will be smoother than a sample grown with a high Ga flux. If the exponent were equal to one then the amount of surface smoothing that takes place would depend only on the film thickness and not on the growth rate.

For Ga fluxes below 1.5 ML/s, the flux dependence of the linear smoothing coefficient agrees with the behaviour predicted by the non-linear continuum growth equation presented in Section 2.2. Equation 2.11 predicts

that $\nu \propto F^{\frac{x+4}{2x+4}}$. The critical island size, x, is not an accurately measured quantity and still needs to be determined. Critical island sizes of 2 and 3 yield exponents in the flux dependence of the linear smoothing coefficient ($\nu \propto F^{\frac{3}{4}}$ and $F^{\frac{7}{10}}$) that are comparable to the fits in Figures 4.2 and 4.3. The critical island size cannot be determined accurately from the flux dependence of ν. Other results presented later in this work will be used to determine the value of x more accurately. The flux dependence of ν suggests that the critical island size is greater than 1, meaning that for a stable island to nucleate on the (001) surface, 3 or more Ga atoms are needed.

For fluxes greater than 1.5 ML/s, the linear smoothing coefficient decreases with increasing Ga flux. This decrease in smoothing may be due to the effect of changing the group V/III ratio on the surface. For these measurements the As_2 flux is held constant and as the Ga flux increases the As_2/Ga ratio becomes smaller and approaches unity. The assumption that the physics during growth on the GaAs surface is dominated by gallium adatoms and that arsenic can be ignored, which is stated in Section 2.2 may no longer apply in this case. This will be discussed more in Section 4.1.3.

The substrate temperature is known to affect the surface morphology of GaAs and is an important parameter in the growth of GaAs and related group III/V hetrostructures. Studying the effect of changes in the substrate temperature provides significant insights into atomic scale mechanisms on the surface. For this work the temperature dependence of the linear smoothing coefficient has been measured over a large range of substrate temperatures at standard growth rates. These results are presented in Figure 4.4.

A weak temperature dependence of ν with an Arrhenius form can be

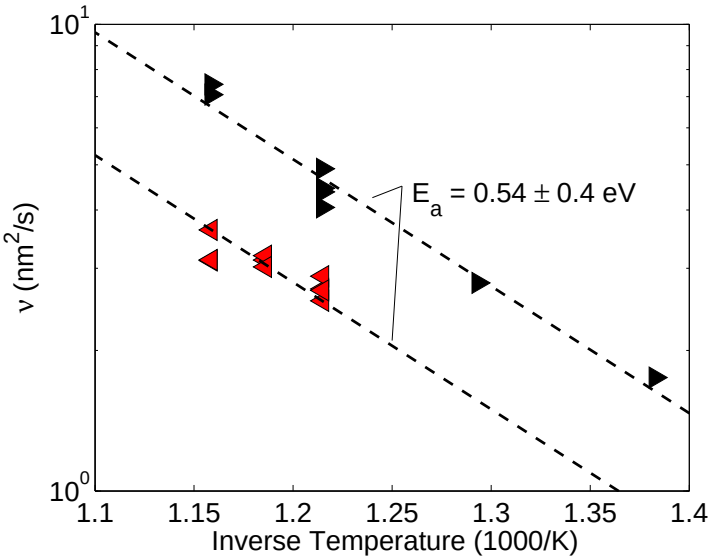

Figure 4.4: Linear smoothing coefficient, ν as a function of temperature at a growth rate of 1 ML/s. Light scattering measurements were taken along the $[1\bar{1}0]$ direction (▶) and the [110] direction (◀).

seen in the $[1\bar{1}0]$ direction data in Figure 4.4. A fit to this data yields an activation energy of 0.54±0.4 eV. Note that there is insufficient data along the [110] direction in Figure 4.4 for an Arrhenius fit; the lower dashed line is drawn solely for comparison. In Equation 2.11 the temperature dependence of ν is associated with the factor $\zeta D^{\frac{x}{2x+4}}$. Fortunately, as discussed in Section 2.2 it is known how both ζ and D depend on temperature, as shown in Equations 2.13 and 2.14. The diffusion constant alone can account for the observed temperature dependence of ν. For a critical nucleus size of 2 ($\nu \propto D^{1/4}$), the activation energy determined from Figure 4.4 of 0.54±0.4 eV will yield a diffusion activation energy of 1.8 eV. Which is in the range of measured diffusion activation energies 1.5-2 eV [58–60].

Even though the diffusion constant could account for the observed temperature dependence of ν, the dimensionless Ehrlich-Schwoebel step edge parameter ζ, which describes the downhill diffusion bias is also expected to have some temperature dependence. However, for GaAs the substrates temperature is expected to have significantly more effect on D then on ζ. If the diffusion bias at a step edge was caused by a negative ES step edge barrier [83], lowering the step edge barrier by a few kT or more, the Ga adatoms will hop in the direction of the lowered barrier with high probability, with temperature having a minimal effect [1, 3]. Examining Equation 2.13, a negative ES barrier or a small incorporation barrier on the order of kT, will produce a temperature independent ζ approximately equal to 0.5. Larger values for ζ can be expected in the presence of a large barrier to attachment of adatoms at step edges from below.

The values of the linear smoothing coefficient, ν presented in this section are consistent with previous measurements of ν. Using kMC simulation of the (001) GaAs surface, Ballestad and Tiedje [1] estimated the linear smoothing coefficient at various Ga fluxes and substrate temperatures, which reported similar values to those presented in this thesis. Also, best fits of continuum growth equations to GaAs surfaces grown with MBE at 1.3 ML/s and 550^{o}C in [27, 57] found ν to have a values of $\sim$1-10 nm^2/s which are consistent with the measurements shown in Figure 4.3. Lavoie [36] made similar observations on smoothing for thermally desorbed GaAs surfaces and roughening from H-etched GaAs surfaces. However, Lavoie measured the smoothing at the start of the growth and interpreted it as being due to the linear term, which is not the case in the initial regime of smoothing. The results presented in this section have a good overall agreement with these previous works. Additionally, in this thesis the first order linear term of the

non-linear continuum growth equation model was linked to experimentally measured smoothing coefficients over a wide range of spatial frequencies, growth rates, and substrate temperatures. Previously in the field of (100) GaAs homoepitaxy, experimental results had not been linked to a physically based smoothing coefficient.

4.1.2 Initial Smoothing

Smoothing that is observed near the start of growth has also been measured over a large range of spatial frequencies, substrate temperatures and gallium fluxes. In this section, this large set of data is used to test predictions made by the non-linear continuum growth equation model as described in Section 2.2. The initial smoothing of the growth does exhibit a behaviour that is similar to an exponential decay of intensity with time. Thus, to start an examination of the initial regime of smoothing the initial smoothing rates (ISR) have been determined by fitting light scattering data to exponential decay of the scattered intensity with time ($I \propto e^{-ISRt}$).

The first result of the initial smoothing rate measurements are presented in Figure 4.5, which shows the spatial frequency dependence of the observed smoothing. The smoothing rates in Figure 4.5 have a weak power law dependence in $\vec{q}$ with an exponent of 0.34 ± 0.4. A weak or no dependence on spatial frequency is not expected. Continuum growth equation models, such as those discussed in Section 2.2, predict that the smoothing will have a non-zero spatial frequency dependence. The linear terms in a continuum growth equation will lead to a strong $\vec{q}$ dependence in the smoothing. This is exemplified in Section 4.1.1 where it was shown that the first order linear term $\nu\nabla^2 h$ leads to a smoothing rate that is $\propto 2\nu q^2$. Note that higher order

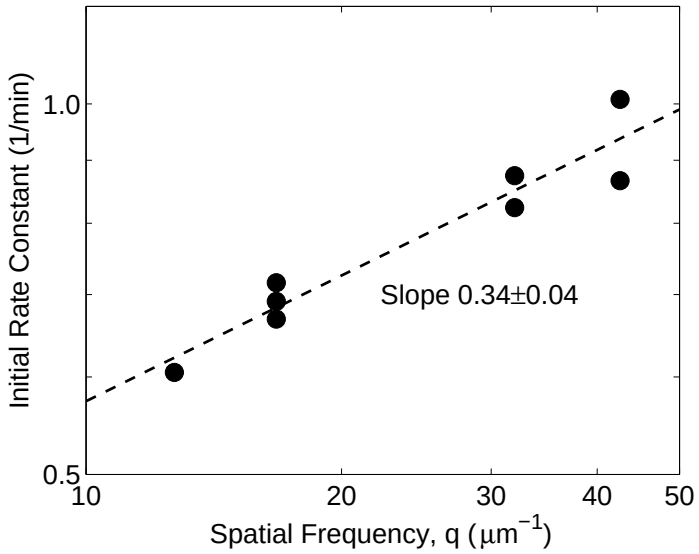

Figure 4.5: Rate constant versus spatial frequency as measured with light scattering near the start of the growth. The GaAs was grown at substrate temperatures of 590^{o}C, Ga fluxes of 1 ML/s and was measured along the [110] crystalline direction.

terms predict a stronger spatial frequency dependence than q^2. It is less clear to what the addition of a non-linear term will do to the predicted spatial frequency dependence of the smoothing, however numerical simulation of various non-linear continuum growth equations, presented in [53] indicate that the strong dependence on spatial frequency is retained when non-linear terms are included in the continuum equation. The measurements presented in Figure 4.5 indicate that a continuum growth equation model is not valid for the initial regime of smoothing seen consistently near the start of the growth in (100) GaAs homoepitaxy.

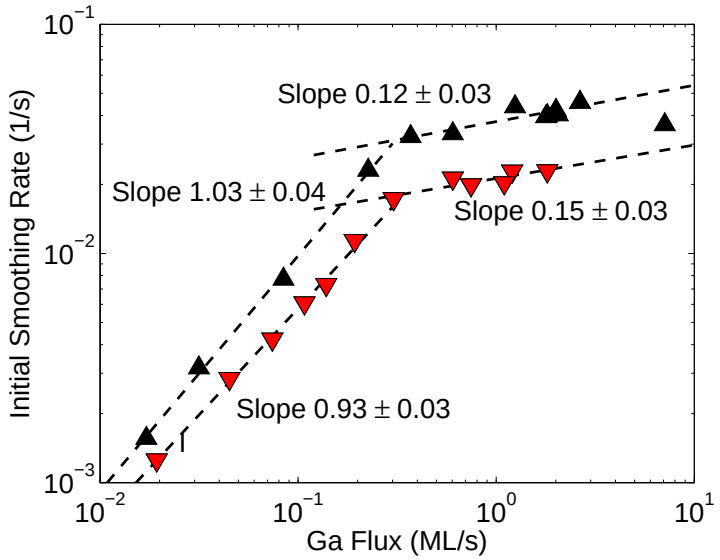

Figure 4.6: The smoothing rate observed at the start of the growth measured over a range of Ga fluxes at a substrate temperature of 590^{o}C at a spatial frequency of 32 μm^{-1}. Data indicated by ▲ was measured along the [1$\bar{1}$0] direction and ▼ was measured along the [110] direction.

The initial smoothing rate has been measured at a multitude of different Ga fluxes which are shown in Figures 4.6 and 4.7. The initial smoothing rate depends on Ga flux in three distinct ways, which are not affected by substrate temperature. For fluxes below 0.2 ML/s the initial smoothing rate increases linearly with Ga flux. A weak flux dependence for the smoothing rate is seen between 0.2 and 2 ML/s. For fluxes greater than 2 ML/s, the initial smoothing rate becomes insensitive to Ga flux similar to ν measured at high Ga flux. As discussed in Section 4.1.1, this behaviour is likely be due to the fact that the As_2/Ga ratio is approaching unity at these physical conditions.

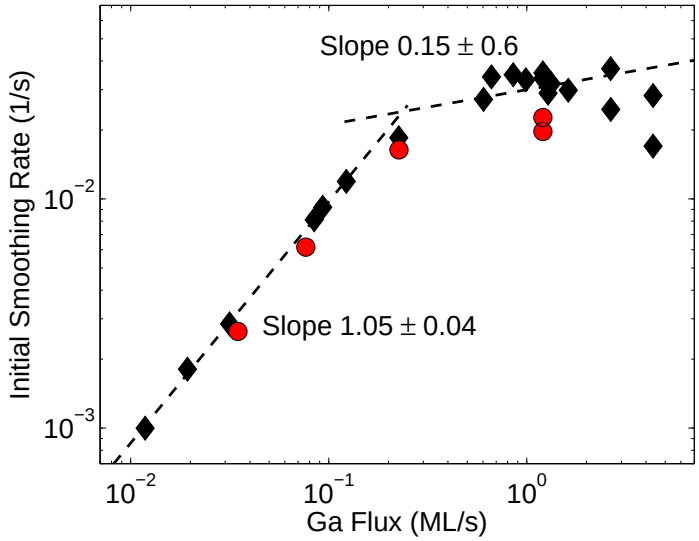

Figure 4.7: The initial smoothing rate measured over a range of Ga flux at an As_2 flux of 8 ML/s and at the substrate temperatures of 550^{o}C (♦) and 500^{o}C (●). The smoothing was measured along the [1$\bar{1}$0] direction and at $q = 32\ \mu\text{m}^{-1}$.

For Ga fluxes between 0.2 and 2 ML/s the initial smoothing rate agrees with the behaviour predicted from the non-linear continuum growth equation. For strong surface topography, as is the case at the start of the GaAs growth, the non-linear term in Equation 2.4 will dominate and the linear term can be neglected. Equation 2.12 predicts that the smoothing depends on Ga flux as $\lambda_2 \propto F^{\frac{2-x}{x+2}}$. A weak power law dependence of the smoothing flux is expected for a critical island size of one $\lambda_2 \propto F^{\frac{1}{3}}$, however no flux dependence is expected for $x = 2$. For the initial smoothing rate the best agreement between the experimental data in Figures 4.6 and 4.7 and the theory occurs when $x = 2$ and no dependence on flux in the smoothing is

expected. Critical island sizes greater than 3 are ruled out as the flux dependence of the initial smoothing rate has a power greater than zero, which conflicts with predicted form of Equation 2.12 for $x > 3$.

For the low flux region (less than 0.2 ML/s) the flux dependence of the initial smoothing rate is stronger than predicted by Equation 2.12. However, for low Ga adatom densities the average Ga diffusion length will increase as the probability of encountering another Ga adatom is reduced. Studies examining growth on vicinal surfaces have observed a transition from nucleation dominated growth to a step-flow mode as the growth rate is decreased [84]. For the randomly rough starting surface, which has large variations in the surface amplitude local areas may appear vicinal and see a similar effect. In this case, the large pits that form on the surface are filling in as fast as the smoothing rate allows. Material is primarily incorporated into the step edges of the surface and nucleation is suppressed. If nucleation is suppressed than S_o will be independent of Ga flux in contrast to Equation 2.10. Consider S_o to be a constant in Equation 2.6. In this case λ_2 will have a linear dependence on Ga flux. The fits to power laws ($ISR \propto F^y$) of the low flux region in Figures 4.6 and 4.7 yield powers ranging from 0.91 to 1.07 which are in agreement with the expected linear dependence predicted by the non-linear continuum growth equation.

For the linear smoothing coefficient, discussed in Section 4.1.1, no change in behaviour is seen in the low flux region. However, if the transition is due to a switch from nucleation dominated growth to a step-flow growth mode only a minor change is expected. Assuming a constant step density as discussed previously, then Equation 2.5 yields a linear dependence on Ga flux. The expected dependence from Equation 2.11 is $\nu \propto F^{\frac{x+4}{2x+4}}$. With $x = 1 or 2$ the exponent is between 0.75 and 0.83 which will be difficult to distinguish from

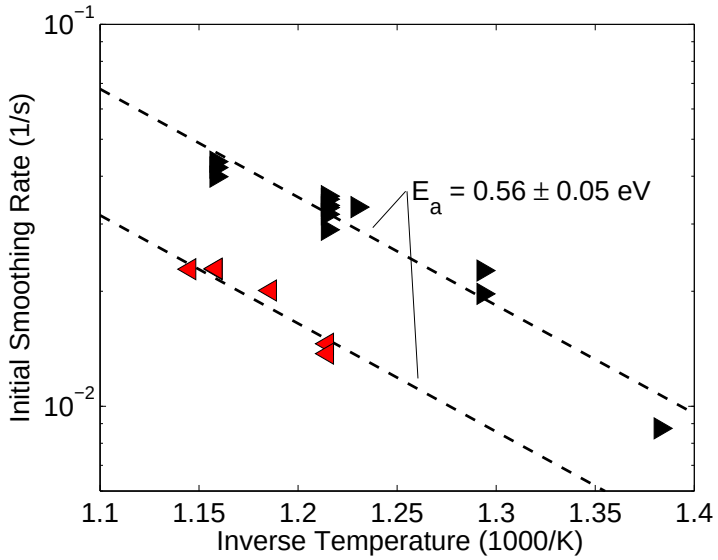

Figure 4.8: The initial smoothing rate measured over a range of substrate temperatures for the Ga flux of 1 ML/s and at q = 32 μm. The ▶ indicates data measured along the $[1\bar{1}0]$ direction and the ◀ along the [110] crystalline direction.

$\nu \propto F$, experimentally. See for example Figures 4.2 and 4.7.

The initial smoothing rate has been measured at various substrate temperatures at standard growth rates. An Arrhenius temperature dependence is seen for initial smoothing rate measured along the $[1\bar{1}0]$ direction and has an activation energy of 0.56±0.5 eV. The temperature dependence of initial smoothing rate shown in Figure 4.8 is weaker than the temperature dependence predicted by the non-linear continuum growth equation model. From Equation 2.12, for low critical island sizes the smoothing is expected to be close to linearly proportional to the diffusion constant ($\lambda_2 \propto D^{\frac{2}{3}}, D, D^{\frac{6}{5}}$ for x = 1, 2, or 3). The activation energy of the diffusion constant, which has been

independently measured, is 1.5 to 2 eV [58–60]. Using this diffusion constant activation energy with Equation 2.12 and x = 1-3, an prediction of the activation energy in the temperature dependence of initial smoothing rate can be made. The range of possible activation energies is quite large, from 1.0 to 2.4 eV. Even with this large predicted range, the measured activation energy in Figure 4.8 does not agree with the non-linear continuum growth equation model. Further indicating that continuum growth equations are not valid in the initial regime of smoothing.

The smoothing of GaAs, starting from a large-amplitude randomly rough surface formed by the thermal oxide desorption does not consistently agree with the behaviour predicted non-linear continuum growth equation model. Despite the inconsistencies, the expected behaviour derived from the non-linear term does agree with some aspects of the light scattering data. The flux dependence of the initial smoothing does agree with the flux dependence predicted for the non-linear smoothing coefficient in Equation 2.4. However, the temperature and spatial frequency dependence of the initial smoothing rate clearly do not agree with predictions made by continuum growth equation models. This indicates that the non-linear continuum growth equation may have some validity, but a deeper understanding of physics of the (001) GaAs surface is needed in order to explain the smoothing observed at early growth times. The smoothing that is seen at the start of the growth may also be beyond the continuum growth equation models presented in Section 2.2. The pits that form on the thermally desorb surface may be too steep to apply continuum growth equation model which assumes low slopes on the surface. Additionally, since the thermal desorption of the native GaAs oxide is a volatile process, small defects or orientation facets that are difficult to observe with AFM might be located on this surface, which is not included

in conventional models of GaAs growth.

4.1.3 Arsenic Flux

In the growth of GaAs with MBE the arsenic flux is often overlooked. As long as the group III/V ratio is large the arsenic flux is thought to have little effect on the quality of growth. Additionally, including arsenic in the theory significantly increases complexity of models used to describe the GaAs system. Due to these factors, only a few studies have been conducted on the effect of arsenic. Of the studies that examine arsenic on GaAs, a majority of them are concerned with the dissociation of As_2 or As_4 on the surface and the absorption of As adatoms into the existing surface reconstruction [45, 85, 86]. Additionally, there have been a few kinetic Monte Carlo simulations of (001) GaAs that have considered arsenic or gallium-arsenic compounds [10, 87]. However, these studies are difficult to relate to the large GaAs surface features that are studied in this thesis. Of the more relevant studies to this work, the Ga incorporation diffusion length has been measured as a function of As_4, and was found to decrease with increasing arsenic [88]. However, the observations in the present work contradict those results. To understand how the results conflict, examine the Ga incorporation diffusion length decreasing with As_2 flux. In this case $S_o \propto F_{As}^{\alpha}$ ($\alpha > 0$). According to Equation 2.5 or 2.6, this predicts that the smoothing coefficients will decrease with increasing As_2, which conflicts with the experimental results presented in Figure 4.9 or 4.10, which show the opposite behaviour.

Changes in the arsenic flux have been measured to have an effect on the smoothing of the GaAs surface. Figures 4.9 and 4.10 show that both ν

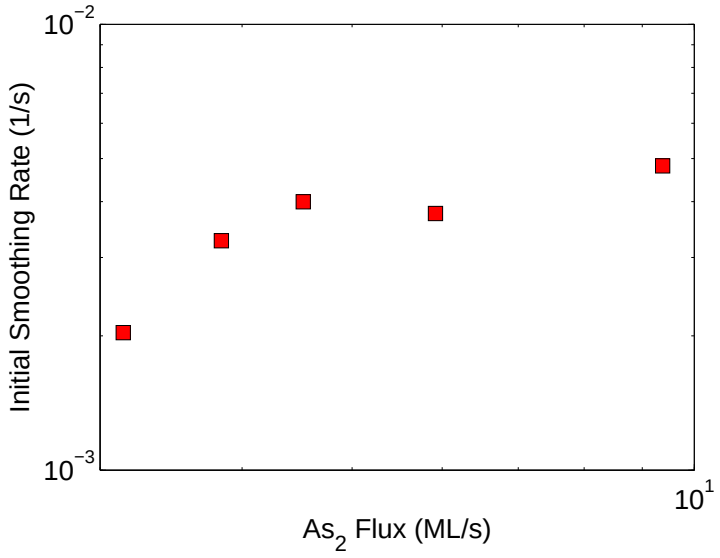

Figure 4.9: The initial smoothing rate as a function of As_2 flux at a growth rate of 0.29 ML/s and a substrate temperature of 550^{o}C measured with light scattering at 17 μm^{-1} along the $[1\bar{1}0]$ crystalline direction.

and the initial smoothing rate increase with increasing As_2 flux for constant Ga flux and substrate temperature (or with increasing group V/III ratio). Additionally, a similar effect was seen in Sections 4.1.1 and 4.1.2, where both linear smoothing coefficient and the initial smoothing rate decreased with decreasing As_2/Ga ratio at Ga fluxes greater than 2 ML/s. In Figures 4.9 and 4.10 the smoothing seemed to saturate at high As_2 flux. This supports the assumption that the effects of arsenic can be ignored for GaAs grown at high As_2/Ga ratio.

Although the non-linear continuum equation model does not include the effects of arsenic directly, these effects may come in through parameters such as the diffusion constant or step edge ES coefficient in non-intuitive

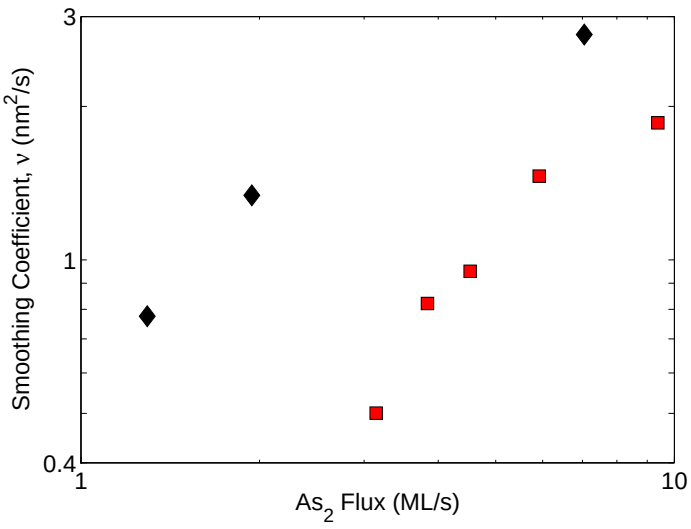

Figure 4.10: Later smoothing coefficient versus As_2 flux. The ♦ indicates a growth rate of 0.39 ML/s, a substrate temperature of 590^{o}C, and a spatial frequency of 32 μm^{-1}. The ■ indicates a growth rate of 0.29 ML/s, a temperature of 550^{o}C, and a spatial frequency of 17 μm^{-1}. Both sets were measured along the $[1\bar{1}0]$ direction.

ways. These parameters depend on binding energies of a gallium adatom on the surface, which will depend on the availability of arsenic. The As_2 dependence of the initial smoothing rate indicates that the diffusion constant increases weakly with As_2, since the initial smoothing rate is expected to have a strong dependence on D. The the initial smoothing rate is expected to have a stronger dependence on the diffusion constant compared to the linear smoothing coefficient, but changing As_2 affects ν more strongly. This suggests that ζ has a relatively strong and proportional dependence on As_2 or that S_o depends on As_2 flux. A possible explanation is that arsenic

increases the sticking coefficient of gallium atoms at the step edges. In this case ζ would be increased and S_o lowered. Another explanation is that diffusion is two-dimensional at high As_2 flux and one-dimensional at low As_2 flux. This Leads to faster adatom motion at low arsenic flux, but more area covered at high As_2 flux. New sites are visited at a much higher frequency for two-dimensional diffusion, even at lower hopping rates.

4.2 Surface Reconstruction

It is necessary to consider the effect of the GaAs surface reconstruction in relation to the observed smoothing. The surface reconstruction is known to depend on the As_2/Ga flux ratio and substrate temperature. A change from one reconstruction to another might cause significant changes in the atomic scale mechanisms of the surface, such as adatom diffusion or interactions with the step edge barriers.

The (001) GaAs surface reconstruction changes twice over the range of substrate temperatures, Ga fluxes, and As_2 used in this work [41]. One of the transitions is seen near the conditions where the smoothing coefficients start to decrease with increasing Ga flux, shown in Figures 4.7 and 4.3 ($\sim$2 ML/s, 550^{o}C). Here the As-rich (2×4) reconstruction changes to the Ga-rich (4×2) surface reconstruction. The drop in the smoothing rates may be associated with the surface changing from an As-rich to a Ga-rich surface reconstruction.

The second transition in the surface reconstruction occurs at an As_2/Ga ratio near 30, where the surfaces changes from the As-rich (2×4) reconstruction to the As-rich c(4×4) reconstruction. This change in surface reconstruction occurs near the transition in the Ga flux dependence of the

initial smoothing rate. Below 0.2 ML/s the initial smoothing rate is linear with Ga flux while above this flux the initial smoothing rate depends weakly on Ga flux as shown in Figures 4.7 and 4.6. No transition is observed around these growth conditions in the Ga flux dependence of the linear smoothing coefficient.

For the (001) GaAs surface the [110] direction is not equivalent to the $[1\bar{1}0]$ direction in terms of surface bonds. A difference in smoothing along the two crystalline directions is expected and has been observed previously [20, 26]. Throughout this work, a noticeable difference has been observed in the smoothing coefficients measured along the [110] and $[1\bar{1}0]$ crystalline directions. For the non-linear smoothing a factor of 2 difference is observed over a large range of Ga flux and substrate temperature. With the linear smoothing coefficient a difference by a factor of about 2.5 is seen between smoothing coefficients measured along the [110] and $[1\bar{1}0]$ directions. This anisotropy in the linear smoothing coefficient is independent of Ga flux and substrate temperature.

4.3 Step Length Density

The atomic step density is an important physical quantity that can be more easily measured than many other microscale quantities used in surface physics, such as the adatom density. Techniques for measurements of the step density include helium atom scattering, RHEED or scanning probe microscopy. For this work the step density was determined from AFM images, as outlined in Section 3.4. The AFM measurements of the step density are then used to calculate the smoothing coefficients, using Equation 2.5.

The flux dependence of the atomic step density, shown in Figure 4.11

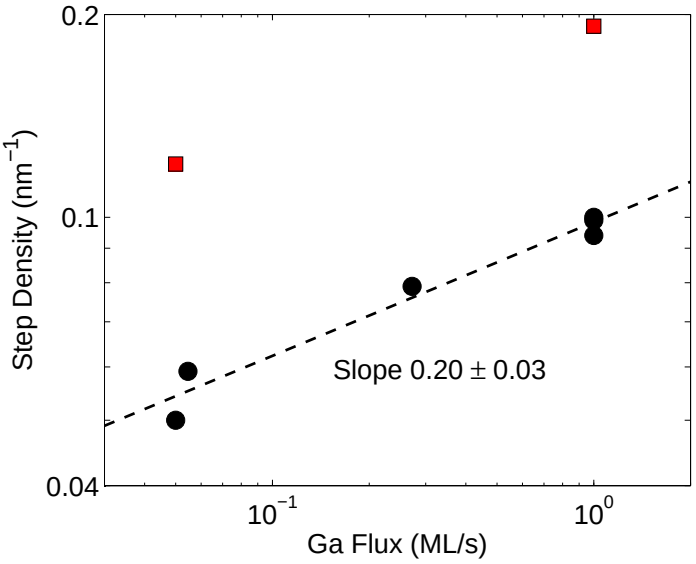

Figure 4.11: Step densities obtained from AFM images of samples grown with different Ga fluxes and substrate temperatures. The GaAs samples were grown to a thickness of 500 nm at a temperature of 590^{o}C (●) or 400^{o}C (■).

agrees with Equation 2.10 which predicts that the step density has a power law dependence on the Ga flux and the diffusion constant. A fit to the data in Figure 4.11 with a power law $S_o \propto F^y$ yields a power $y = 0.2$. A critical island size of 1 or 2 in Equation 2.10, will lead to a flux dependence of $F^{0.25}$ or $F^{0.17}$ for S_o, respectively. Both of these critical island sizes are consistent with the Ga flux dependence of the step density measured by AFM.

The linear smoothing coefficient can be calculated from the measured step densities using Equation 2.5. For calculations of the linear smoothing coefficient the Ehrlich-Schwoebel step edge coefficient, ζ must be es-

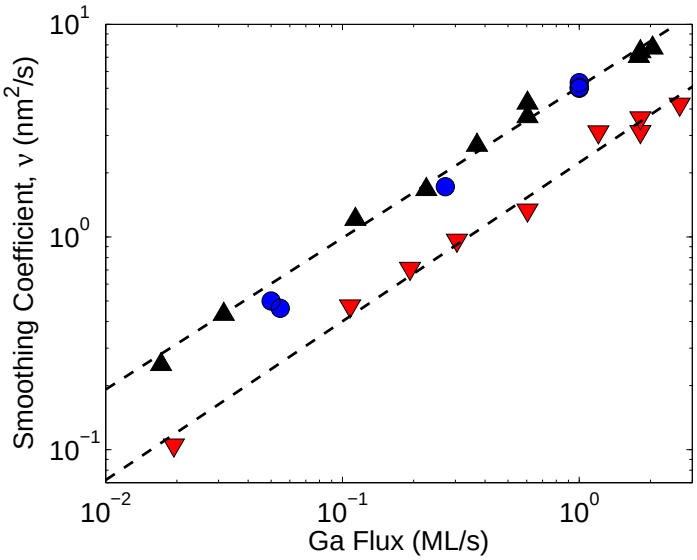

Figure 4.12: Comparison of the linear smoothing coefficient measured with light scattering ([1$\bar{1}$0]: ▲ and [110]: ▼) to ν calculated from Equation 2.5 using $\zeta = 0.5$ and the measured step densities (●).

timated. It is reasonable to assume a weak temperature dependence for ζ as the temperature dependence of $\nu \propto \zeta$ is weak as discussed in Section 4.1.1. Small negative values for the ES step edge barrier, on the order of kT ($0.03 - 0.07$ eV), are physically reasonable for GaAs [1], which Equation 2.13 (assuming no incorporation barrier) yields $\zeta \lesssim 0.5$. Figure 4.12 shows a comparison between ν calculated from S_o and the ν measured by light scattering. The measurements of the step density did not take the GaAs anisotropy into account and represent an average of the [110] and [1$\bar{1}$0] directions, and thus cannot truly agree with the light scattering data which is sensitive to the anisotropy. Taking these factors into account, the linear smoothing coefficients inferred from the step density and light scatter-

ing measurements are in excellent agreement with each other. Additionally, measurements of S_o at different temperatures shown in Figure 4.11 indicate that the step density increases with decreasing temperature, which is consistent with the behaviour predicted by Equation 2.10.

In the non-linear continuum equation growth model the step density is the principal experimental parameter which controls the surface smoothing. AFM measurements of the step density generally compare well with the independent light scattering experiment. This supports the argument that the light scattering apparatus observes the true GaAs surface morphology, and not another effect like scattering off surface contamination. Additionally, it is amazing that a measurement of the discrete atomic steps agrees with a continuum growth equation model, which by nature ignores the discrete elements of the surface. This indicates that the continuum approximation is valid over the range of the growth conditions in this work.

4.4 Growth Interrupts

In the practical fabrication of semiconductor devices with MBE, growth interrupts are occasionally required. It is important to understand what the surface does during these interrupts. For the GaAs system the growth is controlled by the Ga flux. The focus of this work has been on growth rather then annealing during growth interrupts, but limited results on annealing of GaAs have been observed and are presented in this section.

For all samples observed with light scattering the substrate was held at growth temperatures for a significant amount of time before growth was started. As stated before, Figure 3.8 is typical of a light scattering data set. For each of the light scattering runs there is a period of rapid annealing right

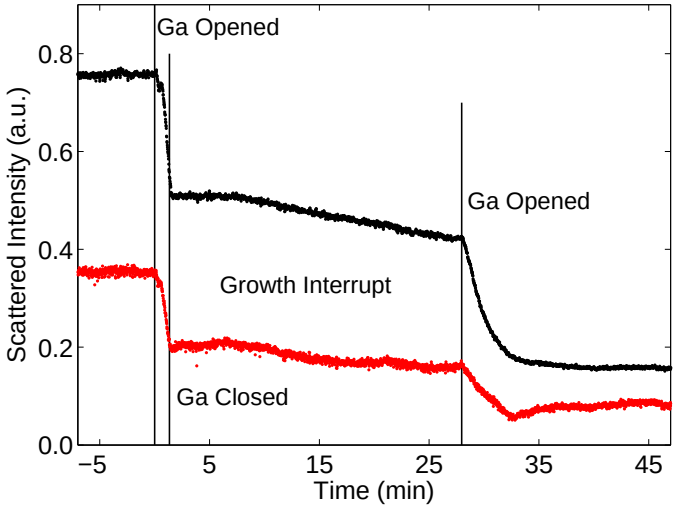

Figure 4.13: A growth interrupt observed with in-situ light scattering for in-plane momentum transfers of 32 μm^{-1} ($\cdots$Upper data) and 42.6 μm^{-1} ($\cdots$Lower data). The light scattering was aligned along the [110] direction and sample was grown at a substrate temperature of 450^{o}C and at a Ga flux of 1.09 ML/s.

after the oxide is desorbed, but the annealing stops at longer times. The light scattering signals consistently repeat this pattern. The reason for this halt in smoothing is unknown, but it is believed that surface contamination prevents the oxide desorbed surface from annealing past a certain surface roughness. Carbon impurities are measured by SIMS to be present on the initial surface as shown in Figure 3.10. The pre-growth annealing is sensitive to both the thermal oxide desorption procedure and surface contamination making measurements of the pre-growth smoothing unreliable.

Examples of the annealing of GaAs observed with in-situ light scattering

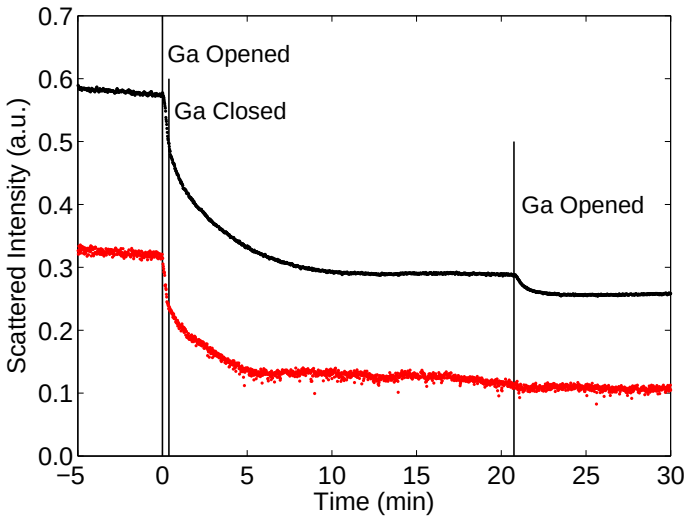

Figure 4.14: Annealing of GaAs as measured with light scattering at 32 μm^{-1} ($\cdots$Upper data) and 42.6 μm^{-1} ($\cdots$Lower data) along the [110] direction. The sample was grown at a substrate temperature of 590^{o}C, and a Ga flux of 1.09 ML/s (when applied). The first Ga cycle was 0.2 minutes.

are shown in Figures 4.13, 4.14, and 4.15. For these runs, the Ga flux was turned on for 93, 40 and 26 seconds respectively. After the brief growth of GaAs a noticeable change can be seen in the light scattering signal after the Ga flux is shuttered. Even after a very brief growth of 26 seconds, as shown in Figure 4.15 the surface continues to anneal.

Surface impurities may have a large effect on the observed smoothing, for annealing during a growth interrupt after a short initial growth. Examine Figure 4.15, where a large impurity bump (as discussed in Section 3.3) is observed after the growth is continued. This experiment suggests that the passivation mechanism of the pre-growth annealing is eliminated by a pulse

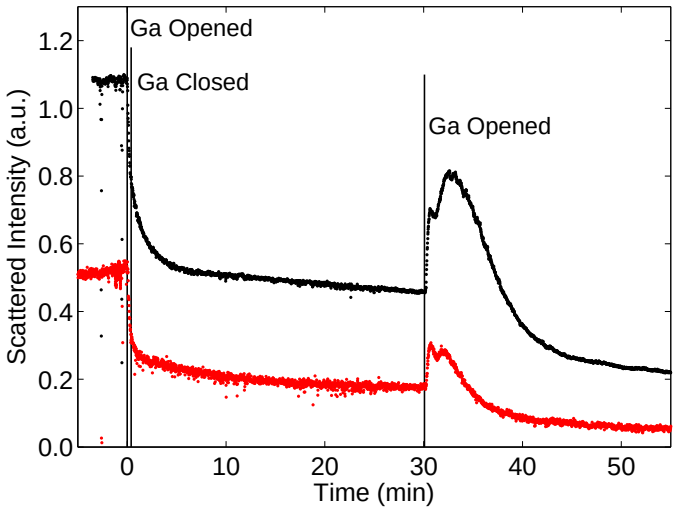

Figure 4.15: A growth interrupt observed with in-situ light scattering displaying an impurity bump, measured along the $[1\bar{1}0]$ direction at 32 μm^{-1} ($\cdots$ Upper data) and 42.6 μm^{-1} ($\cdots$ Lower data). For this sample the substrate temperature was 590^{o}C and the Ga flux was 1.33 ML/s if applied. The first cycle of Ga was 0.37 minutes.

of Ga adatoms. It is believed that the new Ga atoms bury the surface impurities (at least partially) allowing the surface to continue smoothing during the growth interrupt. When the growth is continued the surface impurities are fully covered by the incoming flux of atoms.

The annealing of GaAs is more complex then expected. Figure 4.13 shows an example of a growth interrupt at a low temperature (450^{o}C) and after a long initial growth period. In this figure, the surface initially does not smooth during the anneal, but after 4 minutes the surface begins to smooth again. For the runs displayed in Figures 4.14 and 4.15, smoothing

T (^{o}C)	$\|\vec{q}\|$ (μm^{-1})	Direction	Rate Constant (1/min)	Exponent
450	32.0	[110]	0.0138 (best fit)	-0.1634
450	43.5	[110]	0.0153	-0.197 (best fit)
500	43.5	[110]	0.0381	-
590	32.0	[110]	-	-
590	43.5	[110]	0.197	-
590	32.0	[1$\bar{1}$0]	0.0065 (longer times)	-0.19 (early times)
590	43.5	[1$\bar{1}$0]	-	-0.16

Table 4.1: A summary of smoothing rates during GaAs growth interrupts measured in-situ with light scattering.

is seen immediately after the Ga is shuttered. In all cases the smoothing in a growth interrupt is slower then smoothing observed during the GaAs growth. The behaviour of the smoothing during the growth interrupt is inconsistent, exhibiting a power law dependence on time in some cases and an exponential decay with time at other conditions. Table 4.1 summarizes these results for different substrate temperatures, directions, and spatial frequencies. Numbers in the rate constant column indicate that the smoothing was best characterized by a exponential decay and numbers in the exponent column indicate a power law as the best fit to the data. Numbers in both columns indicate that the fit of the data to both an exponential decay and power law was reasonable.

4.5 Summary and Discussion

In this chapter, in-situ light scattering, RHEED, and ex-situ AFM observations on the GaAs surface during homoepitaxial MBE growth were presented over a large range of substrate temperature, substrate orientation, surface lengthscale, Ga flux and As_2 flux. These measurements were compared to a non-linear continuum growth equation model, a summary of this comparison is displayed in Table 4.2.

For the smoothing of GaAs from thermally de-oxidized surfaces during GaAs homoepitaxy two distinct regimes of smoothing were observed. The experimental measurements taken in the long-time linear smoothing regime were compared to theoretical predictions based on the continuum growth equation model and were found to support it. The agreement between the non-linear growth equation model and the measured Ga flux dependence of the smoothing rates breaks down at low As_2/Ga ratios. However, under these conditions, the effects of arsenic adatoms on the surface are significant, which the non-linear growth equation model does not account for. Additionally, the light scattering measurements of the smoothing that is observed at long times was compared to independent AFM measurements of the step density and found, consistently agreed with each other. These measurements indicate that the smoothing at later times in the growth, when the surface amplitudes are small can be described by a continuum growth equation that is dominated by the first order linear term, $\nu\nabla^2 h$.

The critical island size, an important atomistic growth parameter, can be determined form the experimental measurements The linear smoothing coefficient, ν, and the intrinsic step density, S_o were found to have a power law dependence on Ga flux and the Ga adatom diffusion constant for fluxes

less than 2 ML/s with powers determined by the critical island size. For the the initial smoothing rate a linear dependence on the Ga flux is observed for fluxes less then 0.2 ML/s and a power law dependence on F and D with exponents dependent on the critical island size is observed for fluxes between 0.2 and 2 ML/s. Experimental fits to in-situ light scattering and ex-situ AFM measurements agreed with the critical island size ranging from 1 to 3, however examining all the sets of data, a size of x = 2 is the most consistent. This indicates that the an island consisting of two Ga adatoms is unstable and likely to dissociate. Three Ga adatoms are needed for a stable island to form.

In the continuum growth model it is assumed that there are potential barriers at atomic steps that favour downhill adatom migration. The measured linear smoothing coefficients indicate that adatoms deposited from the vapour onto a stepped surface, migrate in the downhill direction by an average of one interatomic distance, with only a weak dependence on the substrate temperature. This behaviour can be explained by a negative Ehrlich-Schwoebel barrier at step edges and/or by a weak inverse Ehrlich-Schwoebel barrier to adatom incorporation from the lower terrace.

The results from the light scattering measurements on low amplitude smoothing indication that the smoothing can be described by a continuum equation dominated by the first linear term. However, non-linear terms are clearly important in the growth of GaAs since AFM measurements of the shape of the smoothed surface show rounded mounds separated by V-shaped valleys [24]. Continuum equations containing only linear terms predict surface that are symmetric with a vertical inversion, non-linear terms are needed to predict an symmetric surface. The observed lack of inversion symmetry in the surface shape is characteristic of a non-linear continuum

growth equation.

The smoothing that occurs early on in the growth, when surface amplitudes are large, did not consistently agree with predictions from the continuum growth equation model. Even though the measurements taken in the initial regime of smoothing was consistent with some aspects of non-linear continuum growth equation model, such as the Ga flux dependence ($F < 2$ ML/s), the observed temperature and spatial frequency dependence of the initial smoothing were not consistent with predictions from this model. For GaAs growth the starting surface is covered in deep pits, which are a result the thermal desorption of the native surface oxide. The smoothing observed at the start of the growth is dominated by this surface morphology. The angles of the deep pits of the oxide desorbed surface are steep (greater than 5 degrees), and may be beyond the scope of the non-linear continuum growth equation model which assumes low slopes. Additionally, the explosive desorption of the native oxide may leave small artifacts on the surface (not easily observed with AFM), such as small crystallize facets in the pits, which would be beyond the scope of a the BCF based model.

Overall, the substrate temperature and Ga flux dependence of the smoothing rates are consistent with the non-linear continuum growth equation description, in which the parameters in the growth equation are derived from a BCF type atomistic model for epitaxial growth. In this model the step density is the principle experimental parameter which controls the surface smoothing. The smoothing rates measured in the light scattering experiments are in good agreement with theoretical predictions based on independent experimental measurements of the step density obtained from atomic force microscopy images.

Light scattering measurements of long-time smoothing	
Spatial frequency dependence	Agrees
Ga flux dependence: $F > 2$ ML/s	Disagrees, low As_2/Ga ratio effect
$F < 2$ ML/s	Agrees for $x = 2, 3$
Temperature dependence	Agrees for $x = 2$
As_2 flux dependence	Beyond the scope of the model
Light scattering measurements of initial smoothing	
Spatial frequency dependence	Disagrees
Ga flux dependence: $F > 2$ ML/s	Disagrees, low As_2/Ga ratio effect
$0.2 < F < 2$ ML/s	Agrees for $x = 1, 2$
$F < 0.2$ ML/s	Agrees assuming step-flow growth
Temperature dependence	Disagrees
As_2 flux dependence	Beyond the scope of the model
AFM measurements of step densities	
Ga flux dependence	Agrees for $x = 1, 2$
Temperature dependence	Potential agreement, not enough data

Table 4.2: A summary of the different experimental tests of the non-linear continuum growth equation model. The left column contains the various experiments presented in this chapter, the right column describes how the well predictions from the continuum equation model agree with the experimental results.

Chapter 5

GaAs Homoepitaxy on Patterned Substrates

Epitaxial growth on pre-patterned substrates is an important experimental process. The study of it can provide significant insight into the physics of the growth process. A clear understanding of the growth on patterned surfaces is useful for device fabrication [89]. GaAs growth on low-angle (less then 30^o) patterned substrates has been studied previously [11, 12, 90, 91]. In these studies, the time evolution of the surface shape, and the effects of substrate temperature, lengthscale, and duty cycle have been examined and compared to kMC and continuum equation models. This thesis focuses on the effect of growth rate on the surface shape evolution and reveals new features that have not been observed previously. This chapter starts by presenting measurements of the time evolution of the surface shape. Experimental results on the effect of the magnitude of the Ga flux and low-angle slope formation are presented in Section 5.2. The chapter finishes with a discussion on the physical origin of the observed phenomena.

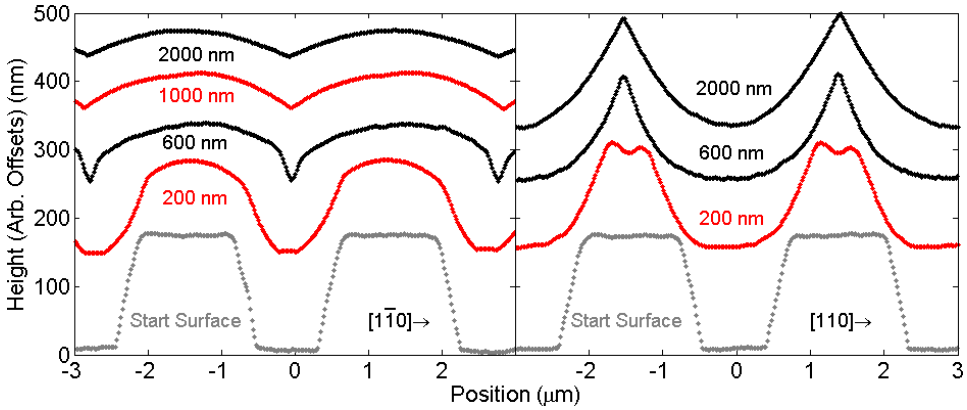

Figure 5.1: AFM line scans of 3 μm pitch gratings aligned perpendicular to the [1$\bar{1}$0] (left) and [110] (right) crystalline axes with GaAs deposited at various depths. The GaAs was grown at 0.86 ML/s and 500^{o}C.

5.1 Time Evolution

The time evolution of the surface shape can be observed by conducting a series of GaAs growths on patterned substrates at the same growth conditions but different thicknesses of deposited material. Figure 5.1 shows the evolution of the surface morphology for GaAs epitaxy starting from 3 μm gratings aligned perpendicular to the [1$\bar{1}$0] and the [110] crystalline directions. The surface shapes produced during GaAs growth on these patterned substrates are complex. The topography of the gratings shown in this chapter are consistently asymmetric. In the left image of Figure 5.1 the ridges of the gratings are observed to become rounded mound-like structures after growth, while the valleys evolve to a pointed and cuspy structure. This mound and V-groove (or W-groove) structure is seen throughout this work, even GaAs grown on randomly roughened substrates will acquire these fea-

tures. This morphology is also similar to the morphology that is seen during unstable growth [22, 23].

However, in this work a new characteristic shape is observed that has not been previously seen in GaAs homoepitaxy. In some of the AFM images the ridges of the line gratings were observed to be cuspy and the valleys to be rounded, as exemplified by the right image in Figure 5.1. These features were often manifested during the growth on gratings aligned perpendicular to the [110] direction. In Figure 5.1 the characteristic shape of the surface was inverted when the alignment of the 3 μm line gratings were rotated by 90^o. At the MBE conditions of the growths in Figure 5.1 the anisotropy seen between the two crystalline directions is not expected to be large. However, massive differences in the lateral smoothing are observed. Additionally, the smoothing is stronger for the downward cuspy surface then the inverted symmetry structure. This indicates that the physics that produced the cuspy structures are sensitive to minor changes in the growth conditions.

The overall time evolution of the patterned surfaces morphology shown in the left image of Figure 5.1 is similar to the time evolution observed in [11], which also examined epitaxial GaAs growth on 3 μm gratings. Though similar surface shape evolutions were observed for these two sets of experiments, the MBE growth conditions differed. In [11], the gratings were aligned perpendicular to the [110] crystalline direction and grown at 1 ML/s, 580^oC, and a low As_2/Ga ratio of 3:1. To a lesser extent the shape evolution of patterned surfaces seen by [12] is also similar to the evolution seen in the left part of Figure 5.1. However, structures like those seen in the right image of Figure 5.1 have not been observed before.

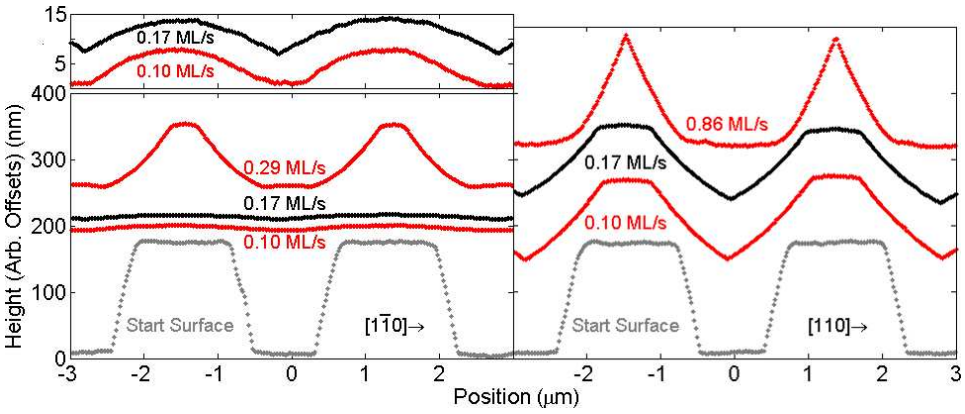

Figure 5.2: AFM line scans of 3 μm pitch gratings aligned perpendicular to the [1$\bar{1}$0] (lower left) and [110] (right) directions grown at various Ga fluxes. The GaAs layers were grown to a thickness of 200 nm, at 590^{o}C. The upper left image is an expanded view of the 0.10 ML/s and 0.17 ML/s line scans shown in the left image.

5.2 Growth Rate Evolution

The effect of growth rate on the surface shape evolution in GaAs homoepitaxy on 3 μm gratings has been studied for a variety of MBE growth conditions. Complex morphologies which are similar to those observed in Section 5.1 are seen for the gratings presented in this section. For example, an inversion in the symmetry of the surface structure can be seen in the right panel of Figure 5.2. For the experiments in this figure the GaAs grown at 0.86 ML/s has upward cuspy features which is in contrast to the gratings grown at lower fluxes. Another interesting feature seen in the AFM images for samples grown at 0.17 and 0.10 ML/s, shown in Figure 5.2, is the vast difference in amplitude reduction between gratings aligned perpendicular to

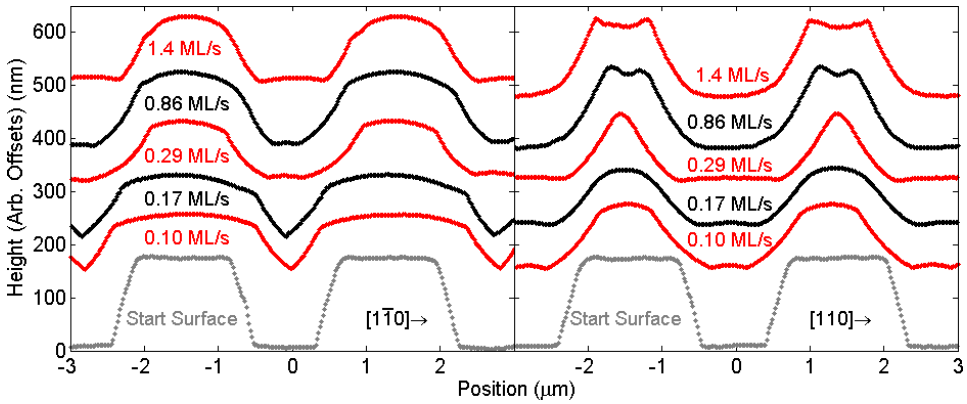

Figure 5.3: AFM line scans of 3 μm pitch gratings aligned perpendicular to [1$\bar{1}$0] (left) and [110] (right) axis grown at various Ga fluxes. The GaAs layers were grown to a thickness of 200 nm at 500^{o}C.

the [1$\bar{1}$0] and [110] crystalline directions. For the low flux growths, the gratings aligned perpendicular to the [1$\bar{1}$0] axis are almost washed out, while the GaAs grown at the exact same conditions but rotated 90 degrees has amplitudes that are similar to the original fabricated pattern. The surface amplitude is smoothed 14 to 16 times faster when the gratings are aligned parallel to the [1$\bar{1}$0] crystal axis.

Note that the material deposited is the same for each set of experiments presented in Figures 5.2 and 5.3. Growths conducted at lower fluxes are held at the growth temperature for longer times, thus the effects of substrate temperature is stronger for these samples. The effect of substrate temperature on patterned surfaces was studied by [11], where temperature was varied for GaAs homoepitaxy on patterned surfaces at conditions that are similar to those used in this work. From [11] it is clear that patterned surfaces grown at low temperatures retain more of the original starting features than surfaces

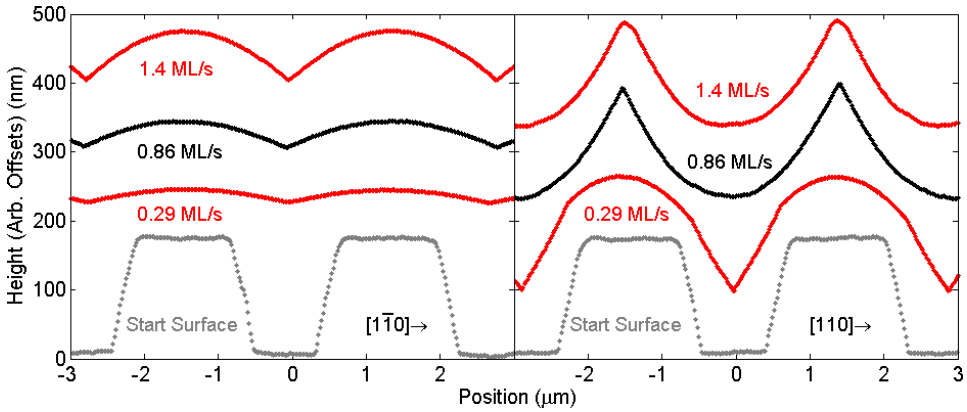

Figure 5.4: AFM line scans of 3 μm pitch gratings aligned perpendicular to the [1$\bar{1}$0] (left) and [110] (right) directions grown at various growth rates. The GaAs layers were grown to a thickness of 2000 nm at a substrate temperature of 500^{o}C.

grown at high temperatures. This will result in less amplitude reduction for growths conducted at low temperature, which can be seen by comparing the gratings grown at 590^{o}C (Figure 5.2) to those grown at 500^{o}C (Figure 5.3). The surface amplitudes and smoothing rates are close to being the same as a function of growth rate for the lower temperature experiments.

More examples of the V-groove and rounded mound morphology and the inversion of these features are seen in Figure 5.3. In the right image in Figure 5.3, the asymmetry of the surface morphology is observed to invert as the growth rate is increased. The AFM line scan of the growth at 0.29 ML/s in the right image of Figure 5.3 exhibits cuspiness at both the ridges and valleys. This is an example of a transition of state in the characteristic surface shape.

Gratings with 2000 nm of GaAs deposition exhibit the same trends as

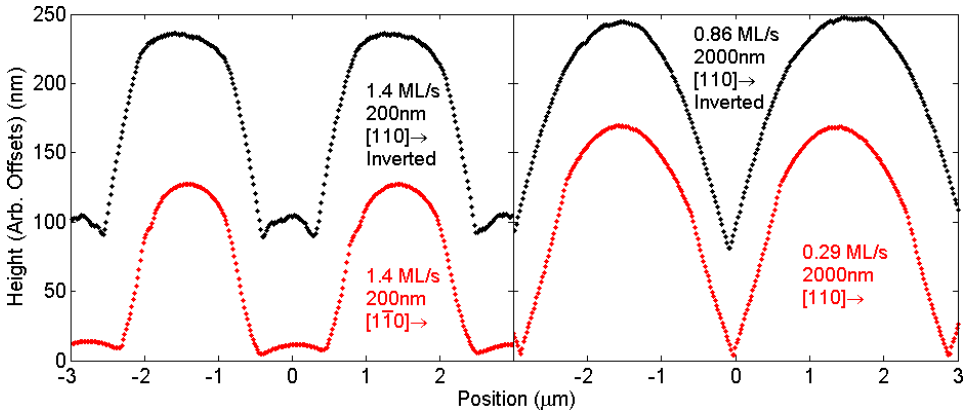

Figure 5.5: Select AFM line scans displayed to compare the V-groove and mound morphology with the inverted symmetry morphology. The upper curves in the left and right images have been flipped with respect to the horizontal axis. All growths were conducted at 500^{o}C.

gratings with 200 nm of growth as shown in Figures 5.3 and 5.4. Again, a significant difference in the surface morphology is seen when the alignment of the gratings is changed with respect to the crystallographic axes. Even with a significant amount of material deposited the growths on gratings aligned perpendicular to the [110] direction, while having lost the original surface shape, retain the initial surface amplitude. The same cannot be said about the growths on gratings aligned perpendicular to the [1$\bar{1}$0] crystalline axis, where the surface amplitude is significantly reduced. Additionally, the two observed characteristic shapes are remarkably similar to each other, as the vertically flipped AFM line scans in Figure 5.5 shows.

Consistently, the smoothing of the patterned structure is weak when the inverted symmetry morphology is manifested. Patterned structures grown under conditions that result in an inversion of symmetry have amplitudes

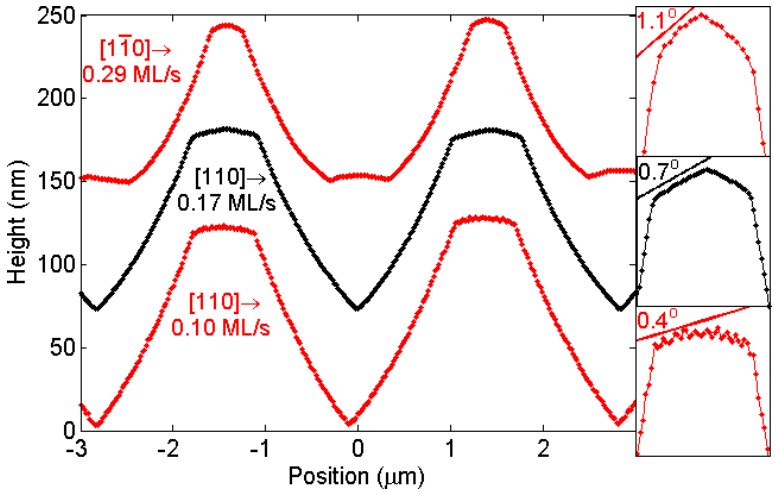

Figure 5.6: AFM lines of 3 μm pitch gratings aligned along the [110] and [1$\bar{1}$0] directions with 200 nm of GaAs growth at 590^{o}C and at Ga fluxes of 0.10, 0.17, and 0.29 ML/s. The small boxes on the right are expanded views of the low angle facets.

that are similar to the initial 3 μm grating, even after 2 μm of material is deposited as shown in the right image of Figure 5.4. Additionally, the smoothing is weak at conditions that manifest downward cuspy structures that are near the inversion symmetry transition. As gallium flux is increased the smoothing become progressively weaker, even changing the symmetry of the growth under certain conditions.

5.3 Slope Section

Another phenomenon seen in GaAs homoepitaxy on large amplitude structured surfaces is the emergence of a low angle facet in the surface morphology [6, 11]. Such facets are observed in the AFM line scans shown in Figure 5.6,

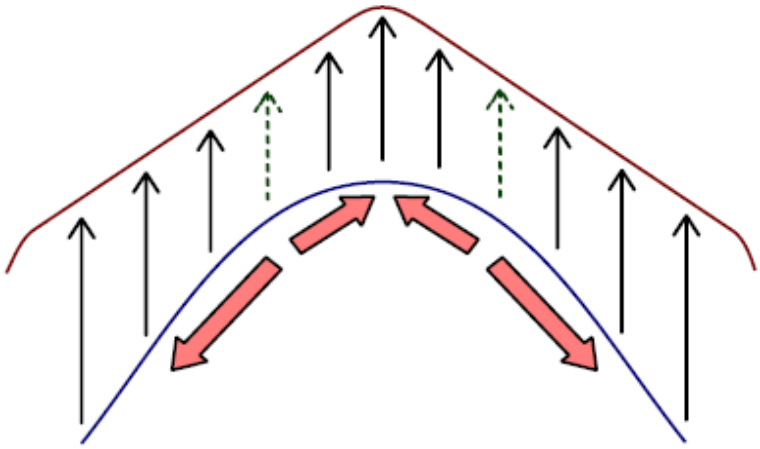

Figure 5.7: Schematic diagram of low angle facet formation that occurs on a patterned substrate. The arrows indicate the local growth rates. A minimum in the step density occurs at the dashed arrow. This figure is reproduced from [6].

where slopes of 0.4^o, 0.7^o, and 1.1^o are measured. These low angle slopes are due to atomic scale mechanisms on the surface and are not related to the formation of other crystalline facet planes. Growth on artificially fabricated structures that include crystalline facets have been studied [84, 92]. These works provide useful insights into homoepitaxy on the (001) GaAs surface. However the angles of commonly seen crystalline facets are significantly larger then the observed low angle slopes measured in this work.

A minimum in the slope dependant step density was found at low slopes and at high substrate temperatures by Jones et al [6] using kMC simulation. This minimum in the step density can lead to the formation of a facet with a slope that corresponds to this minimum. Areas with a low step density

will capture fewer adatoms than high step density areas and thus will have a higher adatom density. The high adatom density in the area of minimum step density will encourage diffusion of these adatoms to areas of high step density. This will lead to a situation depicted in Figure 5.7, where material is moving away from the area of minimum step density. This will result in faster growth rates in regions not at the minimum step density. The slopes of the fast growing regions will move towards the slope that corresponds to the minimum in the step density, eventually matching this slope yielding a facet on the peaks of the gratings as shown in Figure 5.6.

The physical origin of the minimum in the step density, which is described in detail in [6], arises from differences in adatom capture efficiency of vicinal steps of a sloping surface and circular steps of a flat surface. Steps in a parallel configuration are more efficient at capturing free adatoms than steps in a circular configuration. For a growing surface the rate of island nucleation which determines the step density must match the rate of incoming atoms in order to maintain stable epitaxial growth. In order to capture all the incoming adatoms a flat surface with only circular steps will need to have a higher step density than a similar low slope surface with a few vicinal steps. The density of vicinal steps is determined by the slope of the surface and at high slopes the step density will increase as $\nabla h/a$. These factors lead to a minimum in the step density and to the formation of low angle facets.

The observed slopes shown in Figure 5.7 are consistent with the model and AFM images presented by Jones et al [6]. In this thesis low angle facets were not observed for experiments conducted at the low substrate temperature of 500^oC, only for GaAs grown at 590^oC. This agrees with [6], as that work predicted that the minimum in the step density, which drives the formation of a facet, is not present at low substrate temperatures.

Additionally, it should be noted that Equation 2.4 is unable to reproduce the observed slopes as the physics involved is not included in the theory behind this equation.

5.4 Summary and Discussions

Interesting and complex structures have been observed in the surface morphology of patterned GaAs grown at typical MBE conditions. The classic V or W-groove feature accompanied by a rounded peak has been observed throughout this work. Surface shapes similar to these have been observed in other works [11, 12]. Of interest is the observed inversion of the symmetry of this structure, where the peaks are cuspy and the rounded features are located in the valleys, which have not been seen before. Additionally, three examples of the formation of low angle slope were observed.

The nature of the steps on the surface of a patterned substrate will lead to the downward cuspy round mounded surface shape and the inverted symmetry surface morphology. Initially, the 3 μm line grating is composed of nearly flat regions in the peaks and valleys with sloping sections in between. In the nearly flat peaks and valleys of the grating the steps will be circular, as depicted in Figure 5.8. Vicinal steps are imposed on the sloping parts of the grating cycle which will damp the formation of circular steps on the terraces. On the (001) GaAs surface there are two types of steps, those aligned along the [110] direction ($S_{[110]}$) and those along the $[1\bar{1}0]$ direction ($S_{[1\bar{1}0]}$). For gratings fabricated such that the ridges are parallel to a crystalline axis the steps on the sloping regions will be primarily one type of step. In the flat sections of the gratings, the roughly circular step patterns will be composed of both types of atomic step. As illustrated in Figure 5.8, the roughly circular

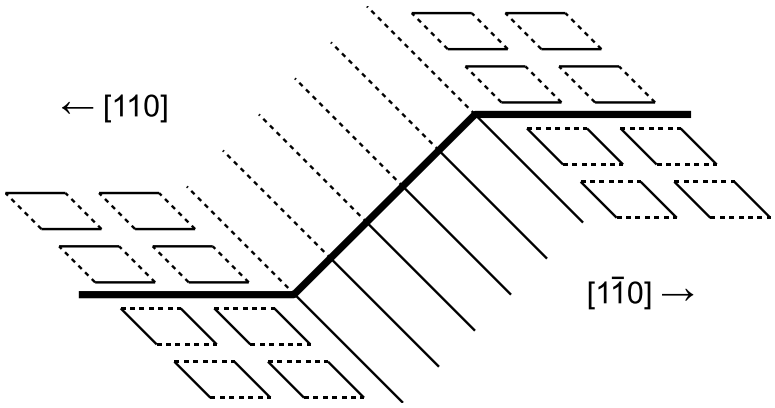

Figure 5.8: Schematic illustration of the steps on gratings aligned perpendicular to the [110] direction (upper part) and the [1$\bar{1}$0] direction (lower part). The dashed lines indicate a weaker adatom capture efficiency for the steps parallel to the [110] direction.

islands are represented as identical squares. At large slope the density of steps that are parallel to the ridges of a grating is $\nabla h/a$, while at zero slope this density of step is $S_o/2$, where S_o is the average density of steps at zero slope. Interpolating between these two points the density of steps parallel to the grating is:

$$S_{\parallel} = \sqrt{(S_o/2)^2 + (\nabla h/a)^2} \tag{5.1}$$

where S_o is determined from Equation 2.10. Subtracting the density of parallel step from the total step density (Equation 2.7), the density of steps perpendicular to the grating:

$$S_{\perp} = S - S_{\parallel} = \sqrt{(S_o)^2 + (\nabla h/a)^2} - \sqrt{(S_o/2)^2 + (\nabla h/a)^2} \tag{5.2}$$

The densities of parallel and perpendicular steps are plotted in Figure 5.9.

Throughout this chapter a significant difference has been observed be-

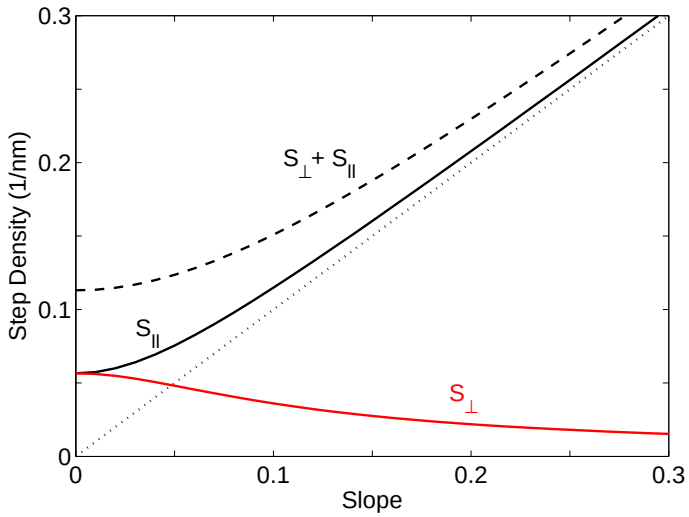

Figure 5.9: Density of steps that are parallel ($S_{\|}$) and perpendicular ($S_{\perp}$) to the ridges of a grating as calculated from the interpolation formulas Equations 5.1 and 5.2, for a Ga flux of 0.1 ML/s and a substrate temperature of 500^{o}C. The dashed line is the total step density and the dotted line is the step density due to the slope ($\nabla h/a$).

tween the smoothing of 3 μm line gratings aligned perpendicular to the $[1\bar{1}0]$ and [110] crystalline directions. For growth on ridges aligned perpendicular to the [110] axis, slower smoothing and a transition to the inverted symmetry structure is seen. It is reasonable that adatoms attach to steps perpendicular to the $[1\bar{1}0]$ direction more efficiently than to steps perpendicular to the [110] direction. For the (001) GaAs surface this argument is reasonable if we consider the surface reconstruction at the temperatures used during growth. STM measurements of the arsenic rich (2×4) surface reconstruction observe rows of arsenic dimers along the $[1\bar{1}0]$ direction [2].

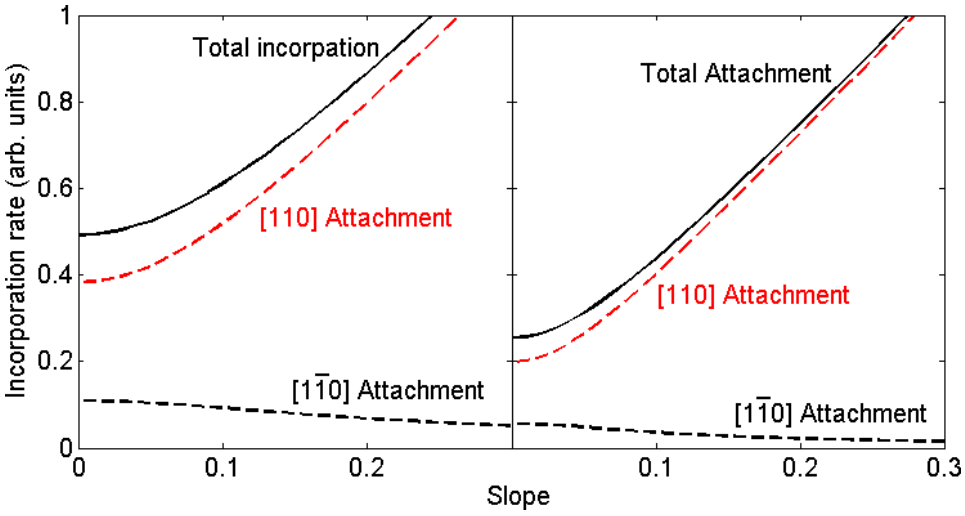

Figure 5.10: Adatom incorporation for grating with vicinal steps perpendicular to the [1$\bar{1}$0] crystalline direction at 1.4 ML/s (left image) and 0.1 ML/s (0.1 ML/s). An anisotropy in the capture efficiency of steps of 4 was used in Equation 5.3.

A step edge along the [110] crystalline axis would correspond to a break in these dimer rows, which adatoms can efficiently attach to.

The adatom incorporation rate will be proportional to the step density times the capture efficiency at the steps:

$$Incorporation\ rate \propto S_{[1\bar{1}0]} + \dot{A}S_{[110]} \tag{5.3}$$

where $\dot{A}$ is a parameter which describes the anisotropy in the step adatom capture efficiency. Figures 5.10 and 5.11 display examples of the incorporation rate determined from Equation 5.3 using the step densities determined from Equations 5.1 and 5.2. The two characteristic surface shapes and the different non-linear smoothing rates at low and high fluxes can be explained in terms of the adatom incorporation rates shown in Figures 5.10 and 5.11.

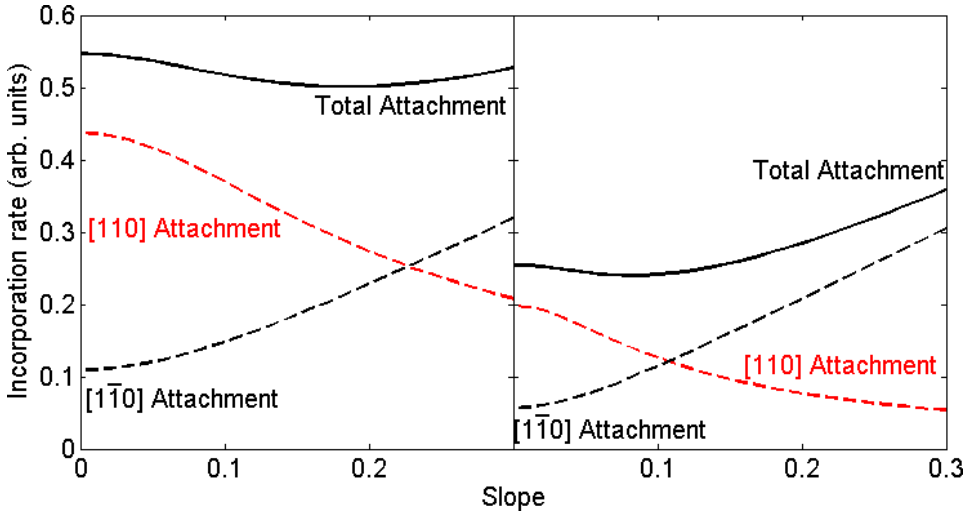

Figure 5.11: Adatom incorporation for grating with vicinal steps perpendicular to the [110] crystalline direction at 1.4 ML/s (left image) and 0.1 ML/s (0.1 ML/s). An anisotropy in the capture efficiency of steps of 4 was used in Equation 5.3.

For gratings aligned perpendicular to the [1$\bar{1}$0] direction, the adatom incorporation rate on the sloping sections of the grating is higher than the incorporation rate on the nearly flat peaks and valleys, as shown in Figure 5.10. Thus, the flat regions will have a higher adatoms density than the sloping parts as adatoms are less likely to incorporate into a step edge. On average Ga adatoms will diffuse from the flat regions onto the sloping parts of the grating in this situation. Thus, if a sloping part of the grating is near a flat region, the sloping part will grow faster at the expense of the flat region which will grow slower than the normal grow rate.

The downward cusp, rounded mound surface shape case is displayed in the left side of Figure 5.12. Consider the smoothing that occurs in the valley

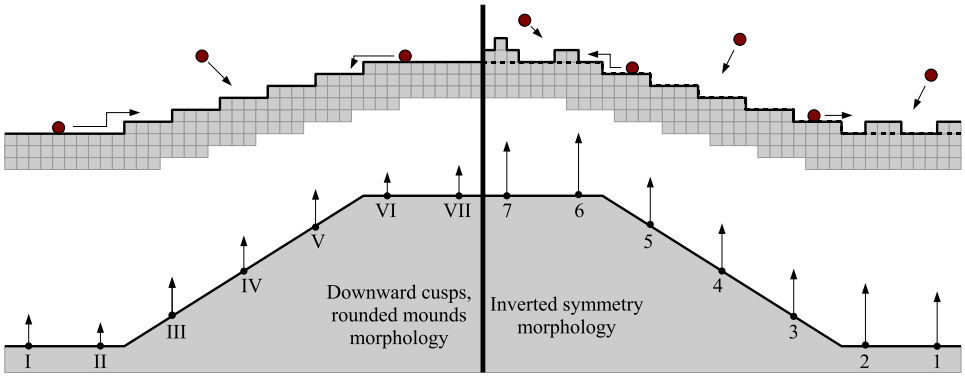

Figure 5.12: Pictorial description of GaAs growth on gratings. The vertical arrows indicate the local growth rate.

of the grating cycle (points I to III). The centre of the valley (point I) is affected less by the distant sloping part of the grating and this area grows at the normal growth rate. The growth rate is reduced in the valley near the sloping part (point II), as adatoms are lost to the nearby sloping region (point III) where the growth rate is increased. The differences in the growth rates of these three points will lead to the formation of the characteristic W-groove shape, as exemplified in the left image of Figure 5.3. The sloping region of the grating is growing faster than the flat valley, which will overtime fill in the valley until the characteristic V-groove shape is seen. At the peaks (points V to VII) the different growth rates in flat and sloping areas will produce rounded features. The sloping part (point V) will grow at a faster rate than the nearby flat region (point VI), this will reduce the difference in slope between these two regions and round the peak. Additionally the faster growth rate in the centre of the peak (point VII) will also round out the flat region.

The non-linear smoothing of the patterned substrates is observed to

decrease as the growth rate is increased. As the Ga flux is increased the step density on a flat surface is increased, as from Equation 2.10. This results in less of a difference between the incorporation rates of the flat and sloping sections of the grating, which can been seen by compare the right and left images of Figure 5.10. In this case the step density is more uniform across the surface and the different parts of the surface will grow at rates that are more similar to each other. This accounts for the observation that smoothing is reduced for growths conducted at high Ga flux.

For gratings aligned perpendicular to the [110] direction a minimum in the adatom incorporation rate can occur, as shown in the left image of Figure 5.11. At high Ga flux and the lengthscales of the 3 μm gratings that were grown on, the adatom incorporation rate on the sloping sections is smaller than the incorporation rate on the flat regions. In this situation adatoms on average will diffuse from the sloping sections onto the flat regions, as depicted in the right side of Figure 5.12. Consider the valley of the grating in this case (points 1 to 3). The flat region near the sloping region (point 2) will have a higher growth rate while the sloping section (point 3) has a lower than average growth rate. This differences in growth rates will round out the valley. At the peak (points 5 to 7) the flat region near the sloping section (point 6) has the highest growth rate. A higher growth rate at this point will result in an inverted W-groove structure as seen in the right image of Figure 5.3. The inverted V-groove structure will form later as material moves away from the sloping section, reducing the width of the peak over time.

As the growth rate is decreased (by decreasing Ga flux) a transition from the characteristic inverted symmetry morphology to the downward cusps, rounded mound surface shape occurs, as observed in the right images

of Figures 5.3 and 5.4. At low fluxes the minimum in the step density is less pronounced and occurs at a lower slope than the minimum that is seen at high fluxes, as shown in Figure 5.11. For the lengthscales of the patterned substrates used in this thesis, at low Ga fluxes the adatom incorporation rate on the sloping sections of the grating aligned perpendicular to the [110] axis is still higher than the incorporation rate on the nearly flat peaks and valleys. These conditions will lead to a weak downward cusp, rounded mound surface shape will manifest.

The anisotropy in the step adatom capture efficiency, $\dot{A}$ was chosen to be 4 as this value causes the minimum at high fluxes to be located at a slope that is similar to the slopes observed in Figure 5.4. A minimum in the incorporation rate, as shown in Figure 5.11, can lead to the formation of a stable slope during the growth, as discussed in Section 5.3. Note that slope selection effect reported by Jones et al [6] was due to a difference in capture efficiency between vicinal and circular configuration of steps that did not include an anisotropy in the adatom capture efficiency of the [110] and $[1\bar{1}0]$ steps. This difference in capture efficiency between vicinal and circular steps was not included in the previous discussion of this section.

The cuspy features that form during the growth on patterned substrates are indicative of non-linear growth in GaAs homoepitaxy. In terms of continuum growth equation models linear terms lead to surface structures that are symmetric when the surface is flipped over the horizontal axis. Non-linear terms will yield structures that are asymmetric when flipped over the horizontal axis. Equation 2.4 predicts the observed downward cuspy structure, as shown by the dashed red line in Figure 5.13, however the inverted symmetry structure is beyond this equation. This non-linear continuum equation was derived assuming that the step density always increases with slope, as

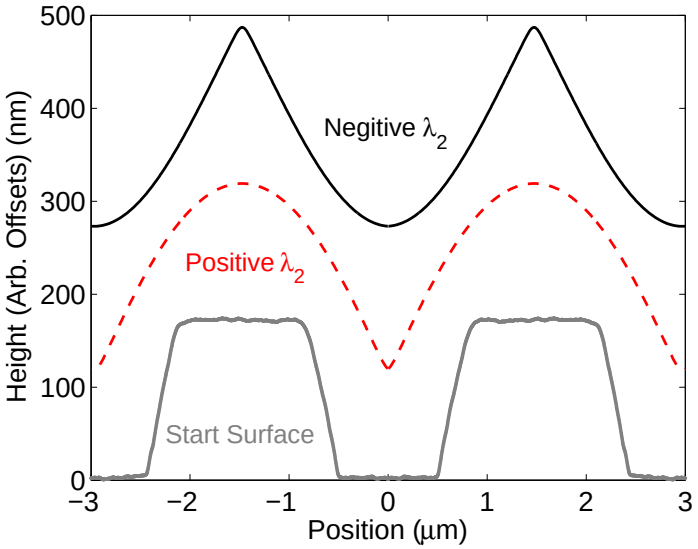

Figure 5.13: Numerical solutions of Equation 3.3 starting on patterned surfaces. The simulations in this figure were ran to a depth of 200 nm at $\nu = 5\ nm^2/s$, and $\kappa = 10^5\ nm^4/s$. The dashed red line represents a simulation run with $\lambda_2 = 10^7 nm^3/s$, and the solid black line represents a simulation run with $\lambda_2 = -8 \times 10^6 nm^3/s$

in Equation 2.7 and did not take the anisotropy in capture efficiencies of different steps into account [1]. As shown in Figure 5.9, the step density will effectively decrease with increasing slope at the conditions that produced the inverted symmetry surface shape. With step density decreasing with slope the non-linear term in Equation 2.4 would be negative ($\lambda_2 < 0$). Equation 2.4 with a negative non-linear term lead to the inverted symmetry surface morphology that is observed in this chapter, as shown by the solid black line in Figure 5.13.

Growth on patterned substrates is a critical step in the manufacturing of

electronic and optical devices. The results presented in this chapter provide a guide to growing on patterned (001) GaAs substrates, which is useful for device fabrication. The surface morphology of a patterned substrate shows less distortion after disposition of an overlayer at high growth rates than growth at low Ga fluxes. The alignment of a pattern respect to the crystalline axes is important, as a pattern aligned along the $[1\bar{1}0]$ direction can evolve into a drastically different shape than the same pattern aligned along the [110] direction. Additionally, the anisotropy in the adatom capture efficiencies of the $[1\bar{1}0]$ and [110] steps indicates that the miscut in vicinal substrates should be aligned along the [110] direction in order to promote faster smoothing.

Chapter 6

Bismuth Assisted GaAs Growth

Interest in the uses of surfactants during MBE growth and device fabrication has increased recently [50, 93]. In the epitaxial growth of the group III-V class of materials several cases of surfactant assisted growth have been reported [5, 35, 38, 94–97]. It is shown that the adatom dynamics of the surface can be drastically altered by a surfactant. In particular these researchers have reported a number of cases in which the optical or electrical properties of the material have been improved, or the surface roughness has been reduced by adding a surfactant into the system. The large size on the Bi atom means that it tends to surface segregate, which makes it an ideal surfactant. During film growth up to one monolayer of bismuth will sit on the surface of GaAs for substrate temperatures less than 500^{o}C in a liquid-like state. Gallium and arsenic atoms are transported through this uppermost layer to the GaAs surface, while bismuth itself does not incorporate into the bulk material [16, 38]. Additionally, these works suggest that Bi modifies surface potentials such that Ga adatom diffusion is increased and that transportation between atomic terraces is increased.

This work focuses on bismuth as a surfactant in the homoepitaxial growth of GaAs under MBE growth conditions that are not favourable to Bi

incorporation or metal droplet formation [9]. Using the methods described in Section 3.3, this work probes the atomic scale mechanisms of MBE growth on the (001) GaAs surface in the presence of the bismuth surfactant. The chapter starts by presenting the observed effects of Bi on the smoothing coefficients (ν and the initial smoothing rate) as measured with in-situ light scattering. Ex-situ AFM measurements of GaAs grown on randomly rough and patterned surfaces are then presented. Finally, the observations of Bi on GaAs are discussed in terms of the continuum growth equation model.

6.1 In-situ Measurements

In-situ light scattering measurements presented in this section have show that the application of bismuth to GaAs homoepitaxy alters the smoothing from what is typically observed during growth on randomly rough GaAs substrates. The smoothing was observed to increase at high spatial frequency, while at low q the smoothing was found to decease. This section will show that the light scattering measurements of the smoothing indicate that Bi changes the characteristic shape seen in the power spectral density of the GaAs surface after growth.

The observed trends seen with in-situ light scattering during the smoothing of the oxide desorbed surface did not change when Bi was applied. In the growth of GaAs with Bi light scattering consistently showed a fast regime of smoothing at the start of the growth followed by a slower linear smoothing at later times, as exemplified in Figure 3.8. As discussed in Section 3.3, an apparent initial regime of growth is seen at early times and an exponential decay with time is seen at later times. The smoothing coefficients measured for GaAs with a Bi surfactant were treated the same way as ν and initial

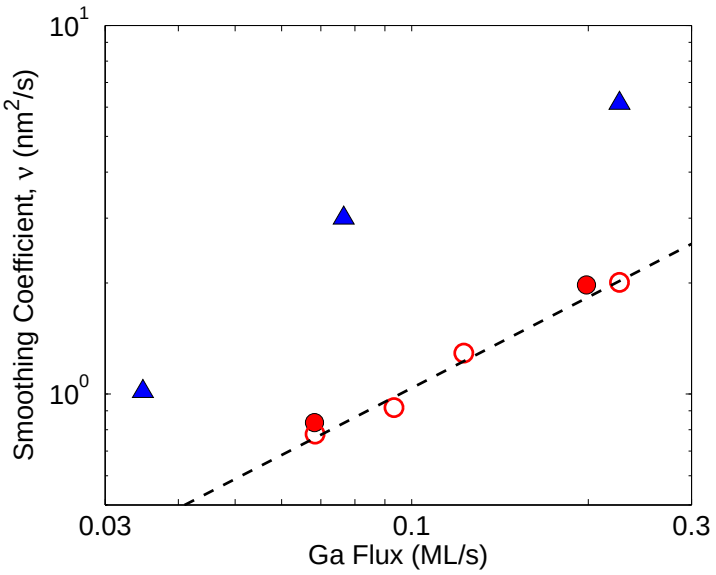

Figure 6.1: Linear smoothing coefficient versus Ga flux with (▲) and without (● 500^{o}C, and ○ 550^{o}C) Bi flux as measured along the [1$\bar{1}$0] direction at 32.0 μm^{-1}. The samples were grown at 500^{o}C and the Bi flux was 3.3 ML/s.

smoothing rate as measured for growth without Bi, as in Chapter 4.

The smoothing coefficients have been measured for GaAs homoepitaxy with Bi applied as a surfactant for smoothing on randomly rough oxide desorbed surface. Light scattering measurements at a spatial frequency of 32 μm^{-1} of ν and the initial smoothing rate are presented in Figures 6.1 and 6.2. Smoothing coefficients presented previously in Chapter 4 are also in these figures in order to illustrate the magnitude to which Bi increases the smoothing. In Figures 6.1 smoothing coefficients from run conducted at 550^{o}C were included since little to no temperature dependence is seen for GaAs grown at low growth rates. Note that the faster smoothing rates

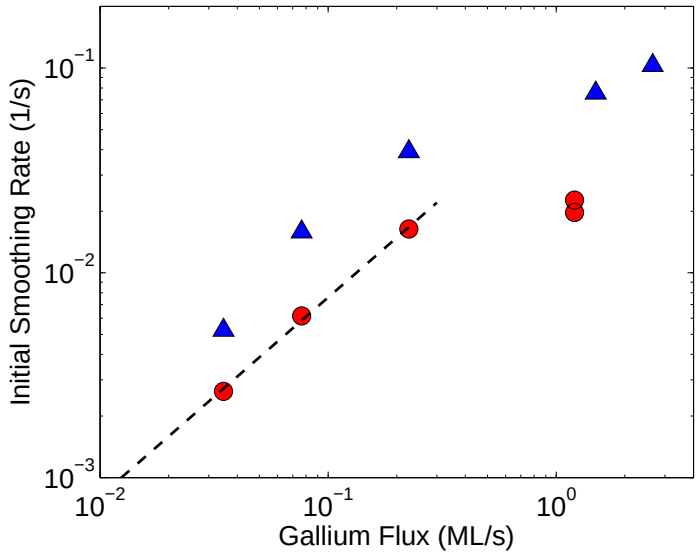

Figure 6.2: Initial smoothing rate versus Ga flux with (▲) and without (●) bismuth surfactant as measured along the $[1\bar{1}0]$ direction at a spatial frequency of 32 μm^{-1}. The samples were grown at a substrate temperature of 500^{o}C and a Bi flux of 3.3 ML/s.

resulted in a significant reduction in the light scattering signal during the time when the linear smoothing coefficient was typically measured, making the measurement of ν more difficult. For a large range of growth rates the smoothing as described by ν and the initial smoothing rate were observed to increase with the addition of a Bi flux, at a substrate temperature of 500^{o}C and a spatial frequency of 32 μm^{-1}. In this case, a Bi flux of 3.3 ML/s increased ν by a factor of 6. Bi had less of an effect on the initial smoothing rate, only increasing it by a factor of three. The surfactant effect was not affected by the growth rate since both smoothing coefficients increased by a

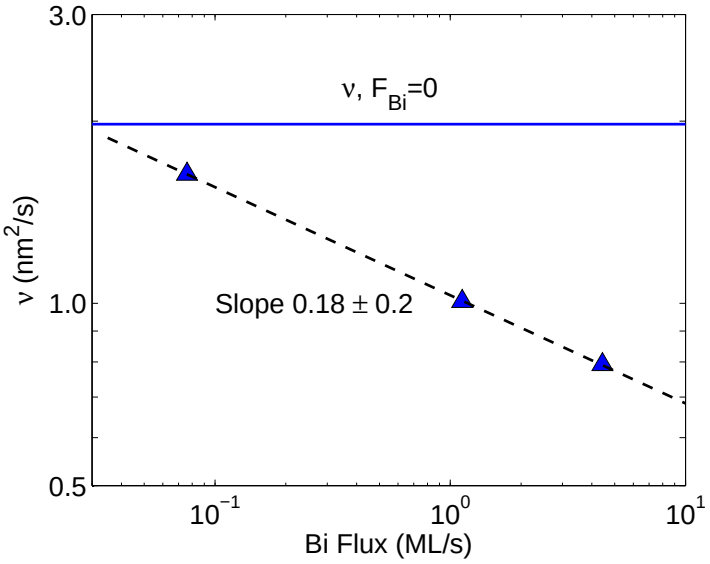

Figure 6.3: Linear smoothing coefficient versus Bi flux as measured with light scattering along the $[1\bar{1}0]$ direction at $q = 17\ \mu\text{m}^{-1}$. The GaAs was grown at 0.29 ML/s and 500^{o}C. The solid line is ν measured without bismuth.

constant factor independent of the Ga flux.

The light scattering measurements at 32 μm^{-1} of the smoothing of the GaAs surface are consistent with other work [5, 38], in that Bi was found to make the GaAs surface smoother than GaAs grown without a surfactant. However, in contrast to measurements at 32 μm^{-1} and other work, the smoothing coefficients observed at a spatial frequency of 17 μm^{-1} were found to decrease with the addition of bismuth. This decrease of the smoothing at large lengthscales when Bi is added system is an unanticipated result since previous studies of Bi on group III-V materials have found that Bi reduced the surface roughness [5, 35, 38, 97]. Figures 6.3 and 6.4 show the

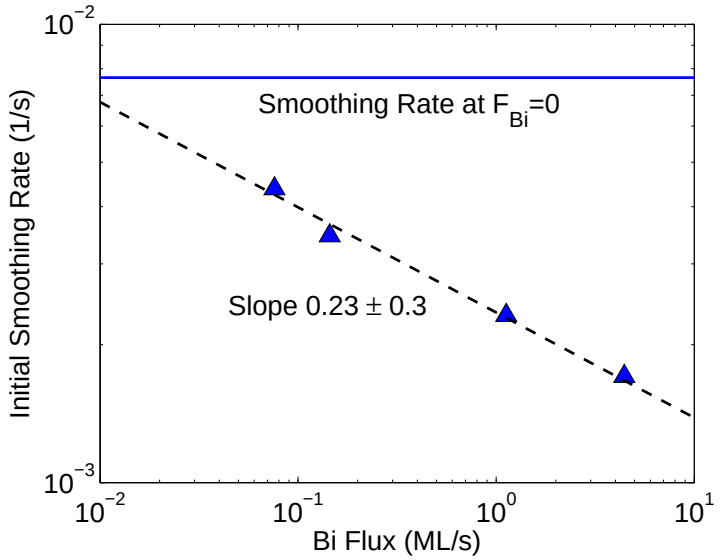

Figure 6.4: Initial smoothing rate versus Bi flux as measured with light scattering along the $[1\bar{1}0]$ direction at a spatial frequency of 17.0 μm^{-1}. The GaAs was grown at 0.29 ML/s and 500^{o}C. The solid blue line is the smoothing coefficient measured without bismuth.

smoothing coefficients versus Bi flux. The growth of GaAs without Bi is represented by the solid lines in Figures 6.3 and 6.4. At $q = 17$ μm^{-1} the Bi flux dependence of ν and the initial smoothing rate are similar to each other. Both ν and the initial smoothing rate were found to decrease with increasing Bi flux as a power law, with respective powers of -0.18±0.2 and -0.23±0.3.

The spatial frequency dependence of the smoothing at long times under the effect of bismuth can be estimated by examining the light scattering measured smoothing coefficients in Figures 6.1 and 6.3 at a Bi flux of 3.3 ML/s and a Ga flux of 0.29 ML/s. If a power law dependence of the smoothing

on spatial frequency is assumed, the estimate yields an exponent near 4. In Section 4.1.1 the smoothing measured at long times was shown to have a power law dependence on spatial frequency with an exponent of close to 2. It was also shown that this $\vec{q}$ dependence is predicted by a continuum growth equation model that is dominated by the first order linear term, $\nabla^2 h$. Similarly, a continuum growth equation model dominated by the second order linear term, $\kappa\nabla^4 h$ predicts the smoothing has a power law dependence on $\vec{q}$ with an exponent of 4. This can be seen by solving a continuum equation dominated by the second order linear term, $\partial_t h = \kappa\nabla^4 h$. A power with an exponent of 4 in spatial frequency dependence as was estimated from the light scattering measurements indicates that the second order linear term dominated continuum equation describes the growth of GaAs with Bi surfactant.

The second order linear term, $\kappa\nabla^4 h$ has been used to study GaAs homoepitaxy before, such as with studies of GaAs surface morphology using the MBE equation [26, 27] which was discussed in Section 2.2. Thus, it is reasonable that continuum growth equation models based on the $\kappa\nabla^4 h$ term would be able to predict phenomena observed during GaAs growth altered by the addition of Bi surfactant. Addition, the physical form of second order smoothing coefficient, κ has been calculated in [98], in this work it was found that $\kappa \propto F/S_o^4$. It should be noted that second order linear term discussed in this Chapter differs from the second order linear term in the continuum equation used for numerical simulations as discussed in Section 3.5. In Section 3.5 a $\kappa\nabla^4 h$ term was added to the non-linear continuum growth equation described by Equation 2.4 in order to promote the stability of this equation during the numerical simulations. In this case the values of κ were sufficiently small, such that they did not effect the outcome of the

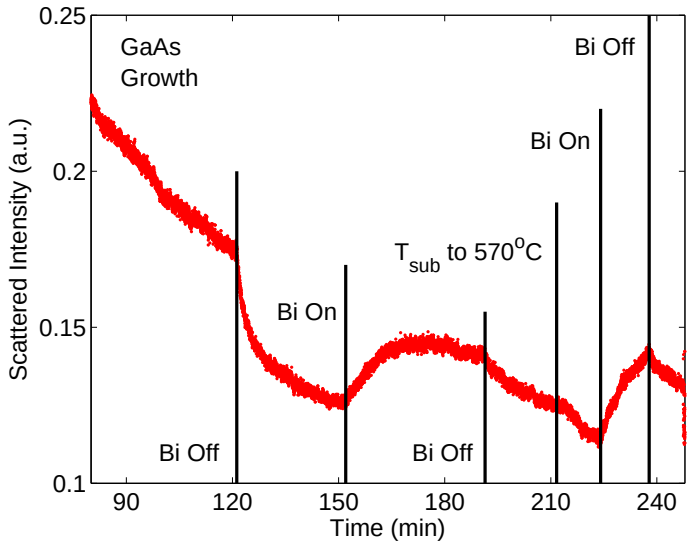

Figure 6.5: Light scattering signal observed during GaAs growth with bismuth cycling on and off. This signal is measured in the linear smoothing regime. The growth conditions are: Ga flux of 0.29 ML/s, Bi flux of 3.5 ML/s, and substrate temperature of 500^{o}C. The light scattering was aligned along the [1$\bar{1}$0] direction and set to 17.0 μm^{-1}. The substrate was later ramped to 570^{o}C.

simulation. In contrast, the observations presented in this chapter indicate that second order linear term is the dominate term in the continuum growth equation model. The second order smoothing coefficient is physically based and significantly increases when Bi is add to the (100) GaAs growth system.

The light scattering measurements suggest that the GaAs surface morphology moves to a new characteristic shape under the influence of Bi. Evidence of this can be seen by examining the dynamics of a single light scattering run. Figure 6.5 show a measured light scattering signal in which Bi

flux is alternated on and off. In this figure the light scattering signal, which is proportional to the PSD at $q = 17.0\ \mu\text{m}^{-1}$, decreases when the Bi flux is turned off and increases when the Bi flux is turned back on. This phenomenon occurs even after the substrate temperature is increased to 570^oC. At this temperature the Bi coverage will be low, as the Bi will only stay on the surface for a short while before evaporating, as shown in Figure 3.1. This experiment indicates that the surface roughness switch to a different asymptotic roughness when Bi is applied and switches back when the bismuth is shuttered. The surface is alternating between two characteristic power spectral density shapes as Bi flux is alternated on and off.

6.2 Ex-situ Observations

The growth of GaAs with Bi as a surfactant has been investigated with ex-situ AFM. Both patterned and thermally desorbed surfaces have been used as starting surfaces. The features normally seen on the GaAs surface are altered by the surfactant. Figure 6.6 shows AFM images of GaAs grown on oxide desorbed surfaces with and without Bi. In this figure a slight change in the structure of the surface features can be seen. For example, the elongation of the mounds in $[1\bar{1}0]$ direction is more pronounced for the samples grown with Bi, as seen in the upper image in Figure 6.6.

The effect that Bi surfactant has on homoepitaxial GaAs growth on patterned substrates has been examined. Figures 6.7 and 6.8 show the shape evolution of 3 μm pitched gratings aligned along the $[1\bar{1}0]$ and [110] crystalline directions. For the gratings in Figure 6.7 the overall structure of the surface shape remains unchanged. In Figure 6.7 the surface amplitudes of the samples grown with Bi are smaller than GaAs grown without Bi.

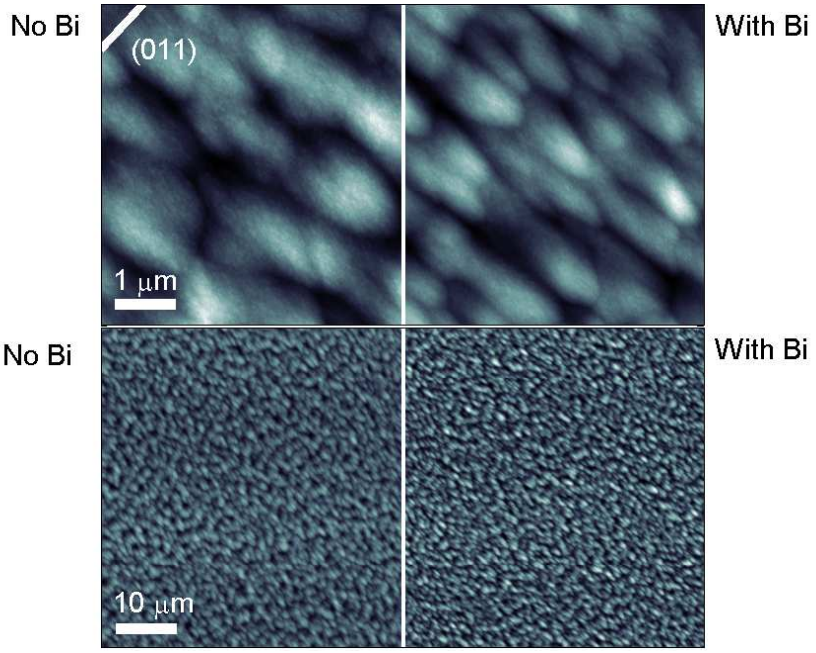

Figure 6.6: AFM images of GaAs surfaces grown without Bi (Left) and with Bi (Right). Each sample had 1.0 μm of GaAs grown at 0.39 ML/s and 500^{o}C. The Bi flux was 3.3 ML/s. The RMS roughnesses are top left: 1.7 nm, top right: 1.4 nm, bottom left: 2.1 nm, bottom right: 2.9 nm.

These results are in contrast to gratings aligned along the [110] direction in Figure 6.8, where the addition of a surfactant results in significant difference in observed features at longer growth times. A similar study has been conducted by Wixom et al [39]. In this study the effect of Bi on the homoepitaxial growth GaAs with Metal-Organic Chemical Vapour Deposition on large patterned surfaces was examined. Although the differences in experimental conditions make a direct comparison difficult, Wixom et al did observe Bi to have a dramatic effect on the evolution of a patterned surface

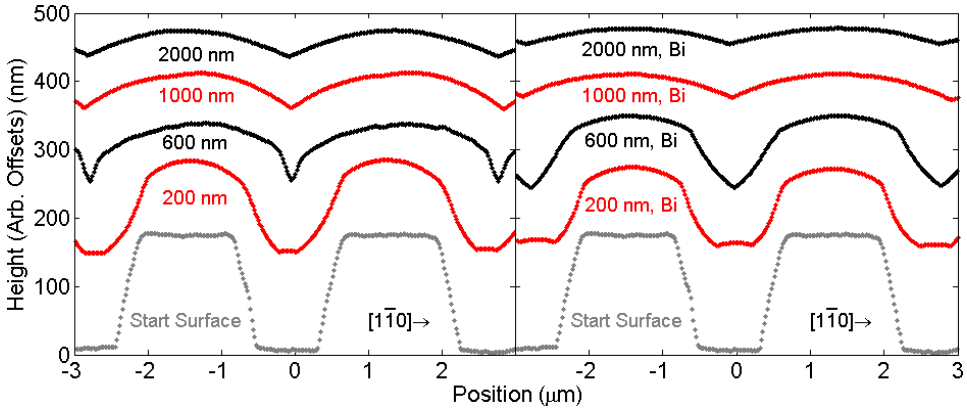

Figure 6.7: AFM line scans of GaAs grown on 3 μm pitch gratings aligned along the [1$\bar{1}$0] direction. The GaAs was grown at 0.86 ML/s and 500^{o}C. The line scans on the right were grown with a Bi flux of 3.2 ML/s.

during growth.

The application of a surfactant effected both characteristic surface shapes that were observed in Chapter 5; i.e. the downward cusp, rounded mound morphology and the inverted symmetry morphology. Bismuth reduces the initial smoothing that occurs during GaAs growth on 3 μm line gratings. Consider how Bi affects the arguments that explained the formation of these characteristic structures, presented in Section 5.4, in order to to explain the observed changes to the surface morphologies in Figures 6.7 and 6.8. The results shown in Figures 6.7 and 6.8 indicate that Bi alters the Ga adatom incorporation at the step edges. The most probable location for Bi to occupy on the (001) GaAs surface is along the step edges. In particular Bi should sit on steps parallel to the [110] crystalline direction, as these locations have the most free dangling bonds. The large Bi atom will have a significant effect on the surface potentials for adatoms at the step edges. It is likely that Bi

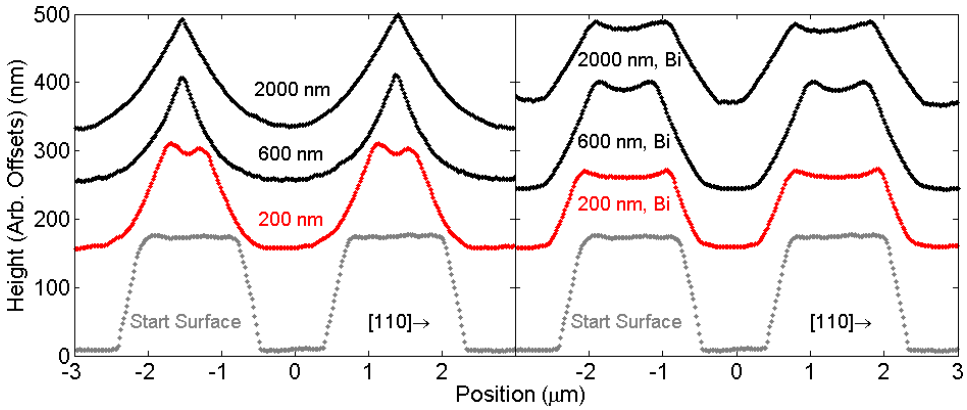

Figure 6.8: AFM line scans of GaAs grown on 3 μm pitch gratings aligned along the [110] direction. The GaAs was grown at 0.86 ML/s and 500^{o}C. The line scans on the right were grown with a Bi flux of 3.2 ML/s.

interferes with the incorporation of Ga atoms into the step edges, reducing the capture efficiency of both circular and vicinal step edges, thus Ga atoms are incorporated more uniformly across the surface. In the downward cusp, rounded mound morphology shown in Figure 6.7, the difference between incorporation rates on the flat and sloping parts of the grating is diminished by the presence of bismuth and the non-linear smoothing on patterned GaAs aligned perpendicular to the $[1\bar{1}0]$ direction is reduced.

In Figure 6.8 the inverted symmetry surface morphology is damped by the application of Bi to the GaAs growth. It is probable that the large Bi atoms block Ga adatoms from accessing the step edge, reducing incorporation of Ga adatoms into the step. Since Bi atoms are more likely to sit on steps parallel to the [110] direction than the $[1\bar{1}0]$ direction, the anisotropy in the step capture efficiency, $\dot{A}$ will be reduced. With a lower value of $\dot{A}$ the minimum in the adatom incorporation rate shown in the left image of Fig-

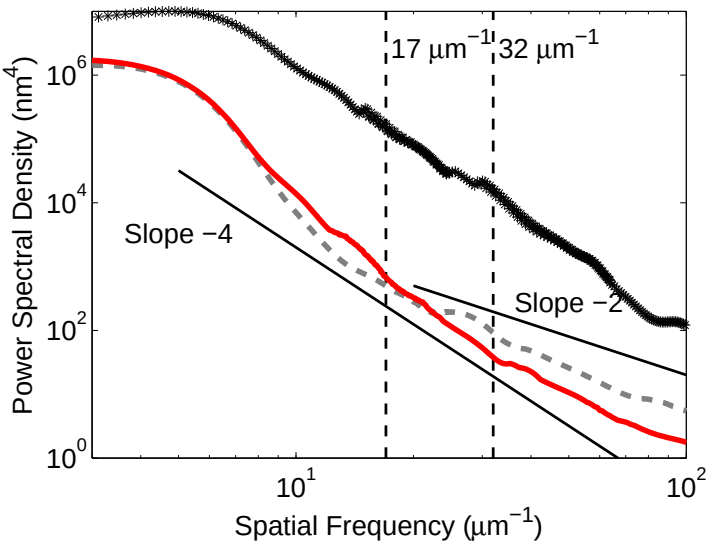

Figure 6.9: Power spectral densities along the $[1\bar{1}0]$ direction as calculated from AFM images of GaAs surfaces grown at a Ga flux of 0.39 ML/s and 500^{o}C to a depth of 1 μm. The Bi flux was 3.3 ML/s. The thermally desorbed starting surface is indicated by $*$, while the solid red line and the dashed grey line indicate GaAs grown with and without Bi, respectively.

ure 5.11 will be less pronounced and the physics that produce the inverted symmetry surface shape is diminished.

The power spectral density of the surface contains additional information about the surface dynamics. Power spectral densities have been extracted from AFM images of the surfaces of grown GaAs films and are presented in Figures 6.9 and 6.10. The PSDs displayed in these figures are consistent with the smoothing presented in Section 6.1. In Figure 6.9 the PSD at $q = 17\ \mu m^{-1}$ of the GaAs grown with Bi is larger than for GaAs homoepitaxy without bismuth. Also, at $q = 32\ \mu m^{-1}$ the PSD for growth

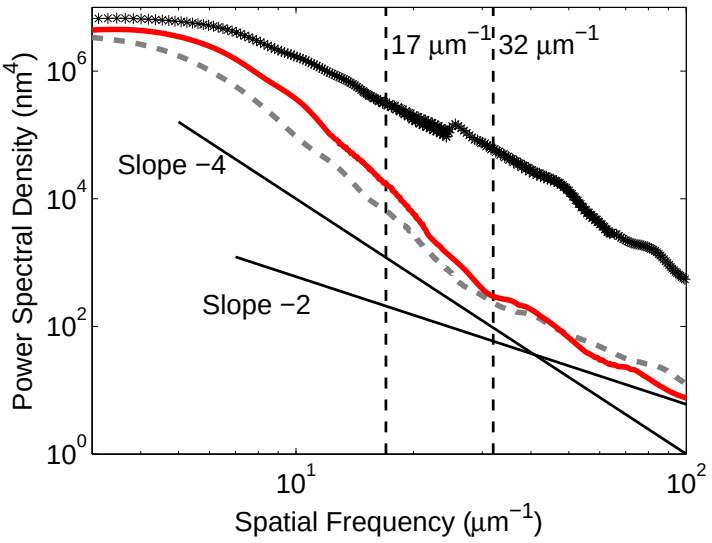

Figure 6.10: Power spectral densities along the [110] direction as calculated from AFM images of GaAs surfaces grown at 0.39 ML/s and 500^{o}C to a thickness of 1.0 μm. The Bi flux was 3.3 ML/s. The thermally desorbed starting surface is indicated by $*$, while $*$ and $\bullet$ indicate GaAs grown with and without Bi.

with Bi is smaller in magnitude than the PSD for growth without a surfactant. This is consistent with the light scattering measurements which showed larger smoothing coefficients for growths with Bi at $q = 32\ \mu m^{-1}$, while the smoothing at $q = 17\ \mu m^{-1}$, was slower with the Bi surfactant. Additionally, the PSD calculated along the [110] direction is consistent with the trends seen in the $[1\bar{1}0]$ direction.

The characteristic shape of the PSD for GaAs grown with Bi shown in Figures 6.9 and 6.10 has changed with respect to GaAs grown without Bi. The GaAs surface smoothing from an oxide desorbed surface during

homoepitaxial growth will saturate to a characteristic shape in the power spectral density. A defining feature in the PSD of (001) GaAs surfaces is that it saturates to a slope of -2 at low q [27]. The samples used to generate Figures 6.9 and 6.10 were grown for significantly longer times than the light scattering apparatus can observe, and the power spectral densities at high spatial frequencies are saturated. For GaAs homoepitaxy the PSD saturates to a slope of -2 at the spatial frequencies presented in Figure 6.9, while the sample grown with Bi flux has saturated to a slope in the PSD closer to -4. The surface morphology the corresponds to a slope in the PSD arises from roughness generated by non-conservative noise on surface. For GaAs grown by MBE this noise is caused by the random deposition of atoms on the surface. Continuum growth equation models predict the observed slope in the PSD. Continuum growth equations have been solved (analytic and numerical solutions) in the presence of non-conservative noise, and the predicted saturated slopes are presented in [53]. As mentioned previously, a slope of -2 in the PSD has been observed before in GaAs grown and indicates a continuum growth equation dominated by the first order linear term, $\nabla^2 h$. A continuum growth equation dominated by the second order linear term would saturate to a slope of -4 in the PSD. However, a slope of -4, seen in the PSD of the sample grown with bismuth, indicates that the second order linear term, $\kappa\nabla^4 h$ is the dominate term. Note that a slope in the PSD of -10/3 is also reasonable for the Bi grown sample shown in Figures 6.9 and 6.10, which would correspond to the MBE continuum equation (Equation 2.3) driven with non-conservative noise. The change in the characteristic shape of the PSD when Bi is added to the (100) GaAs system support a significant change in the physics on the surface.

6.3 Summary and Discussion

The effect of Bi as a surfactant has been observed on the (001) GaAs surface during MBE growth. Both in-situ and ex-situ observations indicate that Bi alters the physics on the GaAs surface. Bismuth was found to increase the rate of smoothing that occurs during GaAs growth at short length scales, while at long length scales bismuth reduced the smoothing coefficients. This result is confirmed by three independent measurements; in-situ light scattering and ex-situ AFM measurements on the smoothing of GaAs from randomly rough surfaces and patterned substrates.

AFM and light scattering measurements at long times on GaAs grown on randomly rough substrates indicate that bismuth on the surface strengthens the second order linear term ($\kappa\nabla^4 h$) and weakens the first order linear term ($\nu\nabla^2 h$) in the continuum growth equation approximation. At the low amplitudes seen for GaAs growth at long times any non-linear terms will be weak and overwhelmed by the linear terms. Comparing the linear terms to each other one finds that at low spatial frequency the first order linear term will dominate, while at high spatial frequency the second order term dominates. From Equation 2.11 the first order linear smoothing coefficient depends linearly on the ES step edge coefficient, ζ and weakly on the diffusion constant. A surfactant on a surface may alter the surface potentials for adatoms at the step edges, as the large Bi atoms are likely to sit there during growth. Thus it is reasonable that ζ is significantly changed by the addition of Bi to the GaAs growth. Form the experimental results we find that the step density is reduced by the Bi surfactant. The second order linear smoothing coefficient likely depends on growth rate and step density as: $\kappa \propto F/S_o^4$ as calculated by Politi and Villain using dimensional analysis [98]. The second order linear smoothing coefficient has the same form of

the second order non-linear smoothing coefficient shown in Equation 2.12 within a numerical constant of order unity. Additionally, bismuth has been reported to increase the Ga adatom diffusion on the surface (001) GaAs surface [16, 39, 99] and reduce the step density by factor of ~ 2. Thus, it is reasonable that the second order linear term is increased such that it is the dominant term, as the in-situ light scattering measurements and AFM measurements suggest.

From the results presented in this chapter it is apparent that Bi changes the characteristics of GaAs homoepitaxy in a complex way. There is more happening on the surface then a simple increase in the rate of smoothing. The addition of bismuth changes the characteristic shape in the PSD of MBE grown GaAs, tending to increase the spatial frequency dependence. This results in GaAs grown with Bi being rougher at low spatial frequency and smoother at high q than for GaAs grown with no Bi. Evidence of this can be seen by examining the PSD of GaAs grown at different conditions in Figure 6.9 and 6.10 and from the in-situ light scattering measurements in Section 6.1.

The results presented in this chapter indicate that bismuth is a good surfactant for the growth of GaAs with MBE. With Bi the surface roughness is significantly reduced at small lengthscales, which is useful for producing the flat interfaces needed for quality devices. Additionally, Bi does not incorporate into the bulk material for the GaAs growth conditions used in this thesis [9]. Also, Bi slows the evolution of the surface shape of large lengthscale patterned surfaces. Thus, using Bi as a surfactant will help preserve micro-scale structures but will smooth out nanoscale roughness associated with the growth process which may adversely affect electronic and optical properties relevant for devices.

Chapter 7

Conclusions

In this thesis elastic light scattering, RHEED, and AFM have been used to measure phenomena that occur during the smoothing of patterned and rough (001) GaAs substrates when grown by MBE. The in-situ light scattering apparatus allows real time monitoring of the surface morphology which is typically unavailable to MBE reactors. With this apparatus the growth rate, substrate temperature, As_2 flux, crystal orientation, spatial frequency and Bi surfactant dependence of the smoothing on randomly roughened GaAs substrates were measured. Complimentary measurements of the surface morphology, atomic step density and PSD on initially rough and patterned GaAs have been taken by ex-situ AFM. This comprehensive study of GaAs homoepitaxy is the first to explore the effects of growth rate on the surface morphology in such detail. An understanding of the evolution of the surface morphology is important for the fabrication of nanoscale devices, which require exact knowledge of the shape of patterned structures or the production of atomically flat interfaces. The set of experimental data presented in this thesis provides an excellent basis for the testing and validation of models describing epitaxial growth.

A non-linear continuum growth model derived from the BCF type atomistic picture was tested in this work. This model was able to predict the experimental phenomena observed at later times in the GaAs growth. The

spatial frequency dependence of the observed smoothing at long growth times indicates that the smoothing can be associated with a continuum equation dominated by the first order linear term, $\nu\nabla^2 h$. The observed Ga flux and substrate temperature dependence of the linear smoothing coefficient were consistent with the dependencies predicted by the continuum growth model for high As_2/Ga ratios. Measurements of the smoothing at As_2/Ga ratios near unity and the As_2 flux dependence were beyond the scope of the non-linear continuum growth model as this model assumes Ga dominated growth, which is not the case at low As_2/Ga ratios. Independent ex-situ AFM measurements of the atomic step densities agree with both the long time smoothing observed with light scattering and the BCF picture of epitaxial growth. As the AFM measured step densities were used to infer the linear smoothing coefficients measured which were consistent with the smoothing coefficients obtained from the light scattering apparatus. Additionally, between the in-situ measurements of the smoothing and the ex-situ measurements of the step density the critical size island nucleus, an important atomistic parameter, was determined to be 2. Overall, the smoothing of the (001) GaAs surface observed with in-situ light scattering for low amplitude surface topography consistently agreed with the continuum growth equation model, in which the parameters in the linear term of the growth equation are derived from a BCF type atomistic model for epitaxial growth.

Several questions remain for the smoothing observed at early times in growth of GaAs on surfaces with the oxide thermally desorbed. The flux dependence of the initial smoothing might be expected to be described by the BCF-based non-linear term in the continuum growth equation model, $\lambda_2\nabla^2(\nabla h)^2$. The predicted flux dependence of the non-linear smoothing coefficient is consistent with the measured flux dependence, and a non-linear

term is clearly present in a continuum equation model that describes of (100) GaAs homoepitaxy, since the GaAs surface exhibits non-linear features such as downward cusps. However, the spatial frequency and substrate dependence of the initial smoothing are clearly not consistent with the continuum growth equation model. It is possible that the reason for the inconsistency has to do with the surface morphology of the initial surface being too steep, exposing new low index crystal planes, which are not considered in the continuum model. The BCF based non-linear continuum growth model is not consistent with the smoothing measured at the start of the GaAs growth. A deeper understanding of the thermal oxide desorbed surface of (100) GaAs or a better model that describes epitaxial growth is needed.

In this thesis, interesting surface morphologies have be observed for GaAs growth on pre-patterned substrates. For gratings with ridges aligned perpendicular to the $[1\bar{1}0]$ crystalline direction and at conditions that result in a low step density for gratings aligned perpendicular to the $[1\bar{1}0]$ direction the resulting surface morphology is characterized by downward cusps and rounded mounds, as previously seen in GaAs growth on patterned substrates [11, 12]. However, growth on gratings with ridges aligned perpendicular to the [110] direction at conditions that resulted in a high atomic step density, produced surface shapes that had cusps pointed upwards and rounded valleys. This surface morphology has not been previously observed in (100) GaAs homoepitaxy. The upward cuspy, rounded valley surface morphology has potential applications in device fabrication since it is persistent and will smooth away as fast patterns aligned to other crystalline directions. The cuspy valleys or peaks indicate that a continuum growth model that describes GaAs homoepitaxy must contain non-linear terms since these features are symmetric with a vertical flip. Linear terms in continuum growth

equation model are unable to predict features that lack up down symmetry. The physical mechanism that causes the observed cuspy structures is the lateral migration and attachment of the adatoms in response to topography dependent variations in the step density. The upward cuspy, rounded valley surface morphology indicates that steps parallel to the [110] crystalline axis are more efficient at capturing adatoms than steps parallel to the $[1\bar{1}0]$ direction.

The in-situ light scattering and ex-situ AFM measurements of the smoothing of randomly rough and patterned substrates in the presence of bismuth significantly alter the characteristic shape of the GaAs surface morphology. These results indicate that Bi alters the ad-atom dynamics on the surface, preferentially accumulate at the atomic step edges during growth, increasing the frequency that adatoms hop between atomic terraces (interlayer transport) of Ga adatoms but decreasing the incorporation rate of these adatoms. Additionally, these experiments suggest that the Bi surfactant increases the diffusion of Ga adatoms on the surface. In terms of the continuum growth equation model, the experimental results indicate that bismuth on the GaAs surface reduces the first order liner term ($\nu\nabla^2 h$) and adds or increases a second order linear term ($\kappa\nabla^4 h$). Overall, bismuth is a good surfactant since it increases smoothing and reduces the roughness at small lengthscales (high spatial frequency), which is useful for making smooth interfaces when growing complex hetrostructures. Also, since Bi decreases the smoothing at large lengthscales, patterned fabricated onto the surface will persist longer during growth, which is useful for device fabrication.

In conclusion, the physics on the surface of (001) GaAs during growth with MBE is found to be more complex then previously thought. Nevertheless, the non-linear continuum growth model is able to explain a wide range

of experimental phenomena, as discussed previously in this thesis. However these is still much more to be learned about the surface shape evolution. For example the effects of changes in the group V/III ratio, a more detailed picture of the Bi surfactant effect, including different concentrations and a description valid for large amplitude topography would be worth pursuing. Extending this work to other semiconductor materials would also be of interest. The set of experimental observations presented in this thesis provide an excellent basis to test and develop models that describe epitaxial growth.

Bibliography

[1] A. Ballestad and T. Tiedje. Emergence of macroscopic structure from atomistic dynamics in epitaxial film growth. *Phys. Rev. B*, 74(15):153405, 2006.

[2] V.P. LaBella, M.R. Krause, Z. Ding, and P.M. Thibado. Arsenic-rich GaAs(001) surface structure. *Surf. Sci. Rep.*, 60:1–53, 2005.

[3] T. Tiedje and A. Ballestad. Atomistic basis for continuum growth equation: Description of morphological evolution of GaAs during molecular beam epitaxy. *Thin Solid Films*, 516(12):3705–3728, 2008.

[4] A. Ballestad. *Epitaxial Growth Dynamics in Gallium Arsenide*. PhD thesis, University of British Columbia, Canada, March 2005.

[5] E.C. Young, S. Tixier, and T. Tiedje. Bismuth surfactant growth of the dilute nitride GaN_xAs_{1-x}. *J. Cryst. Growth*, 279:316–320, 2005.

[6] A.K. Jones, A. Ballestad, Tian Li, M.B. Whitwick, J. Rottler, and T. Tiedje. Faceting at the step flow threshold in epitaxial growth on patterned surfaces. *Phys. Rev. B*, 79:1–6, 2009.

[7] J.F. Geisz and D.J. Friedman. III-N-V semiconductors for solar photovoltaic applications. *Semicond. Sci. Technol.*, 17:769, 2002.

[8] M. Fischer, D. Gollub, M. Reinhardt, M. Kamp, and A. Forchel. GaInNAs for GaAs based lasers for the 1.3 to 1.5 micron range. *J. Cryst. Growth*, 251:353–359, 2003.

[9] X. Lu, D. Beaton, T. Tiedje, R. Lewis, and M.B. Whitwick. Effect of MBE growth conditions on Bi content of $GaAs_{1-x}Bi_x$. *Appl. Phys. Lett.*, 92(19):192110, 2008.

[10] Z. Zhang and B.G. Orr. Two-component simulation for molecular beam epitaxy growth of GaAs. *Phys. Rev. B*, 67(7):075305, 2003.

[11] A. Ballestad, T. Tiedje, J. Schmid, B. Ruck, and M. Adamcyk. GaAs surface shapes during MBE regrowth on patterned substrates. *J. Cryst. Growth*, 271:13–21, 2004.

[12] H.C. Kan, S. Shah, T. Tadyyon-Eslami, and R.J. Phaneuf. Transient evolution of surface roughness on patterned GaAs(001) during homoepitaxial growth. *Phys. Rev. Lett.*, 92(14):146101, 2004.

[13] C. Ratsch, J. Garcia, and R. E. Caflisch. Influence of edge diffusion on the growth mode on vicinal surfaces. *Appl. Phys. Lett.*, 87(14):141901, 2005.

[14] F. Grosse and M.F. Gyure. Ab initio based modeling of III-V semiconductor surfaces: Thermodynamic equilibrium and growth kinetics on atomic scales. *Phys. Rev. B*, 66(7):075320, 2002.

[15] N. Zangenberg, D.A. Beaton, T.Tiedje, S. Tixier, M. Adamcyk, R. Kumaran, J.A. MacKenzie, E. Nodwell, E.C. Young, and G.I. Sproule. Molecular beam epitaxy growth of the dilute nitride $GaAs_{1-x}N_x$ with

a helical resonator plasma source. *J. Vac. Sci. Technol. A*, 25(4):850–856, 2007.

[16] T. Tiedje, E.C. Young, and A. Mascarenhas. Growth and properties of the dilute bismide semiconductor $GaAs_{1-x}Bi_x$ a complementary alloy to the dilute nitrides. *Int. J. Nano.*, 5:964–983, 2008.

[17] A. Ohtake. Surface reconstructions on GaAs(001). *Surf. Sci. Rep.*, 63:295–327, 2008.

[18] E.L. Church, H.A. Jenkinson, and J.M. Zavada. Relationships between surface scattering and microtopographic features. *Opt. Eng.*, 18:125–136, 1979.

[19] M. Adamcyk, T. Pinnington, A. Ballestad, and T. Tiedje. Effect of the starting surface on the morphology of MBE grown GaAs. *Mater. Sci. Eng. B*, 75(2):153–156, 2000.

[20] M.D. Johnson, C. Orme, A.W. Hunt, D. Graff, J. Sudijono, L.M. Sander, and B.G. Orr. Stable and unstable growth in molecular beam epitaxy. *Phys. Rev. Lett.*, 72(1):116–119, 1994.

[21] C. Orme, M.D. Johnson, K.-T. Leung, B.G. Orr, P. Smilauer, and D. Vvedensky. Studies of large scale unstable growth formed during GaAs(001) homoepitaxy. *J. Cryst. Growth*, 150:128–135, 1995.

[22] T. Michely and J. Krug. *Islands Mounds and Atoms: Patterns and Processes in Crystal Growth Far from Equilibrium*. Springer, New York, 2004.

[23] J.W. Evans, P.A. Thiel, and M.C. Bartelt. Morphological evolution during epitaxial thin film growth: Formation of 2D islands and 3D mounds. *Surf. Sci. Rep.*, 61:1–128, 2006.

[24] V.R. Colucci, M.A. Cotta, C.A.C. Mendonca, K.M.I. Landers, and M.M.G. de Carvalho. Surface morphologies in GaAs homoepitaxy: Mound formation and evolution. *Phys. Rev. B*, 58(4):1947–1953, 1998.

[25] V.R. Coluci and M.A. Cotta. Influence of rough substrates on the morphology evolution of epitaxial films. *Phys. Rev. B*, 61(20):13703, 2000.

[26] A. Ballestad, B.J. Ruck, M. Adamcyk, T. Pinnington, and T. Tiedje. Evidence from the surface morphology for nonlinear growth of epitaxial GaAs films. *Phys. Rev. B*, 86(11):2377–2380, 2001.

[27] A. Ballestad, B.J. Ruck, J.H. Schmid, M. Adamcyk, E. Nodwell, C. Nicoll, and T. Tiedje. Surface morphology of GaAs during molecular beam epitaxy growth: comparison of experimental data with simulations based on continuum growth equations. *Phys. Rev. B*, 65(20):205302, 2002.

[28] M.B. Whitwick, T. Tiedje, and Tian Li. Linear smoothing of GaAs(100) during epitaxial growth on rough substrates. *J. Cryst. Growth*, 310:3192–3196, 2008.

[29] T. vanBuuren, M.K. Weilmeier, I. Athwal, K.M. Colbow, J.A. MacKenzie, T. Tiedje, P.C. Wong, and K.A.R. Mitchell. Oxide thickness effect and surface roughening in the desorption of the oxide from GaAs. *Appl. Phys. Lett.*, 59(4):464–465, 1991.

[30] W. K. Burton, N. Cabrera, and F. Frank. The growth of crystals and the equilibrium structure of their surfaces. *Transactions of the Royal Society*, 243(899):266, 1951.

[31] J. Villain. Continuum models of crystal growth from atomic beams with and without desorption. *J. Physique I*, 1(1):19–42, 1991.

[32] A. Pimpinelli and J. Villain. *Physics of crystal growth.* Cambridge University Press, Cambridge, United Kingdom, 1998.

[33] J. Krug. Four lectures on the physics of crystal growth. *Physica A*, 313(1):47–82, 2002.

[34] R.R. Wixon, L.W. Rieth, and G.B. Stringfellow. Te surfactant effects of the morphology of patterned (001) GaAs homoepitaxy. *J. Cryst. Growth*, 269:276–283, 2004.

[35] Ting Liu, S. Chandril, A.J. Ptak, D. Korakakis, and T.H. Myers. Bismuth surfactant effects for GaAsN and beryllium doping of GaAsN and GaInAsN grown by molecular beam epitaxy. *J. Cryst. Growth*, 304:402–406, 2007.

[36] C. Lavoie, T. Pinnington, T. Tiedje, J.L. Hutter, G. Soerensen, and R. Streater. Indium-induced smoothing of GaAs films during MBE growth. *Can. J. Phys.*, 74:S47–S53, 1996.

[37] H.B. Yuen, S.R. Bank, H. Bae, M.A. Wistey, and J.S. Harris Jr. The role of antimony on properties of widely varying GaInNAsSb compositions. *J. Appl. Phys.*, 99(9):093504, 2006.

[38] S. Tixier, M. Adamcyk, E.C. Young, J.H. Schmid, and T. Tiedje. Surfactant enhanced growth of GaNAs and InGaNAs using bismuth. *J. Cryst. Growth*, 251:449–454, 2003.

[39] R.R. Wixon, L.W. Rieth, and G.B. Stringfellow. Sb and Bi surfactant effects on homo-epitaxy of GaAs on (001) patterned substrates. *J. Cryst. Growth*, 265:367–374, 2004.

[40] H.B. Yuen, S.R. Bank, M.A. Wistey, J.S. Harris, M.J. Seong, S. Yoon, R. Kudrawiec, and J. Misiewicz. Improved optical quality of GaNAsSb in the dilute Sb limit. *J. Appl. Phys.*, 97(11):113510, 2005.

[41] L. Däweritz and R. Hey. Reconstruction and defect structure of vicinal GaAs(001) and $Al_xGa_{1-x}As$(001) surfaces during MBE growth. *Surf. Sci.*, 236(1-2):15–22, 1990.

[42] K. Regiński, J. Muszalski, V.V. Preobrazhenskii, and D.I. Lubyshev. Static phase diagrams of reconstructions for MBE-grown GaAs(001) and AlAs(001) surfaces. *Thin Solid Films*, 267:54–57, 1995.

[43] L.L. Chang, L. Esaki, W.E. Howard, R. Ludeke, and G. Schul. Structures grown by molecular beam epitaxy. *J. Vac. Sci. Technol.*, 10(5):655–662, 1973.

[44] A.Y. Cho. Bonding direction and surface-structure orientation on GaAs (001). *J. Appl. Phys.*, 47(7):2841–2843, 1976.

[45] E.S. Tok, J.H. Neave, J. Zhang, B.A. Joyce, and T.S. Jones. Arsenic incorporation kinetics in GaAs(001) homoepitaxy revisited. *Surf. Sci.*, 374:397–405, 1997.

[46] Q. Xue, T. Hashizume, T. Sakata, Y. Hasegawa, A. Ichimiya, T. Ohno, and T. Sakurai. Surface geometry of MBE-grown GaAs(001) surface phases. *Thin Solid Films*, 281:556–561, 1996.

[47] P. Kratzer and and M. Scheffler C.G. Morgan. Density-functional theory studies on microscopic processes of GaAs growth. *Prog. Surf. Sci*, 59:135–147, 1998.

[48] M.R. Pillai, S.-S. Kim, S.T. Ho, and S.A. Barnett. Growth of $In_xGa_{1-x}As$/GaAs heterostructures using Bi as a surfactant. *J. Vac. Sci. Technol. B*, 18(3):1232–1236, 2000.

[49] M. Ahola-Tuomi, P. Laukkanen, R.E. Perälä, M. Kuzmin, J. Pakarinen, I.J. Väyrynen, and M. Adell. Structural properties of Bi-terminated GaAs(001) surface. *Surf. Sci.*, 600:2349–2354, 2006.

[50] P. Laukkanen, M.P.J. Punkkinen, H.P. Komsa, M. Ahola-Tuomi, K. Kokko, M. Kuzmin, J. Adell, J. Sadowski, R.E. Perälä, M. Ropo, T.T. Rantala, I.J. Väyrynen, M. Pessa, L. Vitos, J. Kollár, S. Mirbt, and B. Johansson. Anomalous bismuth-stabilized (2×1) reconstructions on GaAs(100) and InP(100) surfaces. *Phys. Rev. Lett.*, 100(8):086101, 2008.

[51] J.G. Amar and F. Family. Step-adatom attraction as a new mechanism for instability in epitaxial growth. *Phys. Rev. Lett.*, 77(22):4584–4587, 1996.

[52] J. Tersoff, M.D. Johnson, and B.G. Orr. Adatom densities on GaAs: evidence for near-equilibrium growth. *Phys. Rev. Lett.*, 78(2):282–285, 1997.

[53] A.L. Barabási and H.E. Stanley. *Fractal concepts in surface growth*. Cambridge University Press, Cambridge, United Kingdom, 1995.

[54] M. Kardar, G. Parisi, and Y.-C. Zhang. Dynamic scaling of growing interfaces. *Phys. Rev. Lett.*, 56(9):889–892, 1986.

[55] V. Yakhot. Large-scale properties of unstable systems governed by the kuramoto-sivashinski equation. *Phys. Rev. A*, 24:642, 1981.

[56] Tao Sun, Hong Guo, and M. Grant. Dynamics of driven interfaces with a conservation law. *Phys. Rev. A*, 40(11):6763–6766, 1989.

[57] A. Ballestad, B. Lau, J.H. Schmid, and T. Tiedje. Nonlinear growth in GaAs molecular beam epitaxy. *Mater. Res. Soc. Symp. Proc.*, 859E:JJ9.6.1, 2005.

[58] T. Shitara, D.D. Vvedensky, M.R. Wilby, J. Zhang, J.H. Neave, and B.A. Joyce. Misorientation dependence of epitaxial growth on vicinal GaAs(001). *Phys. Rev. B*, 46(11):6825–6833, 1992.

[59] H. Yang, V.P. LaBella, D.W. Bullock, Z. Ding, J.B. Smathers, and P.M. Thibado. Activation energy for Ga diffusion on the GaAs(001)-(2×4) surface: An MBE-STM study. *J. Cryst. Growth*, 201/202:88–92, 1999.

[60] B.A. Joyce. In situ studies of the MBE growth of III-V systems using RHEED and STM. *J. Mater. Sci.: Mater. Electron.*, 14(9):591, 2003.

[61] Paul L. Houston. *Chemical Kinetics and Reaction Dynamics*. Dover Publications, 2001.

[62] J.W. Goodman. *Statistical optics*. John Wiley and sons, New York, 2000.

[63] J.C. Stover. *Optical Scattering*. SPIE, Bellingham, 1995.

[64] E.D. Pallik, editor. *Handbook of Optical Constants of Solids*, pages 429–444. Acedemic Press Inc, 1985.

[65] C. Lavoie, T. Pinnington, E. Nodwell, T. Tiedje, R.S. Goldman, K.L. Kavanaugh, and J.L. Hutter. Relationship between in-situ surface morphology and strain relaxation during growth of InGaAs strained layers. *Appl. Phys. Lett.*, 67(25):3744–3746, 1995.

[66] T. Pinnington, C. Lavoie, and T. Tiedje. Effect of growth conditions on surface roughening of relaxed InGaAs on GaAs. *J. Vac. Sci. Technol. B*, 15(4):1265–1269, 1997.

[67] T. Pinnington, Y. Levy, J.A. MacKenzie, and T. Tiedje. Real time monitoring of InAs/GaAs quantum dot growth using ultraviolet light scattering. *Phys. Rev. B*, 60(23):15901–15909, 1999.

[68] B.D. Cullity. *Elements of X-ray diffraction*. Addison Wesley Inc, 2001.

[69] V.V. Preobrazhenskii, M.A. Putyato, O.P. Pchelyakov, and B.R. Semyagin. Experimental determination of the incorporation factor of As_4 during molecular beam epitaxy of GaAs. *J. Cryst. Growth*, 201/202:170–173, 1999.

[70] T.A. Flaim and P.D. Ownby. Observations on ion gauge sensitivities to various gases. *J. Vac. Sci. Technol.*, 8(5):661–662, 1971.

[71] S.R. Johnson. *Optical Bandgap Thermometry in Molecular Beam Epitaxy*. PhD thesis, University of British Columbia, Canada, December 1991.

[72] M. Beaudoin, A.J.G. deVries, S.R. Johnson, H. Laman, and T. Tiedje. Optical absorption edge of semi-insulating GaAs and InP at high temperatures. *Appl. Phys. Lett.*, 70(26):3540–3542, 1997.

[73] T. Sugaya and M. Kawabe. Low-temperature cleaning of GaAs substrate by atomic hydrogen irradiation. *Japan. J. Appl. Phys.*, 30(3A):402–404, 1991.

[74] A. Khatiri, T.J. Krzyzewski, C.F. McConville, and T.S. Jones. Atomic hydrogen cleaning of low-index GaAs surfaces. *J. Cryst. Growth*, 282:1–6, 2005.

[75] Z.R. Wasilewski, J.M. Baribeau, M. Beaulieu, X. Wu, and G.I. Sproule. Studies of oxide desorption from GaAs substrates via Ga_2O_3 to Ga_2O conversion by exposure to Ga flux. *J. Vac. Sci.*, 22(3):1534–1538, 2004.

[76] Y. Asaoka. Desorption process of GaAs surface native oxide controlled by direct Ga-beam irradiation. *J. Cryst. Growth*, 40:45–51, 2003.

[77] A.J. SpringThorpe, S.J. Ingrey, B. Emmerstorfer, P. Mandeville, and W.T. Moore. Measurement of GaAs surface oxide desorption temperatures. *Appl. Phys. Lett.*, 50(2):77–79, 1986.

[78] W.P. Gomes. *Processing and properties of compound semiconductors, Wet etching of III-V semiconductors, Semiconductors and semimetals, vol. 73.* Academic Press, 2001.

[79] J.H. Schmid. *Evolution of Surface Texture in Thermal Chlorine Etching And Molecular Beam Epitaxy of Gallium Arsenide.* PhD thesis, University of British Columbia, Canada, May 2004.

[80] M. Lax. Temperature rise induced by a laser beam. *J. Appl. Phys.*, 48(9):3919–4003, 1977.

[81] M.B. Whitwick. Light activated Cl_2 etching of GaAs and optical holographic pattern formation. Master's thesis, University of British Columbia, Canada, April 2003.

[82] S. Ritchie, S.R. Johnson, C. Lavoie, J.A. Mackenzie, T. Tiedje, and R. Streate. Semiconductor substrate cleaning and surface morphology in molecular beam epitaxy. *Surf. Sci.*, 374:418–426, 1997.

[83] R.L. Schwoebel and E.J. Shipley. Step motion on crystal surface. *J. Appl. Phys.*, 37(10):3682–3686, 1966.

[84] T. Nishinaga. Atomistic aspects of molecular beam epitaxy. *Prog. Cryst. Growth Char. Mater.*, 48/49:104–122, 2004.

[85] G.R. Bell, M. Itoh, T.S. Jones, and B.A. Joyce. Nanoscale effects of arsenic kinetics on GaAs(001)-(2×4) homoepitaxy. *Surf. Sci. Lett.*, 423:L280–L284, 1999.

[86] A. Ishii, K. Seino, and T. Aisaka. Role of As_2 molecules on Ga-terminated GaAs(001) surface during MBE growth. *J. Cryst. Growth*, 236:511–515, 2002.

[87] C. Heyn and M. Harsdorff. Simulation of GaAs growth and surface recovery with respect to gallium and arsenic surface kinetics. *Phys. Rev. B*, 55(11):55–60, 1997.

[88] A. Yamashik and T. Nishinaga. Arsenic pressure dependence of incorporation diffusion length on (001) and (110) surfaces and inter-surface diffusion in MBE of GaAs. *J. Cryst. Growth*, 198/199:1125–1129, 1999.

[89] P.J. Poole, G.C. Aers, A. Kam, D. Dalacu, S. Studenikin, and R.L. Williams. Selective growth of InP/InGaAs ⟨010⟩ ridges: Physical and optical characterization. *J. Cryst. Growth*, 310:1069–1074, 2008.

[90] T. Tadayyon-Eslami, H.-C. Kan, L. C. Calhoun, and R. J. Phaneuf. Temperature-driven change in the unstable growth mode on patterned GaAs(001). *Phys. Rev. Lett.*, 97(12):126101, 2006.

[91] H.-C. Kan, R. Ankam, S. Shah, K. M. Micholsky, T. Tadayyon-Eslami, L. Calhoun, and R. J. Phaneuf. Evolution of patterned GaAs(001) during homoepitaxial growth: Size versus spacing. *Phys. Rev. B*, 73(19):195410, 2006.

[92] R.S. Williams, M.J. Ashwin, T.S. Jones, and J.H. Neave. Influence of the growth conditions on the ridge morphology during GaAs deposition on GaAs (001) patterned substrates. *J. Appl. Phys.*, 95(11):6112–6118, 2004.

[93] G. Feng, K. Oe, and M. Yoshimoto. Temperature dependence of Bi behavior in MBE growth of InGaAs/InP. *J. Cryst. Growth*, 301-302:121–124, 2007.

[94] N. Grandjean and J. Massies. Kinetics of surfactant-mediated epitaxy of III-V semiconductors. *Phys. Rev. B*, 53(20):13232–13234, 1996.

[95] J.K. Shurtleff, R.T. Lee, C.M. Fetzer, and G.B. Stringfellow. Bandgap control of GaInP using Sb as a surfactant. *Appl. Phys. Lett.*, 75(13):1914–1916, 1999.

[96] Y.G. Sadofyev, S.R. Johnson, S.A. Chaparro, Y. Cao, D. Ding, J.H. Wang, K. Franzreb, and Y.H. Zhang. Sb-mediated growth of Si-doped

AlGaAs by molecular-beam epitaxy. *Appl. Phys. Lett.*, 84(18):3546–3548, 2004.

[97] J.G. Cederberg and S.R. Lee. Surfactant effects associated with Te-doped InPAs alloys. *Appl. Phys. Lett.*, 91(20):201915, 2007.

[98] P. Politi and J. Villain. Kinetic coefficients in a system far from equilibrium. In M.C. Tringides, editor, *Surface Diffusion: atomistic and collective processes*, pages 177–189. Plenum Press, New York, 1997.

[99] Z. Zhang and M.G. Lagally. Atomic-scale mechanisms for surfactant-mediated layer-by-layer growth in homoepitaxy. *Phys. Rev. Lett.*, 72(5):693–696, 1994.

Appendix A

List of Publications

The following is a list of publications produced that use the experimental methods or results presented in this thesis.

- A.K. Jones, A. Ballestad, T. Li, M.B. Whitwick, J. Rottler, and T. Tiedje, *Faceting at the Step Flow Threshold in Epitaxial Growth on Patterned Surfaces*, Phys. Rev. B, 71 (2009), 1-5

- M. Beaudoin, I.C.W. Chan, D. Beaton, M. Elouneg-Jamroz, T. Tiedje, M.B. Whitwick, E.C. Young, J.F. Young, N. Zangenberg, *Bandedge Absorption of GaAsN Films Measured by the Photothermal Deflection Spectroscopy*, J. of Cryst. Growth, 311 (2009), 1662-1665

- M.B. Whitwick, T. Tiedje, and T. Li, *Linear Smoothing of GaAs(001) during Epitaxial Growth on Rough Substrates*, J. Cryst. Growth, 310 (2008), 3192-3196

- X. Lu, D.A. Beaton, R.B. Lewis, T. Tiedje, and M.B. Whitwick, *Effect of Molecular Beam Epitaxy Growth Conditions on the Bi Content of* $GaAs_{1-x}Bi_x$, Appl. Phys. Lett. 92 (2008), 192110

- E.C. Young, M.B. Whitwick, T. Tiedje, and D. Beaton, *Bismuth Incorporation in* $GaAs_{1-x}Bi_x$ *Grown by Molecular Beam Epitaxy with In-situ Light Scattering*, Phys. Stat. Sol. C4 (2007), 1707-1710